Mechanistic Insight of Biomilling for the Synthesis of Metal Oxide and Oxy-hydroxide Nanoparticles

Thesis Submitted to AcSIR
For the Award of the Degree of
DOCTOR OF PHILOSOPHY
In Biological Sciences

By
Chandrashekhar Sharan
Registration Number:10BB11J26114

Under the guidance of
Dr. Pankaj Poddar
Physical and Materials Chemistry Division
CSIR-National Chemical Laboratory
Dr. Homi Bhabha Road
Pune 411008

Dedicated to
my parents . .

Certificate

This is to certify that the work incorporated in this Ph. D. thesis entitled "**Mechanistic Insight of Biomilling for the Synthesis of Metal Oxide and Oxy-hydroxide Nanoparticles**" submitted by **Mr. Chandrashekhar Sharan** to Academy of Scientific and Innovative Research (AcSIR) in fulfillment of the requirements for the award of the Degree of Doctor of Philosophy embodies original research work under my supervision. I further certify that this work has not been submitted to any other University or Institution in part or full for the award of any degree or diploma. Research material obtained from other sources has been duly acknowledged in the thesis. Any text, illustration, table etc., used in the thesis from other sources, have been duly cited and acknowledged.

Chandrashekhar Sharan
(Student)

Dr. Pankaj Poddar
(Supervisor)

DECLARATION

I hereby declare that the work described in this thesis entitled **"Mechanistic insight of Biomilling for the synthesis of Metal Oxide and Oxy-hydroxide Nanoparticles"** submitted for the degree of *Doctor of Philosophy in Biological Sciences* has been carried out by me at the Physical and Materials Chemistry Division of the CSIR-National Chemical Laboratory, Pune, India, under the supervision of Dr. Pankaj Poddar. Such materials as have been obtained by other sources have been duly acknowledged in this thesis. The work is original and has not been submitted in part or full by me for award of any other degree or diploma in any other University.

Chandrashekhar Sharan

(Research Student)

Acknowledgements

There are a great many people to whom I would like to thank, for their support and contribution in research work, provided me over the years.

First and foremost, I would like to express sincere gratitude to my research supervisor Dr. Pankaj Poddar, for being supportive since the day I joined CSIR-NCL, Pune. I am most indebted to him for exposing me to the exciting and interesting field of research. I would also like to thank him for providing me the opportunity to work in various fields in addition to Ph. D. related works. I would like to express my deep felt gratitude to the members of the doctorate advisory committee, the chairperson Dr. Ashish Kishore Lele along with the other members Dr. V. Ravikumar, Dr. Absar Ahmad and Dr. Bashir Mohammad Khan for providing me valuable insight, comments, and suggestions. My special words of thanks should also go to the external expert Dr. Shivprasad Patil (IISER, Pune) for their time to time guidance during the course of my research. It gives me a great pleasure to thank HOD (Dr. Anil Kumar, Dr. Pattayil Alias Joy) and the director (Dr. Sourav Pal, Dr. Ashwini Kumar Nangia) for allowing me to carry out research at CSIR-NCL. I would like to extend my gratitude to the faculty members and staffs of CSIR-NCL for their help. I would also like to acknowledge the support from UGC, for providing the fellowship to pursue my Ph.D.

I also take this golden opportunity to convey my earnest respect to the collaborators Dr. Ramgopal Rao (IIT Bombay), Dr. Samit Chattopadhyay (NCCS, Pune), Dr. Ruchika Kaul Ghanekar (Bharati Vidyapeeth). I would also like to thank my companions Manoj Kandpal, Khusboo Pahwa and Prakash Mansara.

I take this opportunity to thank Dr. Mainak Majumder, Monash University, Melbourne, Australia, for providing opportunity for occupational training to explore the research carried out in his group. My special thanks to Dr. Atanu Basu, the deputy director NIV Pune, Prof. K. P. Sinha, the

Preface

The eco-friendly method for synthesis of nanomaterials with high aqueous dispersibibily, and stability, is of immense importance in nanotechnology. In this context, the biological method following nature's way would be the best choice. Most of the biological methods use the bottom-up approach, in which the nanomaterials are fabricated by the self-assembly of molecules/atoms. Therefore, the exploration of the biological top-down method is of immense interest. This thesis mainly, emphasizes on the use of microorganisms for the synthesis of nanomaterials by the controlled breakdown of bigger (micron-sized) particles into smaller nanoparticles and is termed as "biomilling".

This thesis is divided into five chapters. In the first chapter depicts the general introduction to the thesis. It also gives a glimpse of various methods of synthesis of nanoparticles and the method used in the thesis work i.e. biomilling. The second chapter describes the experimental and characterization techniques which have been used to carry out the work. The third chapter describes the biomilling of metal oxide nanorods into small quasi-spherical nanoparticles and to culminate some of the challenges associated with biomilling. The fourth chapter describes the biomilling of metal oxy-hydroxide nanorods into small quasi-spherical nanoparticles. In this chapter our main emphasis is to understanding about the mechanistic aspects of biomilling. The fifth chapter describes the conclusions and future perspective of the work described in this thesis. In short, the aim of this thesis is to provide the wealth of information for the top–down biological synthesis of nanomaterials.

Table of Contents

List of Abbreviations

1	μM	Micromolar
2	μm	Micrometer
3	2X	Twice concentration
4	3D	3-dimensional
5	AFM	Atomic force microscopy
6	AR	Analytical reagent
7	B.E.	Binding energy
8	CSIR	Council of scientific and industrial research
9	DLS	Dynamic Light Scattering
10	DNA	Deoxyribonucleic acid
11	EDS	Energy-dispersive X-ray spectrum
12	EELS	Electron Energy Loss Spectroscopy
13	EFM	Electric force microscope
14	EM	Electron microscopy
15	ESCA	Electron spectroscopy for chemical analysis
16	eV	Electron volts
17	fcc	Face-centered cubic
18	FTIR	Fourier Transform Infra-Red

19	FWHM	Full-width half maximum
20	GR	Guaranteed reagent
21	h	Hour
22	HR-TEM	High resolution transmission electron microscopy
23	ICP-AES	Inductively coupled plasma atomic emission spectroscopy
24	ICP-OES	Inductively coupled plasma-optical emission spectroscopy
25	IR	Infra-Red
26	JCPDS	Joint Committee on Powder Diffraction Standards
27	kDa	Kilo Dalton
28	LDOS	Local density of states
29	MFM	Magnetic Force Microscope
30	MGYP	Maltose Glucose Yeast extract Peptone
31	min	Minute
32	M_r	Relative molecular mass/weight
33	mV	Milivolt
34	NA	Numerical aperture
35	NCIM	National center for industrial microorganisms
36	nm	Nanometer
37	NPs	Nanoparticles
38	NRs	Nanorods

39	PAGE	Polyacrylamide gel electrophoresis
40	PFM	Piezorespose force microscopy
41	Phe	Phenyalanine
42	PL	Photoluminescence
43	PXRD	Powder X-ray diffraction
44	RT	Room temperature
45	*S. cerevisiae*	*Saccharomyces cerevisiae*
46	SAED	Selected area electron diffraction
47	SDS	Sodium dodecyl sulphate
48	SEM	Scanning electron microscopy
49	SNOM	Scanning near field microscopy
50	SPM	Scanning probe microscopy
51	SPR	Surface plasmon resonance
52	STM	Scanning tunneling microscopy
53	TCA	Trichloroacetic acid
54	TEM	Transmission electron microscopy
55	TGA	Thermogravimetric analysis
56	Trp	Tryptophan
57	Tyr	Tyrosine
58	UHV	ultra-high vacuum

59	UV	Ultra-Violet
60	UV-vis	Ultra-violet visible
61	WDS	Wavelength dispersive X-Ray
62	XPS	X-ray photoelectron spectroscopy
63	XRD	X-ray diffraction

List of Figures

Chapter III: The Synthesis of Metal Oxide Nanoparticles using Biomilling and Understanding the Role of Proteins

Chapter IV: The Mechanistic Insight into the Biomilling of Metal Oxy-Hydroxide Nanoparticles

(G), and selected area electron diffraction (SAED) pattern (H).1

List of Tables

Chapter I

Introduction

The eco-friendly synthesis of functionalized, quasi-spherical, highly water dispersible, and stable nanomaterials is an essential part of the research in nanotechnology. In the current world scenario, there is a growing need to develop environment friendly methods for the synthesis of nanomaterials and this thesis is a deliberate effort towards it. The work mainly emphasizes on biomilling; a biological top-down method of synthesis of nanoparticles, and to understand its mechanistic aspects.

This chapter provides an introduction to the thesis. It gives an overview and important aspects of multidisciplinary research of bionanotechnology. It started with the theme of motivation then the diverse methods of synthesis of nanoparticles, including the method which we used in the thesis "biomilling", were described. Furthermore, the few important applications of nanomaterials have been depicted. Finally, the chapter-wise description of the work done in this thesis was illustrated.

1.1   Theme and Motivation

"Look deep into nature, and then you will understand everything better."
— *Albert Einstein*

People have been turning to nature to solve their problems; for millions of years. Scientists also often look to nature, to see if there's already a solution to the problem they are facing. How does butterfly display beautiful colors? What produces the dazzling colors of peacock's feathers? The answers to mysteries lie in the nature's spectacular architectures, which constitutes miniature optical mirrors and filters made of organic crystal or physisorbed water layers, arranged periodically. When such periodicity is in the range of ten to few hundreds of nanometers; which is also the periodicity of refractive index, these structures interferes with the visible light and modify the transmitted, reflected or absorbed light.[1] Nature is the grandmaster who builds and transforms materials into different shapes, and sizes with different properties. It is remarkable to see how the highly complex tasks have been performed in nature with simple, yet highly efficient machinery. The way nature works, is quiet energy efficient and environment friendly.

Scientists throughout the world have been developing the green synthetic methods, for the synthesis of nanomaterials. The living organisms as well as other biological materials, have been used for the synthesis of various nanomaterials.[2] Now a days, number of biological methods for synthesis of nanomaterials, have been established by scientists, throughout the world.[3–6] Some examples are biosynthesis,[4,7–10] biomimetic synthesis,[11,12] bio-templated synthesis,[13] biomineralization,[14–17] bioreduction,[18,19] bio-inspired materials synthesis,[20] bioremediation[21] etc. To carry out these processes, various genera of living

organisms and their products have been used such as bacteria,[22] fungi,[23,24] viruses,[25,26] plant extracts,[27] plant metabolites,[28] antibiotics,[29] enzymes,[23,30,31] proteins,[32] nucleic acids[33] and so on.

The work of this thesis is greatly inspired by the natural phenomena such as 'the biological weathering of rocks'[34,35] and 'bioleaching',[36,37] which constitute many physical, chemical as well as biological processes. Here, our main concern is biological weathering, in which plants, animals and/or consortium of micro-organisms (bacteria, fungi, algae or yeasts) release the chemical compounds, such as organic acids, metal chelating agents, acidifying molecules etc. These processes are the elegant ways of extraction of inorganic nutrients from rocks.[34,38] The motivation behind this work came from the enthusiasm to understand and to harness the natural resources for the synthesis of nanomaterials. With this inspiration from nature, microorganisms for the controlled breakdown of bigger (micron-sized) particles into smaller nanoparticles (NPs) were used and this rather a newly developed process in our laboratory was termed as "**biomilling**". This nomenclature has been derived from analogues physical process "ballmilling" which is used to grind the bigger particles into NPs using mechanical energy. In the biomilling process, no harsh chemicals are used therefore, it can be considered as a 'green top-down method' for synthesis of NPs.

1.2   Various Approaches for the Synthesis of Nanoparticles

The most valuable and challenging part of nanotechnology is the fabrication of nanomaterials. It can be done by two antagonistic ways, either by breaking down the bigger particles "top-down" or by the assembly of atoms or molecules "bottom-up" approaches. Now a days, a number of chemical, physical and biological processes, are used

for the synthesis of nanomaterials. Some of these methods, for the synthesis of nanoparticles are shown in figure 1.1. Among all the methods, the physical methods are, in general, energy intensive; and chemical methods use hazardous chemicals that pose adverse effects on the environment. The nanomaterials synthesized by these methods are mostly incompatible for biological uses. Many times, these nanomaterials are unstable at physiological conditions required for the well-being of organisms. Therefore, the alternative environment-friendly methods are of immense interest. For the search of such environment-friendly methods, the scientist often looks towards the nature.
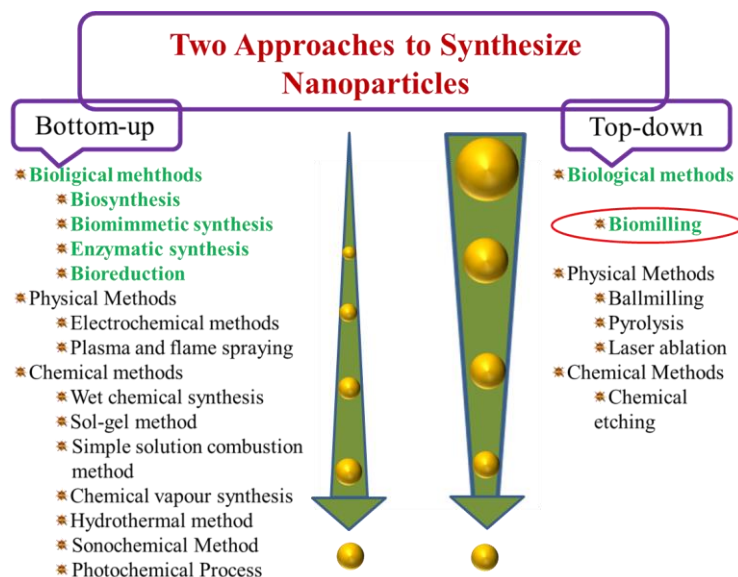
Figure 1.1: *The various approaches for the synthesis of nanoparticles.*

In last two decades, the biological methods have gained their popularity for being environment friendly as well as biocompatibility, and are termed as "green synthesis methods".[30] During this period, many different biological methods such as biosynthesis, biomimetic synthesis, bioreduction, bioremediation, bio-template synthesis, enzymatic synthesis, protein/peptide-mediated synthesis, nucleic acid mediated synthesis etc. have

been developed; however, all these methods use the bottom-up approach. Therefore, the exploration of top-down method would be of great significance.

1.2.1   Bottom–up Approaches of Synthesis of Nanoparticles

Feynman suggested that the atoms can be arranged in the way we want,[39] but it requires a deep understanding of the individual molecular structures, their assemblies, and dynamic behaviors. In the bottom–up approach, the functional nanometer size objects are constructed by the self-assembly of molecules/atoms.[40] The molecular self-assembly involves mostly weak and non-covalent interactions. These interactions include (i) hydrogen bonds, (ii) ionic bonds (electrostatic interactions), (iii) van der Waals interactions etc.[2] Individually, these interactions are feeble, however; numerous interactions together make them strong enough to hold the atoms/molecules together in the form of stable nanoparticles.

1.2.2   Top–down Approaches of Synthesis of Nanoparticles

The top–down methods for synthesis of nanomaterials are the counterpart of the bottom– up approaches which involve the breaking-down of bulk materials into nanoparticles. Instead of building an object from the bottom up, atom-by-atom, early craftsmen invented the **top-down** approach.[41] They use tools to shape and transform existing matters like clay, plant fibers, and metals etc. to create functional products. With the advancement of the techniques, today a number of methods are available for patterning of surfaces, like nanolithography using photons (X-ray, UV), scanning probe, electron or ion beams.[42] Likewise, the assembly and manipulation of atoms can also be done using STM.[43] However, for producing the materials in nano-dimension, this method is less popular,

except few physical methods e.g. ball milling,[44] laser abalations[45] etc. Our lab has deliberately taken initiative to explore the green top-down approach for the synthesis of nanoparticles below 10 nm and named biomilling.[46,47] In this thesis, we have used this approach for synthesis of nanomaterials, however, with some improvements.[48,49]

1.3 Synthesis of Nanoparticles by Physical Methods

1.3.1 Ball Milling

A ball mill is a type of grinder used to grind and blend materials. A schematic of ball-mill is shown in figure 1.2. This is most commonly used in mineral processing industries *e.g.* paints, pyrotechnics, ceramics and selective laser sintering etc. The ball milling technique, which is generally regarded as a traditional technique, has the history of several centuries. However, the use of this method for synthesis of nanomaterials was first time realized in 1999.[50,51] Thenceforth, this method has been used by many researchers for synthesis of different nanomaterials including one-dimensional nanomaterials.[44,52–54]
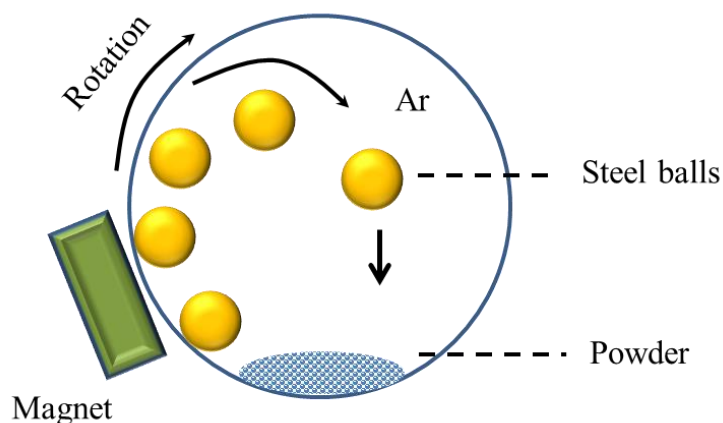
Figure1.2: *Schematic of high-energy vertical rotating ball mill.*

1.3.2 Spray Pyrolysis

Spray pyrolysis is a process in which, a solution is spread on a heated surface, which allows the constituents to react to form a thin film. The chemical reactants are selected such that the products other than the desired compound are volatile at that temperature.[55] This process is well suitable for the deposition[56] and synthesis of oxide nanomaterials,[57] synthesis of carbon nanotubes[58] etc. This method is widely used for the deposition of a transparent conductive coating of SnO_2 on glass substrate, which is widely used for making dye sensitize solar cells.[59]

1.3.3 Laser Ablation

Laser ablation is the process of removing material from a solid (or occasionally liquid) surface. Pulsed laser ablation in liquids used for the synthesis of nanoparticles in solvent/liquid. The target material is evaporated and condenses in the solvent thus forming nanoparticles. The synthesis of gold nanoparticles by laser ablation is shown by a schematic in figure 1.3. This method can be considered as top-down physical method of synthesis of nanoparticle.[45,60,61] It has also been used for the reshaping of nanoparticles from irregular into spherical shape.[62]
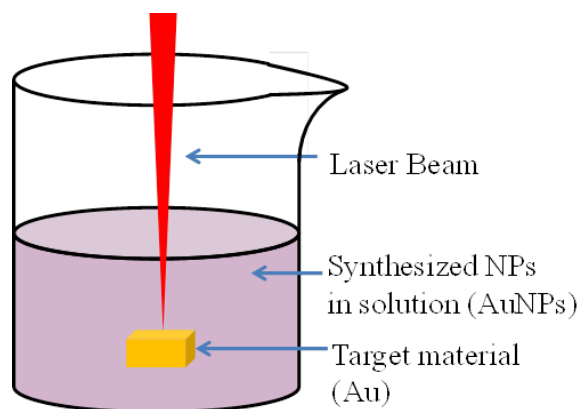
Figure 1.3: *Schematic showing synthesis of gold nanoparticle by laser ablation.*

1.3.4   Nanofabrication, Nanolithography and Nano-manipulation

With the advent of STM, it has been possible to precisely move individual atoms or molecules. Nowadays, scanning probe lithography (SPL) method has gained popularity for nanofabrication. With the help of today's sophisticated instruments; it is possible to have nano-scale precise control for the construction of spatially defined nanostructures. It is also possible to do this on surfaces with reactive or adhesive ligands for the subsequent attachment of polymers, inorganic materials, biomolecules etc.[63,64]

1.4   Synthesis of Nanoparticles by Chemical Methods

This method is the most commonly used method of synthesis of nanomaterials.

1.4.1   Wet Chemical Synthesis

Wet chemical synthesis comprises of all the chemical methods that carried out in the liquid phase.[65–68] In this method, an inorganic metal salt is dissolved in a solvent are added to basic solutions under controlled condition, in order to precipitate out the nanomaterials to be synthesized which then washed, dried and sometimes calcined, to obtain final nanoparticles. Some common methods are – Hydrothermal/solvothermal method,[67] sol – gel method, co-precipitation method,[68] micro-emulsion techniques/water–oil micro-emulsions method, polyol method etc.

1.4.2   Sol-gel Method

The colloidal suspension, in which solid particles of few hundred nanometers in size dispersed in a liquid phase are known as sol, whereas solid macromolecules immersed in a solvent to form jelly-like material, can be considered as a gel. In this method, the chemical transformation of sol into a gel state occurs, which upon subsequent post-treatment, transform into respective solid/metal oxide nanomaterials. The structure and composition

of nano-oxides formed with this method depends upon the reaction conditions, pH of solution, ion source and nature of precursors.[65]

1.4.3   Micro-emulsion Method

The micro-emulsions are transparent solutions consisting of small droplets of an immiscible phase (non-polar or polar). It generally consists of an aqueous phase and organic/oil phase. The surfactants are added to lower the interfacial tension between the immiscible dispersed and continuous phases to stabilize the droplets. The self-assembly take place in order to form nanoparticles with the size ~1–100 nm. The size of formed nanoparticles can be tailored by varying the concentrations of the dispersed phase and the surfactant phases.

1.4.4   Co-precipitation Method

In this process, the basic solutions commonly sodium hydroxide or ammonium hydroxides were added to inorganic salt precursors usually chloride, oxy-chloride, nitrates etc., to precipitate respective metal hydroxide. After filtration, washing and calcination, it forms respective metal oxide nanoparticles.[68] This method is especially useful for the synthesis of large amount of nanoparticles, however, the control of particle size distribution is limited.[65]

1.4.5   Hydrothermal Method

This method is carried out in a specialized vessel that could with stand high temperature and pressure commonly known as hydrothermal bomb. In the vessel, heterogeneous reaction takes place in presence of aqueous solvents, under high temperature and pressure.[67]

1.4.6 Microwave Assisted Method

The electromagnetic radiation with frequencies between 300 MHz (wavelength 1 m) to 300 GHz (wavelength 1 mm) are called microwave. The house hold microwave produces frequency ~2.45 GHz (λ=12 cm). This non-ionizing radiations cause the dielectric heating, primarily by absorption of the energy in water. The application of microwave heating is used for the synthesis of nanoparticles since 1986.[69]

1.4.7 Electrochemical Method

In this method the electrons act as reactant. The electrochemical redox reaction is carried out generally using platinum or steel electrodes. It can be considered as an environment friendly process with no pollution.[70]

There are many more chemical methods like – chemical vapor synthesis, sono-chemical method, photochemical process etc.

1.5 Synthesis of Nanoparticles by Biological Methods

"When nature finishes to produce its own species, man begins using natural things in harmony with this very nature to create an infinity of species."

–Leonardo da Vinci

Living organisms have diverse metabolic capabilities to synthesize various metabolites and interact with minerals present in the environment. The minerals they use for their growth and metabolism to form protective structures. To do so, these minerals/ions are firstly taken into the cell through various mechanisms and then incorporated into the necessary physiological pathways and biosynthetic structures of the body. The formation of inorganic minerals is termed as bio-mineralization and the mineral formed by organisms are called

bio-minerals. This bio-mineralization is widespread phenomenon found in various groups of organisms including plants, animals and microorganisms.[16,71–73] Some of these organisms are – diatoms, sponges, mollusks, crustaceans, coral forming organisms etc.

The bio-mineralization forms all the level of hierarchical structures from mega structures like the coral reef, to down to nano-meter structures. Coral reefs are elegant example of a mega structure built by colonies of tiny animals found in marine waters. These structures are mostly made of calcium carbonate secreted by coral organisms. The largest coral reef is "The Great Barrier Reef", comprising over 2,900 individual reefs and 900 islands stretching for over 3,48,000 square kilometers of Queensland, Australia.[72,74] In contrast the beautiful color of some butterfly wings, bird's feathers and scales of fishes, are an elegant example of synthesis and patterning of nano-crystals. In order to generate these light effects, the mirrors or filters are arranged in multilayers; with vary in refractive index of alternate layers.[1]

The bio-minerals perform a large number of vital functions required for the survival of an organism. Some of the functions include a protective covering around the body (exoskeleton), provide mechanical strength to body (endoskeleton), resistance to pests and predators, act as buoyancy device, optical receptors in eyes, gravity receptor etc. Some magneto-tactic bacteria, used to synthesize intracellular magnetic nanomaterials, which helps bacterium to move in response to magnetic field (magneto-taxis).[75]

The bio-mineralization process served as a source of inspiration for the nanotechnologist for the biosynthesis of nanoparticles. Although human beings have been using living-organisms especially microorganisms for ages, in the production of cheese, curd, wine, beer, bread etc., but the possibility of using such microorganisms in the

deliberate synthesis of nanoparticles is a relatively new procedure. For this, both the unicellular as well as multicellular organisms have been employed; and the synthesis has been done via both the extracellular as well as intracellular ways. The synthesis of nanoparticles using organisms is broadly categorized as the "biosynthesis". In this method, all genera of organisms have been extensively explored for the synthesis of nanoparticles *viz.* fungi including unicellular yeasts, bacteria, viruses, plants, plant cell extract, animal cells etc. With the advancement of this method, researchers started exploring the use of biological products instead of intact living organisms. Today, a number of methods are available in this category such as protein-mediated synthesis, peptide-mediated synthesis, enzymatic synthesis, DNA/RNA-mediated synthesis, antibiotic-mediated synthesis and so on. Researchers further explored the use of biological materials as a scaffold, for the synthesis of nanoparticles. This method is termed as biomimetic synthesis or bio-template synthesis.

1.5.1 Biosynthesis: Using Biological Resources for the Synthesis of Nanoparticles

The "biosynthesis of nanomaterials" is a generalized term comprises of all kind of biological method of synthesis of nanomaterials. However, this term has long been representing the bottom-up synthesis of nanomaterials, using living organism or their products. It includes animal cells, plant cells, microbes, plant extract etc. as well as their metabolites such as enzymes, proteins, amino acids, nucleic acids etc.[8,76–94]

1.5.2 Biomimetic Synthesis: Imitating Nature for the Synthesis of Nanoparticles

One way of designing materials at the nano-scale level is to mimic natural biomaterials, since nature has been evolving synthesis of such materials for billions of years. In this

approach, biological materials used as a template on which molecules assembled to synthesize nanoparticles.[12,95,96] This approach has used for the synthesis of a vast array of nanomaterials, such as silver nanoparticles,[97] silver nanoplates,[93] α-Fe$_2$O$_3$,[11] SiO$_2$,[98] etc.

1.5.3 Bioleaching: A Means of Synthesis of Nanoparticles

Bioleaching is the process that employs microorganisms for the dissolution of metals from their mineral sources. The microorganism secretes organic acids, metal chelators or complexing agents in the environment, which is responsible for the leaching of metals from mineral ores.[99] The solubilization of metals in this process involves – (a) formation of organic and inorganic acids (proton formation), (b) excretion of complexing agents (ligand formation) and (c) oxidation and reduction reactions.[36] This process is widely used by mining industries for the extraction of metals.

The bioleaching process was used in our lab for the synthesis of silica nanoparticle by bioleaching of sand (Figure 1.4). This is a two-step process involving bioleaching of sand in the form of silicic acid, which is then converted into silica nanoparticles. In this process, the proteins secreted by the fungus *Fusarium oxysporum,* is considered to be responsible for the hydrolysis of silicon to silicic acid, as well as stabilizing and capping agent to form a nanoparticles.[37] This method can be considered as a top-down biological method of synthesis of nanoparticles.
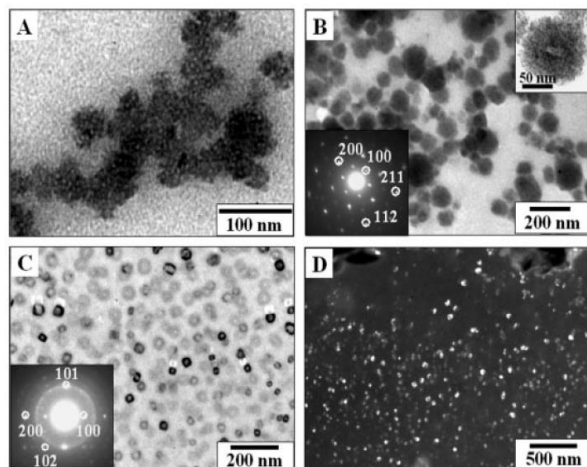
Figure 1.4: TEM image showing silica nanoparticles (NPs) synthesized by exposure of sand to the F. oxysporum, before (A, B) and after calcination (C, D) at 400 ^{o}C for 2 h. The lower insets of images showing SAED pattern of corresponds to respective images.[37]

1.6 Biomilling: Method used in this Thesis

The top-down method for the biological synthesis of nanoparticles developed recently in our group, involved the breakdown of bigger/micron size particles down to few nanometers. To carry out this environment-friendly process, the nature inspired us to harness the microbial capability in order to avoid the use of harmful chemicals. In nature, there are many biological phenomena that directly correlate the mineral utilization in order to sustain the life of living organisms. Such phenomena have been well utilized in weathering of rocks, bioleaching,[100–103] biofouling,[104,105] biofilm formation[101,106] etc. Most of these phenomena start with the physical adhesion of microbes to the surface via van der Waals forces, followed by secretion of enzymes, acidifying compounds and metal chelators that lead to breakdown the materials, in order to extract nutrients. The nutrient conversion in rocks and soil is a quite well known process and has been well studied since

1950s.[102,103] However, this method for the synthesis of nanoparticles is realized merely a decade ago in 2005.[37]

This method is especially important for the synthesis of nanoparticles with size less than 10 nm which otherwise is very challenging with present chemical methods, especially, for complex oxide nanomaterials *viz.* perovskite family of compounds. The synthesis of a type of nanomaterials needs calcination at high temperature. In general, the high temperature leads to the grain growth and agglomeration of nanoparticles with improper crystallinity.[46] Therefore, for such compounds this method would be very useful.

This top-down biological method was first time demonstrated for the synthesis of BiOCl nanoparticles by break-down of thin chemically synthesized nanoplates and termed as "biomilling". For this purpose, an alkalotolerant and thermophilic fungus, *Humicola sp.* (HAA-SHC-2), was isolated from self-heating compost. The biomilling was carried out by the fungal mycelia (20g) suspended in 100 mL of an aqueous suspension of chemically synthesized BiOCl nanoplates (edge lengths 150–200 nm). The reaction was carried out at pH 9 and 50 $^{\circ}$C in dark under constant shaking speed of 200 rpm (Figure 1.5).[46]

Till date, this method has been effectively applied for the synthesis of binary oxides (ZnO,[48] Gd_2O_3,[47]), oxy-hydroxides (α-FeO(OH)[49]) as well as of ternary oxides such as BiOCL,[46] $BaTiO_3$.[107]
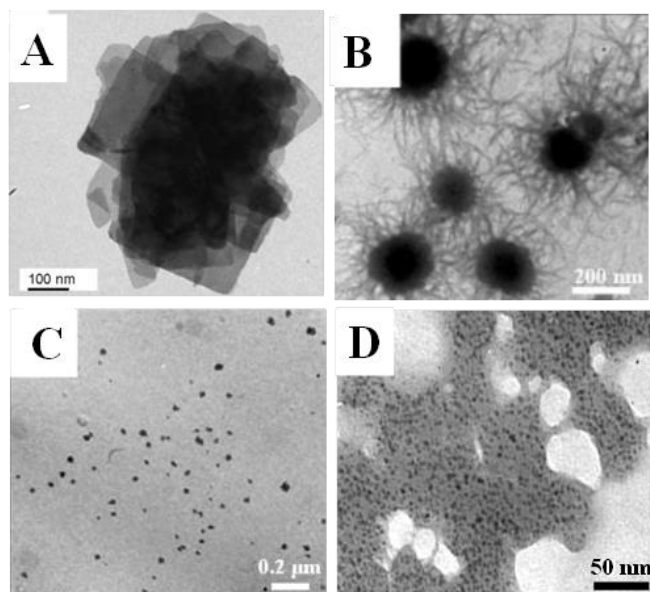
Figure 1.5: *TEM image showing BiOCl nanoparticles synthesized by biomilling of BiOCl nanoplates (A) after biomilling for18 h (B), 48 h (C), and 72 h (D), respectively.*[46]

1.7   The Improvements in Biomilling Method

The biomilling method for the synthesis of nanoparticles is quite a new method as compared to other methods of synthesis of nanoparticles. Being in its infancy, it was facing many challenges (Please see chapter 2 for detail). Therefore, this method needs to be improved in order to gain its popularity and feasibility, for large-scale production of nanoparticles, with minimum efforts. In this thesis, efforts made for the improvement in the method as well as to gain deep understanding about the mechanism of this process.

In this improved method, the material to be biomilled, is kept in a dialysis bag which has a finite pore size, and allows the small biomolecules to pass across the membrane but retains back the microbial cells inside the bag (Figure 1.6). Therefore, the cells are not in the direct contact with the material to be biomilled; however, the secreted biomolecules (proteins) can pass across the membrane and interact with the materials.

After the completion of biomilling, the biomilled nanoparticles remain in the dialysis bag, which eases the recovery of biomilled nanoparticles. Apart from it, this methods has many advantages –

a) Isolate the biomilled NPs with minimum efforts:

    After the biomilling, the biomilled nanoparticles remain confined within the dialysis bag, which after washing with deionized water can be used at it is. By this way, we get biomilled nanoparticles easily separated from the complex mixture of biomass without need of an extra step.

b) Separate the top-down biomilling and bottom-up biosynthesis processes (if the organism itself, has NP synthesis ability by extra/intracellular reduction of free zinc ions to form NPs):

    The ions which have been leached out of the precursor nanorods, could easily have passed out through the pores and get accumulated into the microbial cells. Therefore, the metal ion precursor is not available for the biosynthesis of nanoparticles. It suggests that the nanoparticles obtained in biomilling is due to breakdown of parental rod shaped nanoparticles rather than the biosynthesis of leached out ions.

c) Differentiate the yeast cell involvement in the biomilling process:

    The biomilling were carried out with live cells and dead cells. We observed that the biomilling occur in the presence of the live cells but not dead one.
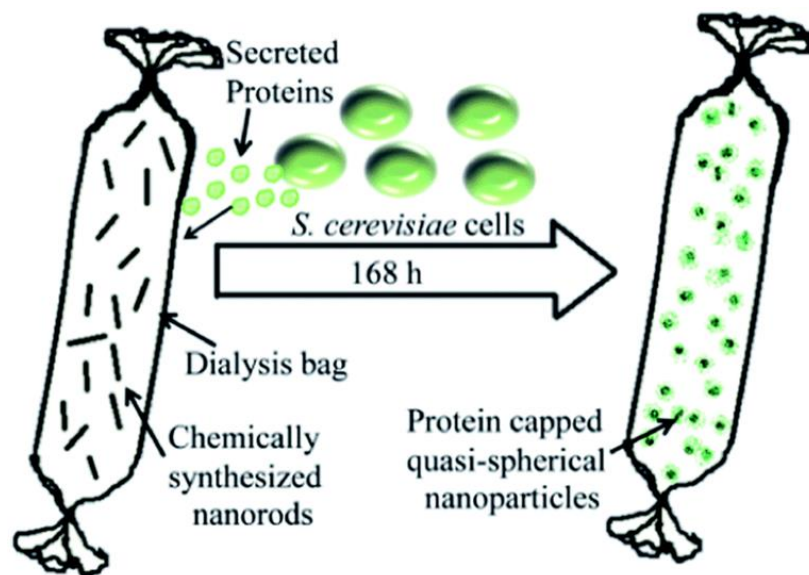
Figure 1.6: The schematic depicting the improved biomilling process.

1.8   The Interaction of Nanomaterials with Living Beings

How the nanomaterials interact with the living systems, has always been of great importance for biomedical applications. A lot of studies have been done on the biocompatibility of nanoparticles.[108–118] The International Union of Pure and Applied Chemistry (IUPAC) defined biocompatibility (biomedical fields) as "ability to be in contact with a living system without producing an adverse effect". It has also defined (biomedical therapy) as "ability of a material to perform an appropriate host response for a specific application".[119]

When a foreign body (antigen) is administrated to a living organism, it provokes the immune response to nullify their pathological effects. The immune response of the body is a complex phenomenon and is greatly differ from one organism to other, even, one cell or tissue type to other. Therefore, the biocompatibility of nanoparticles is the quite an important parameter, in order to use nanomaterials for the biomedical applications.

1.9   The Applications of Nanoparticles

Some of the potential applications emerging out which are based on the nanoparticles are shown in the figure 1.7. Some of these applications of nanoparticles include: biosensors,[120] medical diagnostics,[121] nanomedicine,[122] drug delivery,[113,123,124] cellular and molecular imaging,[125] regulating stem cell behaviour,[126] bio-photonic for sensing,[127] tissue engineering,[128] antifouling agents,[129] catalysis,[130–132] nano-electro-mechanical systems (NEMS) and micro-electro-mechanical (MEMSMEMS),[133–135] optical devices,[136] information storage media,[137] single electron transistors,[138] LEDS,[139] LASERS,[140] environmental safety,[141] self-cleaning coatings[142] and so on.
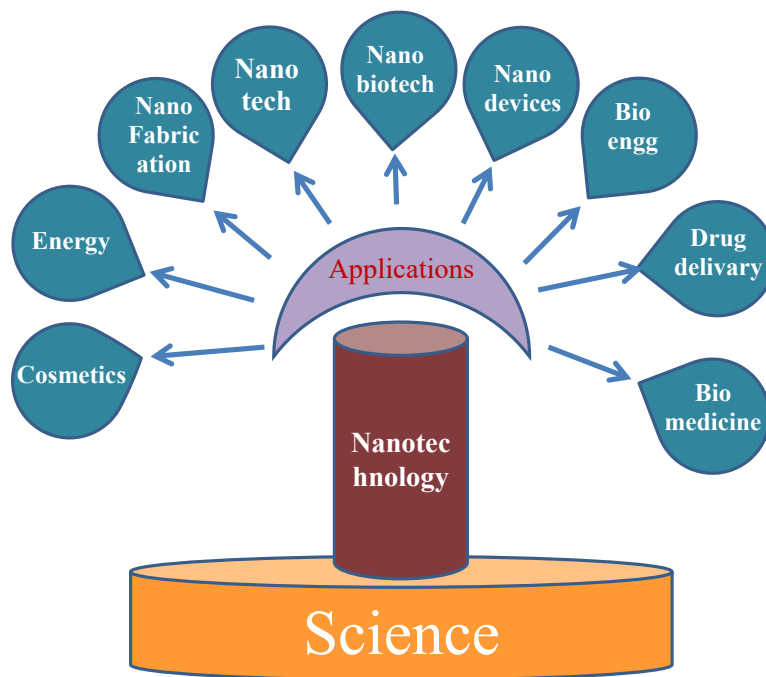
Figure 1.7: *Diagrammatic representation of applications of nanoparticles.*

1.10 Outline of the Thesis

The work involved in this thesis explored the biomilling method for the synthesis of nanomaterials. This method relies on the use of microorganisms for the break-down of micron sized particles into nanoparticles which is an environmental friendly, green top-down approach. In this thesis, the metal oxide and oxy-hydroxide nanoparticles were synthesized. We made efforts to culminate some of the challenges associated with the process and to make better understanding about the mechanistic aspects underlying this process.[46,107]

The first chapter is the general introduction about the thesis. It started with the motivation behind this work. The various methods of synthesis of nanoparticles and the method used in the thesis work (biomilling) have been described. Furthermore we have described the efforts that we made for the improvement of the method.

The second chapter describes the experimental and characterization techniques such as atomic force microscopy (AFM), transmission electron microscopy (TEM), scanning electron microscopy (SEM), UV-visible spectroscopy, fluorescence spectroscopy, X-ray diffraction, energy dispersive analysis of X-rays, inductively coupled plasma-optical emission spectroscopy (ICP-OES), gel electrophoresis. These characterization techniques have been used extensively for the characterization of materials. In this chapter, the working principles, the working modes and other detailed of instruments used in this thesis have been described.

The third chapter describes the biomilling of metal oxide nanorods into small quasi-spherical NPs. Our choice of the material for this study was rod-shaped ZnO nanoparticles. The microorganism chosen for this purpose is a yeast *Saccharomyces cerevisiae*. It is a

unicellular eukaryotic organism. Apart from this, their proteomic and genomic databases are also available. The protein of the used organism forms "corona" around the NPs. As yeasts have been used as probiotic as well as in making of food preparations from ancient times, are proved to be non-cytotoxic for human. The dynamic nature of protein corona and the expression profile of intracellular as well as extracellular proteins of the yeast (microorganism) were investigated. The efforts were made to address some of the challenges associated with the biomilling process: (1) isolate the biomilled NPs with minimum efforts, (2) separate the top-down biomilling and bottom-up biosynthesis processes (if the organism itself, has NP synthesis ability by extra/intracellular reduction of free zinc ions to form NPs), and (3) differentiate the yeast cell involvement in the biomilling process.

The fourth chapter describes the biomilling of metal oxy-hydroxide nanoparticles. The α-FeO(OH) nanorods were chosen as a model system because α-FeO(OH) is abundant, eco-friendly and non-toxic toward the living organism. The rod-shaped α-FeO(OH) particles were synthesized by chemical route, and biomilled into nanoparticles below 10 nm size using *S. cerevisiae*. The special emphasis has given to develop the understanding about the mechanistic aspects of biomilling using a combination of techniques such as UV-vis, FTIR, AFM, and XPS.

The fifth chapter describes the conclusions and future perspective of the work described in this thesis.

1.11   References

1   C. Brechignac, P. Houdy and M. Lahmani, *Nanomaterials and Nanochemistry*, Springer-Verlag Berlin Heidelberg, 2007.

2   S. Zhang, *Mater. Today*, 2003, **6**, 20–27.

3   M. Gericke and a. Pinches, *Hydrometallurgy*, 2006, **83**, 132–140.

4   H. Korbekandi, S. Iravani and S. Abbasi, *Crit. Rev. Biotechnol.*, 2009, **29**, 279–306.

5   T. Klaus-Joerger, R. Joerger, E. Olsson and C. Granqvist, *Trends Biotechnol.*, 2001, **19**, 15–20.

6   D. Mandal, M. E. Bolander, D. Mukhopadhyay, G. Sarkar and P. Mukherjee, *Appl. Microbiol. Biotechnol.*, 2006, **69**, 485–492.

7   A. Bharde, A. Wani, Y. Shouche, P. A. Joy, B. L. V Prasad and M. Sastry, *J. Am. Chem. Soc.*, 2005, **127**, 9326–9327.

8   R. Y. Sweeney, C. Mao, X. Gao, J. L. Burt, A. M. Belcher, G. Georgiou and B. L. Iverson, *Chem. Biol.*, 2004, **11**, 1553–1559.

9   R. Ramanathan, A. P. O. Mullane, R. Y. Parikh, P. M. Smooker, K. Suresh, A. P. O'Mullane, R. Y. Parikh, P. M. Smooker, S. K. Bhargava and V. Bansal, *Langmuir*, 2011, **27**, 714–9.

10   J. H. Lee, M. G. Kim, B. Yoo, N. V Myung, J. Maeng, T. Lee, A. C. Dohnalkova, J. K. Fredrickson, M. J. Sadowsky and H.-G. Hur, *Proc. Natl. Acad. Sci.*, 2007, **104**, 20410–20415.

11   M. T. Klem, M. Young and T. Douglas, *J. Mater. Chem.*, 2010, **20**, 65–67.

12   C. Tamerler and M. Sarikaya, *Acta Biomater.*, 2007, **3**, 289–299.

13   C. Reuther, L. Hajdo, R. Tucker, A. A. Kasprzak and S. Diez, *Nano Lett.*, 2006, **6**, 2177–2183.

14   A. Arakaki, K. Shimizu, M. Oda, T. Sakamoto, T. Nishimura and T. Kato, *Org. Biomol. Chem.*, 2015, **13**, 974–89.

15   J. Miot, N. Recham, D. Larcher, F. Guyot, J. Brest and J.-M. Tarascon, *Energy Environ. Sci.*, 2014, **7**, 451–460.

16   K. Naka, *Biomineralization I*, Springer Berlin Heidelberg, 2007, vol. 270.

17   Y. Cai and R. Tang, *J. Mater. Chem.*, 2008, **18**, 3775–3787.

18   G. Canizal, P. S. Schabes-Retchkiman, U. Pal, H. B. Liu and J. a. Ascencio, *Mater. Chem. Phys.*, 2006, **97**, 321–329.

19   F. Mouxing, L. Qingbiao, S. Daohua, L. Yinghua, H. Ning, DENG. Xu, W. Huixuan and H. Jiale, *Chinese J. Chem. Eng.*, 2006, **14**, 114–117.

20   J. Huang, L. Lin, D. Sun, H. Chen, D. Yang and Q. Li, *Chem. Soc. Rev.*, 2015, **44**, 6330–6374.

21   A. Sanyal, D. Rautaray, V. Bansal, A. Ahmad and M. Sastry, *Langmuir*, 2005, **21**, 7220–7224.

22   S. Singh, U. M. Bhatta, P. V Satyam, A. Dhawan, M. Sastry and B. L. V Prasad, *J. Mater. Chem.*, 2008, **18**, 2601–2606.

23   A. Ahmad, P. Mukherjee, D. Mandal, S. Senapati, M. I. Khan, R. Kumar and M.

Sastry, *J. Am. Chem. Soc.*, 2002, **124**, 12108–12109.

24   N. Durán, P. D. Marcato, O. L. Alves, G. I. De Souza and E. Esposito, *J. Nanobiotechnology*, 2005, **3**, 1–8.

25   C. E. Flynn, S.-W. Lee, B. R. Peelle and A. M. Belcher, *Acta Mater.*, 2003, **51**, 5867–5880.

26   S. Balci, K. Noda, A. M. Bittner, A. Kadri, C. Wege, H. Jeske and K. Kern, *Angew. Chemie - Int. Ed.*, 2007, **46**, 3149–3151.

27   G. R. Salunke, S. Ghosh, R. J. Santosh Kumar, S. Khade, P. Vashisth, T. Kale, S. Chopade, V. Pruthi, G. Kundu, J. R. Bellare and B. A. Chopade, *Int. J. Nanomedicine*, 2014, **9**, 2635–53.

28   D. K. Singh, R. Jagannathan, P. Khandelwal, P. M. Abraham and P. Poddar, *Nanoscale*, 2013, **5**, 1882–1893.

29   R. Jagannathan, P. Poddar and A. Prabhune, *J. Phys. Chem. C*, 2007, **111**, 6933–6938.

30   U. Kumar, A. K. Ranjan, C. Sharan, A. A. Hardikar, A. Pundle and P. Poddar, *Curr. Nanosci.*, 2012, **8**, 130–140.

31   R. Das, R. Jagannathan, C. Sharan, U. Kumar and P. Poddar, *J. Phys. Chem. C*, 2009, **113**, 21493–21500.

32   S. S. Behrens, *J. Mater. Chem.*, 2008, **18**, 3788–3798.

33   L. Berti and G. a Burley, *Nat. Nanotechnol.*, 2008, **3**, 81–87.

34   C. Calvaruso, M. P. Turpault and P. Frey-Klett, *Appl. Environ. Microbiol.*, 2006, **72**, 1258–1266.

35   N. P. Rosenstock, *Fungal Biol. Rev.*, 2009, **23**, 107–114.

36   D. Mishra, D. Kim, J. Ahn and Y. Rhee, *Met. Mater. Int.*, 2005, **11**, 249–256.

37   V. Bansal, A. Sanyal, D. Rautaray, A. Ahmad, M. Sastry, B. V. Bansal, A. Sanyal, V. Bansal and A. Sanyal, *Adv. Mater.*, 2005, **17**, 889–892.

38   R. Landeweert, E. Hoffland, R. D. Finlay, T. W. Kuyper and N. Van Breemen, *Trends Ecol. Evol.*, 2001, **16**, 248–254.

39   P. Avouris, *Acc. Chem. Res.*, 1995, **28**, 95–102.

40   R. Baron, B. Willner and I. Willner, *Chem. Commun.*, 2007, **4**, 323–332.

41   D. S. Goodsell, *Bionanotechnology: lessons from nature*, John Wiley & Sons, Inc., 2004.

42   Y. Xia, J. a. Rogers, K. E. Paul and G. M. Whitesides, *Chem. Rev.*, 1999, **99**, 1823–1848.

43   A. Piednoir, E. Perrot, S. Granjeaud, A. Humbert, C. Chapon and C. R. Henry, *Surf. Sci.*, 1997, **391**, 19–26.

44   N. Salah, S. S. Habib, Z. H. Khan, A. Memic, A. Ajam, E. Alarfaj, N. Zahed and S. Al-Hamedi, *Int. J. Nanomedicine*, 2011, **6**, 863–869.

45   P. V. Kazakevich, A. V. Simakin, V. V. Voronov and G. A. Shafeev, *Appl. Surf. Sci.*, 2006, **252**, 4373–4380.

46   B. Mazumder, I. Uddin, S. Khan, V. Ravi, K. Selvraj, P. Poddar and A. Ahmad, *J. Mater. Chem.*, 2007, **17**, 3910–3914.

47   I. Uddin, P. Poddar, U. Kumar and N. Phogat, *J. Green Sci. Technol.*, 2013, **1**, 48–53.

48   C. Sharan, P. Khandelwal and P. Poddar, *RSC Adv.*, 2015, **5**, 1883–1889.

49   C. Sharan, P. Khandelwal and P. Poddar, *RSC Adv.*, 2015, **5**, 91785–91794.

50   Y. Chen, J. Fitz Gerald, J. S. Williams and S. Bulcock, *Chem. Phys. Lett.*, 1999, **299**, 260–264.

51   C. Yieng, J. F. Gerald, L. T. Chadderton and L. Chaffron, *J. Metastable Nanocrystalline Mater.*, 1999, **2-6**, 375–380.

52   L. P. The, *New Phys. Sae Mulli*, 2012, **62**, 483–487.

53   S. Bid, A. Banerjee, S. Kumar, S. K. Pradhan, U. De and D. Banerjee, *J. Alloys Compd.*, 2001, **326**, 292–297.

54   Y. Chen, C. P. Li, H. Chen and Y. Chen, *Sci. Technol. Adv. Mater.*, 2006, **7**, 839–846.

55   J. B. Mooney and S. B. Raddubg, *Annu. Rev. Mater. Sci.*, 1982, **12**, 81–101.

56   S. A. Studenikin, N. Golego and M. Cocivera, *J. Appl. Phys.*, 1998, **83**, 2104–2111.

57   T. Xia, M. Kovochich, M. Liong, L. Ma, B. Gilbert, Ḱ. H. Shi, J. I. Yeh, J. I. Zink and A. E. Nel, *ACS Nano*, 2008, **2**, 2121–2134.

58   C. N. R. Rao, A. Govindaraj, G. Gundiah and S. R. C. Vivekchand, in *The*

Chemistry of Nanomaterials: Synthesis, Properties and Applications, 2004, vol. 59, pp. 4665–4671.

59   S. Sadhu, A. Jaiswal, S. Adyanthaya and P. Poddar, *RSC Adv.*, 2013, **3**, 1933–1940.

60   T. Tsuji, K. Iryo, N. Watanabe and M. Tsuji, *Appl. Surf. Sci.*, 2002, **202**, 80–85.

61   M. A. Gondal, Q. A. Drmosh, Z. H. Yamani and T. A. Saleh, *Appl. Surf. Sci.*, 2009, **256**, 298–304.

62   X. Hu, H. Gong, Y. Wang, Q. Chen, J. Zhang, S. Zheng, S. Yang and B. Cao, *J. Mater. Chem.*, 2012, **22**, 15947–15952.

63   J. D. Batteas and J. C. Garno, in *Applied Scanning Probe Methods*, 2006, vol. B. Bhushan, pp. 105–136.

64   A. K. Raychaudhuri, in *The Chemistry of Nanomaterials: Synthesis, Properties and Applications*, 2004, vol. 2, pp. 688–723.

65   M. Mohapatra and S. Anand, *Int. J. Eng. Sci. Technol.*, 2010, **2**, 127–146.

66   S. Talam, S. R. Karumuri and N. Gunnam, *ISRN Nanotechnol.*, 2012, **2012**, 1–6.

67   J. Wang and L. Gao, *J. Mater. Chem.*, 2003, **13**, 2551–2554.

68   J. A. Rodriguez and M. Fernandez-Garcia, *Synthesis, Properties and Applcations of Oxide Nanomaterials*, Wiley-interscienc; A John Wiley & Sons, Inc., 2007.

69   Y. Ni, S. Yang, J. Hong and P. Zhen, *Scr. Mater.*, 2008, **59**, 127–130.

70   Á. Llavona, A. Prados, V. Velasco, P. Crespo, M. C. Sánchez and L. Pérez, *CrystEngComm*, 2013, **15**, 4905–4909.

71   A. Schulz, H. Wang, P. van Rijn and A. Böker, *J. Mater. Chem.*, 2011, **21**, 18903–18918.

72   Great barrier Reef Marine Park Authority Annual Report 2014-15, 2015, 1–230.

73   K. Simkiss and K. Wilbur, *Biomineralization*, Academic Press New York, 1989.

74   Australian government department of Environment, .

75   D. Faivre and D. Schüler, *Chem. Rev.*, 2008, **108**, 4875–4898.

76   N. Kroger, R. Deutzmann, C. Bergsdorf and M. Sumper, *Proc. Natl. Acad. Sci.*, 2000, **97**, 14133–14138.

77   X. Li, H. Xu, Z.-S. Chen and G. Chen, *J. Nanomater.*, 2011, **2011**, 1–16.

78   L. Wen, Z. Lin, P. Gu, J. Zhou, B. Yao, G. Chen and J. Fu, *J. Nanoparticle Res.*, 2009, **11**, 279–288.

79   S. A. Kumar, A. A. Ansary, A. Ahmad and M. I. Khan, *J. Biomed. Nanotechnol.*, 2007, **3**, 190–194.

80   L. Du, H. Jiang, X. Liu and E. Wang, *Electrochem. commun.*, 2007, **9**, 1165–1170.

81   A. Ahmad, S. Senapati, M. I. Khan, R. Kumar and M. Sastry, *Langmuir*, 2003, **19**, 3550–3553.

82   R. Herrera-Becerra, C. Zorrilla and J. A. Ascencio, *J. Phys. Chem. C*, 2007, **111**, 16147–16153.

83   S. S. Shankar, A. Ahmad and M. Sastry, *Biotechnol. Prog.*, 2003, **19**, 1627–1631.

84   M. Sastry, A. Ahmad, M. I. Khan and R. Kumar, *Curr. Sci.*, 2003, **85**, 162–170.

85   S. He, Z. Guo, Y. Zhang, S. Zhang, J. Wang and N. Gu, *Mater. Lett.*, 2007, **61**, 3984–3987.

86   S. Senapati, A. Ahmad, M. I. Khan, M. Sastry and R. Kumar, *Small*, 2005, **1**, 517–520.

87   V. Bansal, D. Rautaray, A. Bharde, K. Ahire, A. Sanyal, A. Ahmad and M. Sastry, *J. Mater. Chem.*, 2005, **15**, 2583–2589.

88   L. F. A. Raj and J. E, *Orient. J. Chem.*, 2015, **31**, 51–56.

89   A. Syed and A. Ahmad, *Colloids Surfaces B Biointerfaces*, 2012, **97**, 27–31.

90   P. Mohanpuria, N. K. Rana and S. K. Yadav, *J. Nanoparticle Res.*, 2008, **10**, 507–517.

91   P. Mukherjee, A. Ahmad, D. Mandal, S. Senapati, S. R. Sainkar, M. I. Khan, R. Parishcha, P. V Ajaykumar, M. Alam, R. Kumar and M. Sastry, *Nano Lett.*, 2001, **1**, 515–519.

92   S. Singh, V. D'Britto, A. Bharde, M. Sastry, A. Dhawan and B. L. V. Prasad, *Int. J. Green Nanotechnol. Phys. Chem.*, 2010, **2**, 80–99.

93   J. Xie, J. Y. Lee, D. I. C. Wang and Y. P. Ting, *ACS Nano*, 2007, **1**, 429–439.

94   R. G. Haverkamp, A. T. Marshall and D. van Agterveld, *J. Nanoparticle Res.*, 2007, **9**, 697–700.

95   M. Sarikaya, *Proc. Natl. Acad. Sci.*, 1999, **96**, 14183–14185.

96   C. Tamerler and M. Sarikaya, *Philos. Trans. A. Math. Phys. Eng. Sci.*, 2009, **367**,

1705–1726.

97   R. R. Naik, S. J. Stringer, G. Agarwal, S. E. Jones and M. O. Stone, *Nat. Mater.*, 2002, **1**, 169–72.

98   C. Gautier, R. Courson, P. J. Lopez, J. Livage and T. Coradin, *MRS Proc.*, 2007, **1008**, 1008–T01–04.

99   K. Bosecker, *FEMS Microbiol. Rev.*, 1997, **20**, 591–604.

100   T. Rohwerder, T. Gehrke, K. Kinzler and W. Sand, *Appl. Microbiol. Biotechnol.*, 2003, **63**, 239–48.

101   G. Curutchet, E. Donati, C. Oliver, C. Pogliani and M. R. Viera, *Methods Enzymol.*, 1999, **337**, 171–186.

102   L. Arrieta and R. Grez, *Appl. Microbiol.*, 1971, **22**, 487–490.

103   R. B. Duff, D. M. Webley and R. O. Scott, *Soil Sci.*, 1963, **95**, 105–114.

104   G. D. Bixler and B. Bhushan, *Philos. Trans. R. Soc. A Math. Phys. Eng. Sci.*, 2012, **370**, 2381–2417.

105   M. E. Callow and J. A. Callow, *Marine biofouling: a sticky problem*, 2002, vol. 49.

106   R. M. Donlan, *Emerg. Infect. Dis.*, 2002, **8**, 881–890.

107   I. Uddin, A. Jaiswal and P. Poddar, *Int. J. Innov. Biol. Reaserch*, 2013, **2**, 1–5.

108   W. Wu, Q. He and C. Jiang, *Nanoscale Res. Lett.*, 2008, **3**, 397–415.

109   Y. Mei, A. Kumar, W. Gao, R. Gross, S. B. Kennedy, N. R. Washburn, E. J. Amis and J. T. Elliott, *Biomaterials*, 2004, **25**, 4195–201.

110   Y. Kong, C. Bae, S. Lee, H.-W. Kim and H. Kim, *Biomaterials*, 2005, **26**, 509–517.

111   J. Selvakumaran, M. P. Hughes, J. L. Keddie and D. J. Ewins, in *2nd Annual International IEEE-EMBS Special tpoic Conference on Microtechnologies in Medicine & Biology*, 2002, pp. 261–264.

112   M. M. Van Schooneveld, E. Vucic, R. Koole, Y. Zhou, J. Stocks, D. P. Cormode, C. Y. Tang, R. E. Gordon, K. Nicolay, A. Meijerink, Z. A. Fayad and W. J. M. Mulder, *Nano Lett.*, 2008, **8**, 2517–2525.

113   K. C.-W. Wu, Y. Yamauchi, C. Hong, Y. Yang, Y. Liang, T. Funatsu and M. Tsunoda, *Chem. Commun. (Camb).*, 2011, **47**, 5232–4.

114   E. Casals, T. Pfaller, A. Duschl, G. J. Oostingh and V. Puntes, *ACS Nano*, 2010, **4**, 3623–3632.

115   A. K. Gupta and M. Gupta, *Biomaterials*, 2005, **26**, 3995–4021.

116   K. Vallières, P. Chevallier, C. Sarra-Bournet, S. Turgeon and G. Laroche, *Langmuir*, 2007, **23**, 9745–9751.

117   N. Lee and T. Hyeon, *Chem. Soc. Rev.*, 2012, **41**, 2575–2589.

118   C. Ding, A. Zhu and Y. Tian, *Acc. Chem. Res.*, 2014, **47**, 20–30.

119   M. Vert, Y. Doi, K.-H. Hellwich, M. Hess, P. Hodge, P. Kubisa, M. Rinaudo and F. Schué, *Pure Appl. Chem.*, 2012, **84**, 377–410.

120   K. Besteman, J. Lee, F. G. M. Wiertz, H. A. Heering and C. Dekker, *Nano Lett.*, 2003, **3**, 727–730.

121 A. M. Smith, S. Dave, S. Nie, L. True and X. Gao, *Expert Rev. Mol. Diagn.*, 2006, **6**, 231–244.

122 S. Logothetidis, *Nanomedicine and Nanobiotechnology*, Springer Berlin Heidelberg, Berlin, Heidelberg, 2012.

123 J. W. Rasmussen, E. Martinez, P. Louka and D. G. Wingett, *Expert Opin. Drug Deliv.*, 2010, **7**, 1063–77.

124 K. D. Wani, B. S. Kadu, P. Mansara, P. Gupta, A. V. Deore, R. C. Chikate, P. Poddar, S. D. Dhole and R. Kaul-Ghanekar, *PLoS One*, 2014, **9**, e107315.

125 A. Ito, M. Shinkai, H. Honda and T. Kobayashi, *J. Biosci. Bioeng.*, 2005, **100**, 1–11.

126 K.-C. Wu, C.-L. Tseng, C.-C. Wu, F.-C. Kao, Y.-K. Tu, E. C So and Y.-K. Wang, *Sci. Technol. Adv. Mater.*, 2013, **14**, 1–11.

127 J. L. West and N. J. Halas, *Annu. Rev. Biomed. Eng.*, 2003, **5**, 285–292.

128 G. Ciardelli, in *Applied Scanning Probe Methods X*, 2008, vol. 10, pp. 257–283.

129 M. Zanoni, O. Habimana, J. Amadio and E. Casey, *Biotechnol. Bioeng.*, 2016, **113**, 501–512.

130 W. Weiss and W. Ranke, *Prog. Surf. Sci.*, 2002, **70**, 1–151.

131 J. F. Hamilton and R. C. Baetzold, *Science*, 1979, **205**, 1213–1220.

132 P. Mukherjee, C. Ranjan Patra, R. Kumar and M. Sastry, *Phys. Chem. comm.*, 2001, **4**, 1–2.

133 M. Kandpal, C. Sharan, P. Poddar, K. Prashanthi, P. R. Apte and V. Ramgopal Rao,

Appl. Phys. Lett., 2012, **101**, 104102.

134   M. Kandpal, C. Sharan, V. Palaparthy, N. Tiwari, P. Poddar and V. R. Rao, *RSC Adv.*, 2015, **5**, 85741–85747.

135   C. P. Wong, K.-S. Moon and Y. Li, *Nano-Bio-Electronic, Photonic and MEMS Packaging*, Springer Science + Business Media LLC, Boston, MA, 2010.

136   M. Willander, L. L. Yang, A. Wadeasa, S. U. Ali, M. H. Asif, Q. X. Zhao and O. Nur, *J. Mater. Chem.*, 2009, **19**, 1006–1018.

137   M. Cavallini, J. Gomez-Segura, D. Ruiz-Molina, M. Massi, C. Albonetti, C. Rovira, J. Veciana and F. Biscarini, *Angew. Chemie - Int. Ed.*, 2005, **44**, 888–892.

138   C. Thelander, T. Mårtensson, M. T. Björk, B. J. Ohlsson, M. W. Larsson, L. R. Wallenberg and L. Samuelson, *Appl. Phys. Lett.*, 2003, **83**, 2052–2054.

139   M. Willander, O. Nur, S. Zaman, A. Zainelabdin, N. Bano and I. Hussain, *J. Phys. D. Appl. Phys.*, 2011, **44**, 224017.

140   Q. Li, J. B. Wright, W. W. Chow, T. S. Luk, I. Brener, L. F. Lester and G. T. Wang, *Opt. Express*, 2012, **20**, 17873.

141   P. P. Simeonova, N. Opopol and M. I. Luster, in *NATO Science for Peace and Security Series*, Springer, 2007, pp. 1–276.

142   V. A. Ganesh, H. K. Raut, A. S. Nair and S. Ramakrishna, *J. Mater. Chem.*, 2011, **21**, 16304.

Chapter II

Characterization Techniques

This chapter describes the basics and working principles of different techniques used in this thesis for the characterization of materials.

2.1   Introduction

"The most important discoveries of the laws, methods and progress of nature have nearly always sprung from the examination of the smallest objects which she contains."

Jean Baptiste Pierre Antoine Monet de Lamarck

(French naturalist, 1744–1829)

Materials science deals with the structure, the properties, and the interactions in systems composed of atoms and molecules. Detailed state-of-the-art calculations covering only a few dozen atoms are at the other end of the precision range, dealing with the minute interactions between single atoms.[1] In order to get the insight of these interactions and measurement of properties of materials, different characterization techniques have been used, and are presented in this chapter. While pursuing the work, a range of techniques including atomic force microscopy (AFM), transmission electron microscopy (TEM), UV-visible spectroscopy, fluorescence spectroscopy, Fourier transformed infra-red (FTIR) spectroscopy, X-ray diffraction (XRD), energy dispersive analysis of X-rays (XPS), Dynamic light scattering (DLS), inductively coupled plasma-optical emission spectroscopy (ICP-OES), thermogravimetric analysis (TGA), polyacrylamide gel electrophoresis (PAGE) were used. This chapter briefly explains the basic principles, some relevant information of instrument and their use in the characterization of materials.

2.2   Atomic Force Microscopy (AFM)

An AFM is a high resolution microscope, which is a type of scanning probe microscope (SPM). The SPM has demonstrated the resolution down to the atomic (angstrom) level. The SPM includes STM, AFM, MFM, EFM, PFM, kPFM, Stylus profiler and scanning near field optical microscopy (SNOM) techniques which is also known as near field

scanning optical microscopy (NSOM) etc. In SPM, a physical probe raster scans over the sample surface in order to construct an image. During the raster scan the interactions (force or current gradient) between probe and sample is monitored. The quantitative interaction at each data points are plotted, in the form of a three–dimensional image. Although these instruments have been primarily meant for imaging, these have been widely used for the quantitative measurements of the various physical and chemical interactions occurring at the surfaces.

The first SPM invented was the scanning tunneling microscope (STM) which was developed at the IBM research laboratory in Zurich by Gerd Binnig and Heinrich Rohrer in 1982. For this superb invention, they shared the Nobel Prize for physics in 1986.[2] The STM works by monitoring the tunneling current at each points of the path on which the probe moves over the sample surface. The most rewarding feature of this instrument is its capability of providing up to atomic resolution. Unfortunately, there is a drawback that STM can only be used for conductive or semi-conductive samples; which greatly limits the applicability of this instrument.

In order to extend the use of SPM for non-conductive samples, few years later AFM has been discovered by Binnig and Rohrer in 1986. It uses a very sharp tip (with diameter few nanometer) attached at the end of a cantilever having very low spring constant (0.005–50 N/m). Similar to STM, the AFM probe also raster scan over the surface, either in continuous or intermittently in touch with the sample typically at constant force. Binnig et al. (1986) estimated the interatomic forces between AFM probe and sample, by considering the binding energy of ionic bonds, van der Waals bonds, and those of reconstructed surfaces. The energies of these bonds are in the order of 10 eV, 10 meV,

and 1 meV, respectively (1 eV = 1.6 x 10^{-19} J). For distances on the order of 0.16 Å, the calculated respective forces are 10^{-7} N, 10^{-11} N, 10^{-12} N respectively. They considered mechanical "springs", composed of levers with their associated tips, that have a mass of 10^{-10} kg and a resonance frequency of 2 kHz, corresponding to a spring constant k = 0.016 N/m small as 10^{-4} Å, the associated forces acting on the lever will be 1.6 x 10^{-16} N.[3] Under the influence of these vanishingly small forces, the probe moves overt the surface and gives topography information of the sample.

The interaction force between tip and sample leads to the bending of cantilever, which in turn deviate the laser light falling over the cantilever to the quadrupled detector. This detector consists of four sensors, one at each quadrant. The differential intensity of light falling on upper two detectors with respect to lower two, gives the vertical deflection signal. Whereas, the differential intensity of light falling on left two detector with respect to right two, gives the lateral deflection signal. These differential vertical signal is used to provide the feedback signal to the scanner, in order to keep the sample at constant distance with the probe or at under constant forces between the two. These signals are also used to generate images of *i.e.* the 3D map of vertical or lateral force or heights.

With this technique various physical and mechanical properties of the samples can also be determined for example magnetic measurement,[4] electric force measurement, piezoresponse force measurement,[5] elasticity measurement,[6] adhesive force measurement[7–11] chemical force measurement,[12,13] capillary force measurement[14] and so on. This technique has also been widely applied for the study of biological specimens, for example study of biomolecules[15], single cell spectroscopy,[16,17] force measurement,[16] elasticity

measurement,[6,18,19] enzyme-ligand interactions,[20] protein-DNA interaction,[21,22] drug membrane interaction,[23] cancer cell detection[24–27] etc.

To extend the applicability of AFM for different kind of samples, various modes have been developed. Some of these modes are- **(A) Contact mode AFM:** To measures topography of a sample, the AFM probe moves in contact with the sample. The topography image obtained from the deflection of the cantilever. In this mode the probe is in constant touch with the sample which can damage the sample, hence oscillating (tapping and non-contact) modes have been developed.[28] **(B) Tapping Mode AFM:** To measures topography of a surface, probe oscillates in with periodically in contact with the sample. The change of the vibration amplitude or phase of the oscillating cantilever used to build the topography image of sample.[29–31] **(C) Non-Contact mode:** Probing tip is not in contact with the sample surface, and surface structure is obtained from the change of the vibration amplitude or resonant frequency of the oscillating cantilever.[32,33] **(D) Phase Imaging:** In oscillating modes (also called dynamic mode) the probe oscillates near resonance frequency of cantilever. When the vibration amplitude of the oscillating cantilever is held constant, the phase shifts occur, due to attractive or repulsive forces acting between probe and sample. The shift data is used to build a phase map of material, which depicts the elasticity of materials.[34–36] **(E) Electric Force Microscope (EFM):** To measures electric field gradient distribution above sample surfaces.[37] **(F) Magnetic Force Microscope (MFM):** To measures magnetic domain arrangements in a magnetic sample surface.[4,38] **(G) Piezorespose Force Microscopy (PFM):** To measures piezoelectric properties and d_{33} coefficient of a material.[5,39–41] **(H) Lithography:** Unlike imaging, this mode is used to mechanically etch or indent a sample surface to make a pattern. This mode can also be

used to arrange the atoms or molecules in a predefined pattern on a samples.[42–45] A schematic representation of working principle and some of the modes scanning probe are shown in figure 2.1.
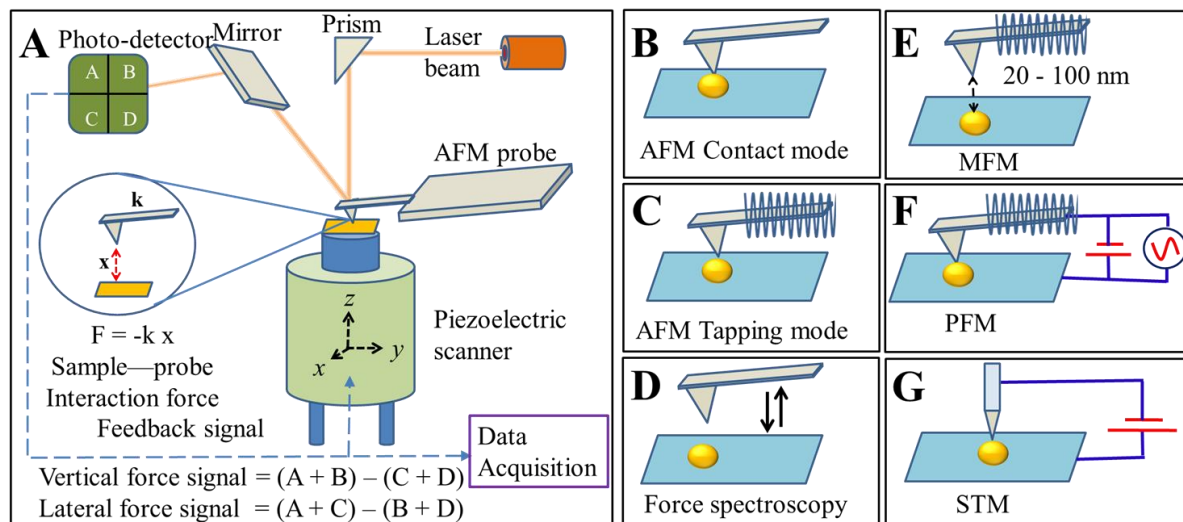
Figure 2.1: *Schematic of scanning probe microscope showing various components (A) and s working modes (B, C, D, E, F, and G).*

The AFM images presented in the thesis, were carried our using a Multimode scanning probe microscope equipped with a Nanoscope IV controller from Veeco Instrument Inc., Santa Barbara, CA. The samples generally prepared on cleaned silicon-wafer or freshly cleaved mica, and dried under nitrogen gas. The measurements were performed at ambient conditions.

2.3 Transmission Electron Microscopy (TEM)

The TEM is firstly developed by Ernst Ruska in Berlin (1931). In a TEM, the electrons transmit through a thin specimen and are detected by detector. With TEM (resolution 0.2 nm), it is even possible to image individual atomic planes or columns of atoms.

In principle the electron microscope (EM) is similar to the optical microscope, except instead of visible light EM uses a beam of electrons as a source of illumination. The resolution of the microscope is greatly limited by the diffraction at the objective lens. In order to visualize an object clearly, the resolution of image should be high.

The resolution can be defined as minimum distance between two objects that reveals them as separate entities. Smaller δ will have higher the resolution. Abbe and Rayleigh independently showed that resolution depends on the wavelength of the illumination source and is given by the **Abbe equation**.[46] It states that the smallest distance that can be resolved (δ) is given by–

$$\delta = \frac{0.61\lambda}{\mu \sin \beta}$$

where, λ is the wavelength of source of illumination, μ is the refractive index of viewing medium, β is defined as semi angle of collection of radiation by lens i.e. (1/2) of the cone of light entering, an objective lens. The '$\mu\sin\beta$' is referred to as the numerical aperture (NA) of an objective lens. For simplicity, the numerical aperture can be considered as unity.

In 19th century, Rayleigh defined that, the resolution is limited by the diffraction of light. According to his postulate, the two point sources can only be considered as resolved, if the diffraction maxima of one source point overlap with the first diffraction minima of second source point. In this condition, the two sources can be said to be just resolved, and distance more than this can be is said to be resolved.[47] The Rayleigh criteria, is demonstrated by in figure 2.2. The airy disks patterns and their respective intensity of light

distribution demonstrate the resolved (A, a), just resolved (B, b) and un-resolved (C, c) conditions.
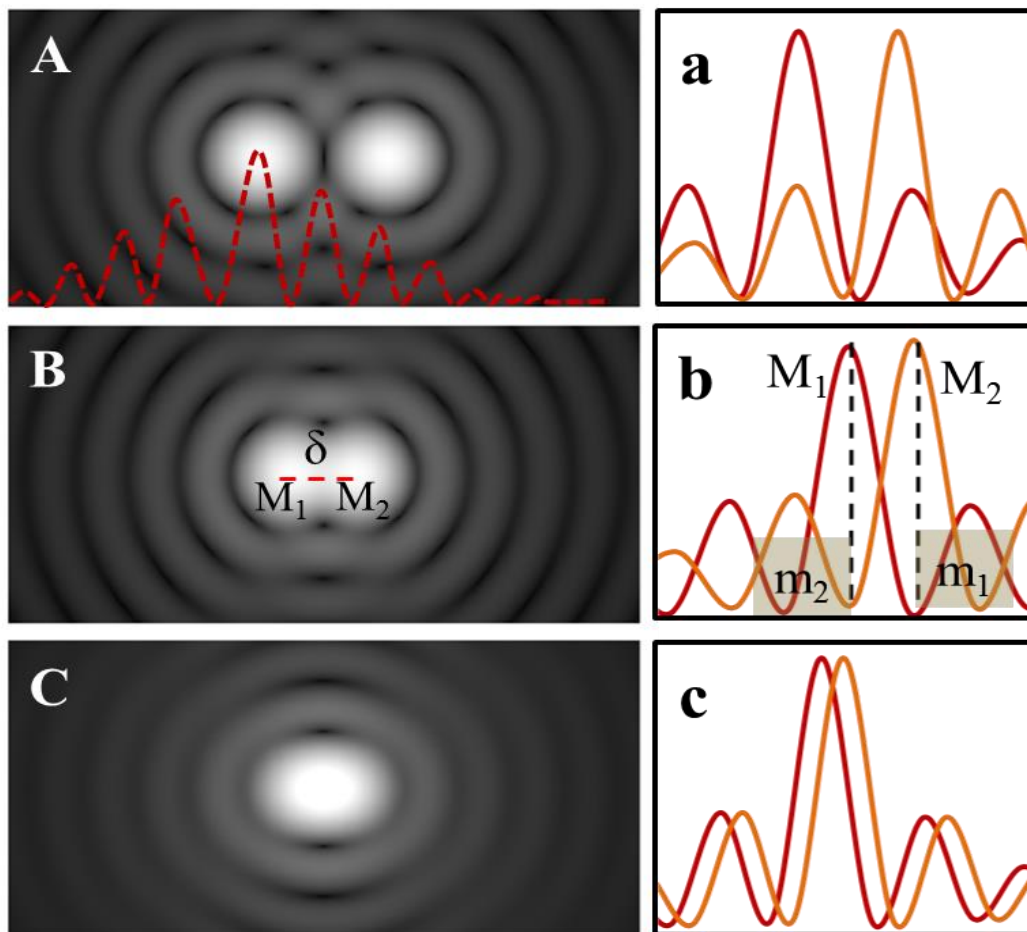
Figure 2.2: *Schematic of Rayleigh criteria, showing resolution in terms of airy disks patterns.*

However, there are some microscopes which could overcame the Abbe's limit of resolution, such as scanning near field optical microscopy (SNOM),[48] scanning holography microscopy,[49] the structured illumination microscopy (SIM), point localization techniques including photo activated localization microscopy (PALM), and stochastic optical reconstruction microscopy (STORM). As the wavelength of an electron beam can be up to

100,000 times shorter than that of visible light photons. At accelerating potential to 50 kV, the wavelength of electron beam is about 5 pm (0.005 nm), so a TEM can achieve better than 50 pm resolution.[50] and useful magnifications of up to about 10,000,000x whereas most light microscopes are limited by diffraction to about 200 nm resolution and useful magnification up to 2000x. Therefore, the electron microscope has a much higher resolving power than that of a light microscope and can reveal the structure of far smaller objects. As electron beam strikes the specimen an X-ray is generated that can be used for elemental mapping and structural analysis of specimen. (For detail please see, X-ray diffraction section of this chapter)

2.3.1   Energy Dispersive Analysis of X-rays (EDS)

As high energy of electrons is continuously bombarded to the atoms of the specimen, due to which two important types of X-rays may be generated. The continuum or Bremsstrahlung X-rays, and characteristic X-rays.

Continuum or Bremsstrahlung X rays are generated when an incoming, beam electron passing close to the atomic nucleus, is slowed due to the Colombian attraction force between the electron and nucleus of the atom (in-elastic scattering) with the release of X-ray energy, figure 2.3 A. The energy of X-ray depends on how close the electron passes to the nucleus. Closer it passes, more the deceleration the electron hence, higher energy X-rays are generated. Since this event is random, different electrons will lose different amounts of energy, therefore the continuum X-ray shows a broad energy distribution (figure 2.4). On other hand, the characteristic X-rays are generated, when the high energy beam electrons interact with the inner shell electrons of the specimen atoms, so that an inner shell electron is ejected as secondary electron, figure 2.3 B. The removal of

this electron temporarily ionizes the atom until an outer shell electron fill into the vacancy, to stabilize the atom.
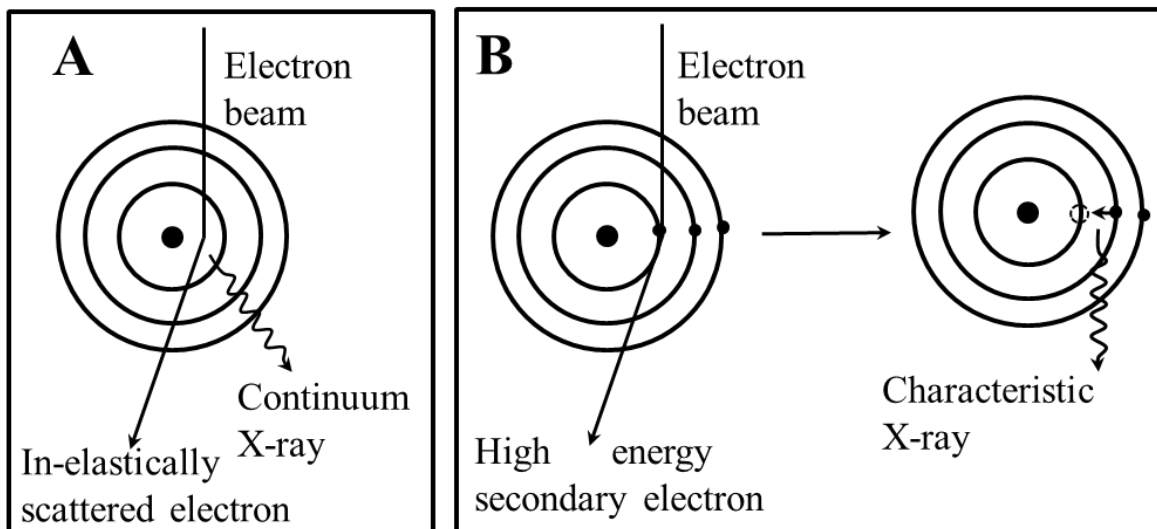
Figure 2.3: *Generation of continuum X-ray (a) and characteristic X-ray (b) upon bombardment of electron beam to the atoms present in the sample.*

Since the electron comes from higher energy levels, a specific amount of energy released in the form of X-rays, therefore the energy distribution is quiet intense and are discrete (figure 2.4). These discrete energy peaks are the unique characteristic of an element and are used for the elemental analysis of sample.[51]
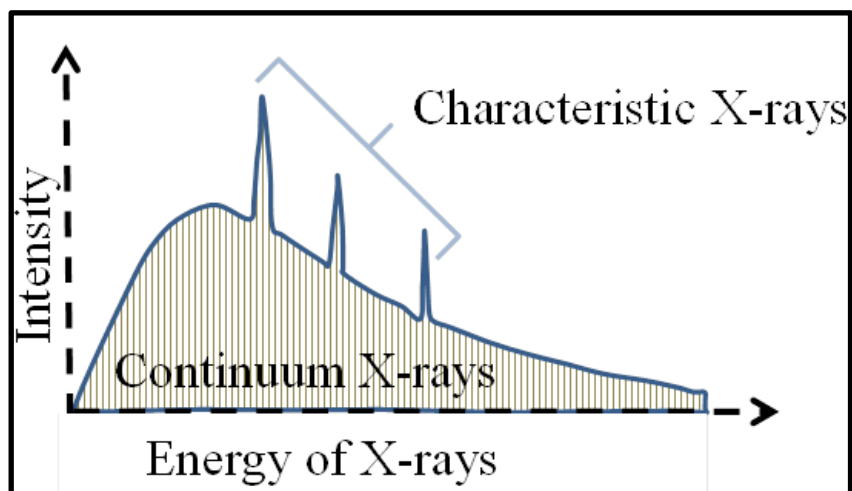
Figure 2.4: *Schematic showing energy of an X-ray generated from atoms of specimen. The continuum X-rays shows the broad energy distribution whereas, characteristic X-rays (peaks) show discrete energy levels.*

The characteristic X-ray, radiated from the sample is detected and used for the compositional analysis of elements present in the sample. With at present energy dispersive X-ray analysis systems, it is possible to map many elements simultaneously, and assigning a specific colors to each of the elements.

In electron microscopy, the X-rays can be used in various ways (table 2.1) for the analysis of samples[51]

In TEM analysis, a thin specimen is illuminated with electrons in which the electron intensity is uniform over the illuminated area. At the bottom of the microscope the un-scattered electrons hit a fluorescent screen, which gives rise to a "shadow image" of the specimen. Depending on the thickness and the density of the materials presents in specimen, differential contrast produced in the image.

Table 2.1: Summary of the main features of various analytical procedures.

Procedure	Energy dispersive X-Ray (EDS)	Wavelength dispersive X-Ray (WDS)	Electron Energy Loss Spectroscopy (EELS)	Electron diffraction
Microscope system needed	TEM or STEM or SEM	TEM or STEM or SEM	TEM or STEM	TEM or SEM
What Identified	Elements with atomic number greater than 6 (11 normally)	Elements with atomic number greater than 3	Elements with atomic number greater than 3	Chemical identity of crystal
Quantitative	Yes	Yes	Yes	No
Smallest area analyzed	10 nm	10 – 100 nm	0.3 – 0.4 nm	1 – 10 nm
Detection limit	10^{-13} g	10^{-10} g	10^{-19} g	Not applicable
Specimen Type	Ultrathin, Thin, Bulk*	Ultrathin, Thin, Bulk	Ultrathin	Ultrathin

* Ultrathin = 50 – 100 nm, Thin = 0.1 – 2 μm, Bulk = >2 μm thick sample

2.3.2   Different Modes of Imaging in TEM

In TEM image using the central spot, or we use some or all of the scattered electrons. In the case of bright-field imaging an aperture is inserted into the back focal plane to block most of the diffracted electrons. The beam of electron which passes through the aperture is used to generate the image. In dark-field imaging, the direct beam is blocked, and one or more of the diffracted beams, are allowed to pass through the aperture to generate image. The dark-field imaging is useful to get the information like planar defects; stacking faults, amorphous and crystalline nature of sample etc. In selected area electron diffraction (SAED), an aperture is used to define the area from which a diffraction pattern is formed in a TEM specimen. The resulting patterns used for the determination of a lattice spacing

measurement and to get the information about amorphous, crystalline and polycrystalline materials.

In this thesis, the topography, anisotropy and size distribution of biomilled nanoparticles were studied using FEI Tecnai TM G^2 F30 transmission electron microscope, equipped with field emission electron gun operated at accelerating potential of 200–300 kV. The aqueous samples were mounted on the copper grid of mesh size 200 μm, pre-coated with conducting carbon and allowed to dry completely.

2.4   Optical Spectroscopy

The spectroscopy is the study of the interaction of radiation with matter. The radiation is an electromagnetic sine wave having both electric and magnetic components, whose direction is perpendicular to each other. It is characterized by energy (E), which is linked to the frequency (ν) and wavelength (λ) with **Planck relationship**:

$$E = h\nu = \frac{hc}{\lambda}$$

Where, h is Planck's constant (6.625 x 10^{-34} J-s), c is the speed of light (2.998 x 10^8 m/s).

The electromagnetic radiations interact with a matter since; it contains positive and negative charges. With spectroscopy technique we study the electromagnetic phenomenon.[52]

In the medium, the absorption of light causes a transition from an energetic ground state to a particular excited state. Depending on the energy of light and on the chemical nature of the interacting compound, the excited states may differ very much in nature.[53]
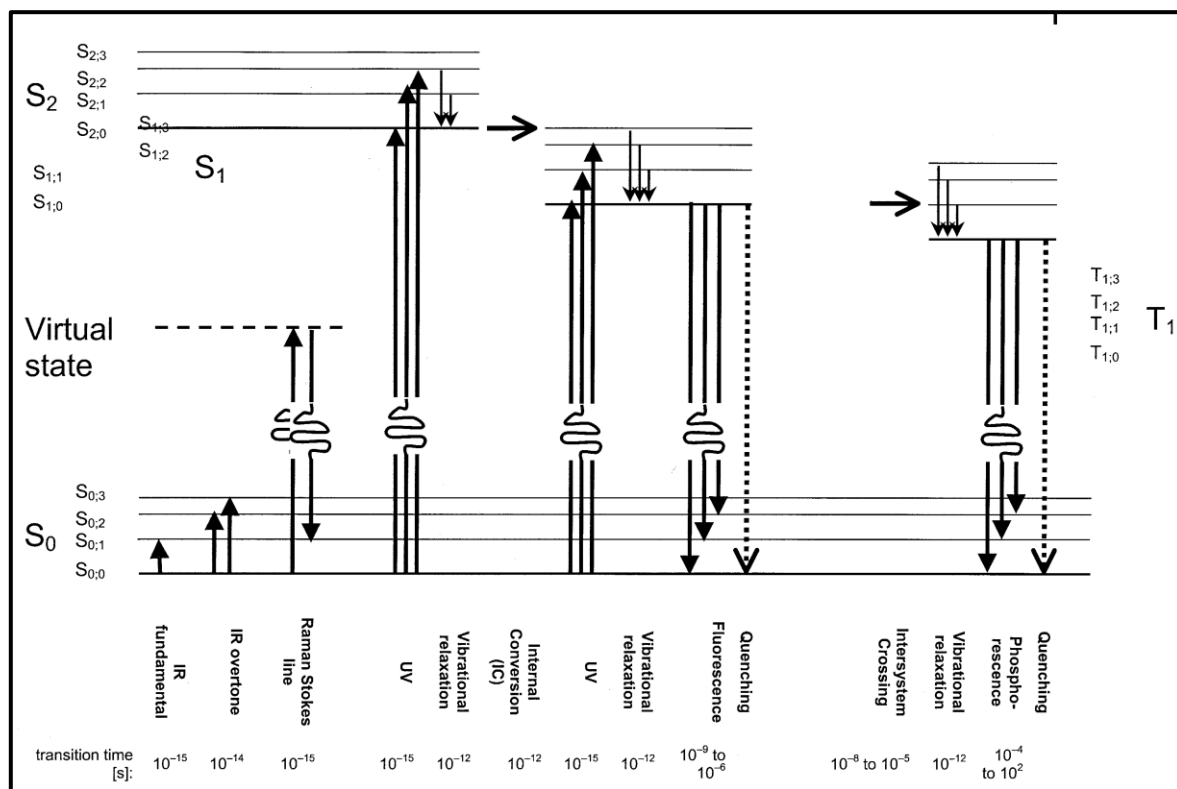
Figure 2.5: *Schematic shows the vibrational and electronic transitions. The distance between electronic states has been compressed by a factor of at least 10, compared to the distance between vibrational states. The S_0 depicts ground state, S_1 & S_2 exited state and T_1 transition states.*[53]

The absorption of light in UV/vis range causes electronic and vibrational excitations. Relaxation back from excited states to ground state may cause emission, luminescence or fluorescence (figure 2.5). Spectroscopic methods can be used for the study of concentrations, energies, conformations, or dynamics of molecules etc. It is sensitive to small changes in molecular structure or surroundings.

2.4.1 UV-visible Spectroscopy

The Beer–Lambert Law: A beam of light passing through a solution it transfers energy to the absorbing molecules as it as it passes across the solution. The relation between measured intensities and concentration of absorbing molecules/analytes is expressed in the Lambert-Beer law. The **Lambert's law** stated that absorbance of a material sample is directly proportional to its thickness (path length), whereas **Beer's law** stated that absorbance is proportional to the concentrations of the attenuating species.

The decrease in the intensity or irradiance (I), over the course of a small volume element is proportional to the irradiance of the light entering the element, the concentration of absorbers (C), and the length of the path through the element (dx).

$$\frac{dI}{dx} = -\varepsilon I C$$

The proportionality constant (ε) depends on the wavelength of the light and on the absorber's structure, orientation and environment. Integrating this equation shows that if light with irradiance I_0 is incident on a cell of thickness l, the irradiance of the transmitted light will be

$$I = I_0\, e^{-\varepsilon C l} = I_0\, X\, 10^{-\varepsilon C l}$$

It can be also expressed in its logarithmic form:

$$A = \log\frac{I_0}{I} = \varepsilon C l$$

Where, A is the absorbance or optical density of the sample (A = εCl) and ε is called the molar extinction coefficient or molar absorption coefficient.[54]

In this thesis, the absorbance spectra were recorded using a Jasco UV-vis dual-beam spectrometer (Model V-570) operated at a resolution of 2 nm.

2.4.2 Fluorescence Spectroscopy

The fluorescence of a molecule is the light emitted spontaneously due to transitions from excited singlet states (usually S_1) to various vibrational levels of the electronic ground state, i.e. $S_{1,0} \rightarrow S_{0,v}$. The various events takes place during the transition process are illustrated in figure 2.6.
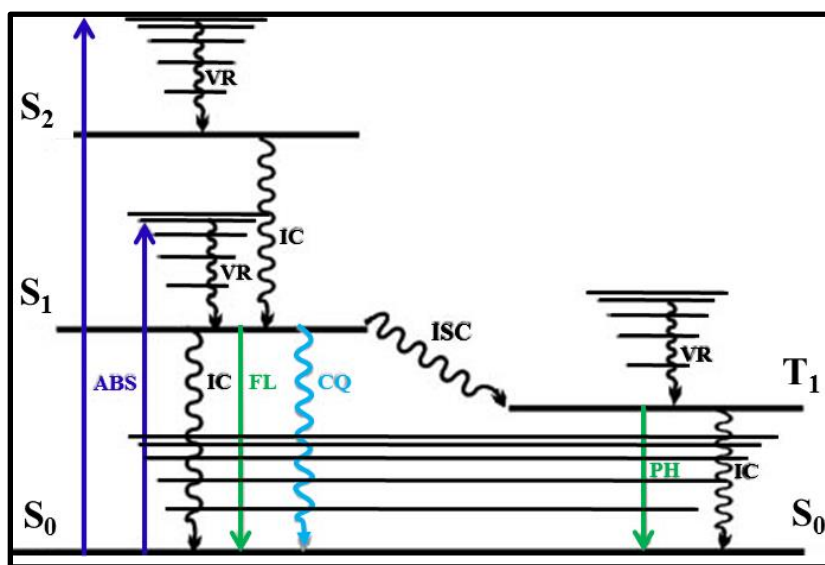
Figure 2.6: *Jablonski diagram illustrating the creation and fate of a molecular excited singlet state, including absorption (ABS), fluorescence (FL), phosphorescence (PH), internal conversion (IC), intersystem crossing (ISC), vibrational relaxation (VR) and collisional quenching (CQ). Not included are processes like solvent relaxation, energy transfer and photochemical reactions.*[55]

The fluorescence spectroscopy is a widely used analytical instrument in material sciences. Some of the important parameters are – fluorescence intensity at a given wavelength $F(\lambda)$, the emission spectrum (emission intensity on emission wavelength), quantum yield (ϕ), lifetime (τ) and polarization (P).[55]

In this thesis, the fluorescence emission spectra were recorded using a Cary Eclipse photoluminescence spectrophotometer from Varian equipped with a xenon flash lamp.

2.4.3   Fourier Transformed Infra-red Spectroscopy (FTIR)

The absorption of electromagnetic radiation in infra-red region by a matter, leads to the excitation of molecules to a higher vibrational state. The absorption of a particular frequency is strong, if the photon energy coincides with the vibrational energy levels of the molecule. The vibrational spectrum of a molecule is unique to a molecule and used as a molecular fingerprint of the matter. The absorption takes place in the wavenumber range of 400 to 4000 cm^{-1}.

An FTIR is a multiplex instrument, in which the spectral information is encoded in such a manner that the intensity distribution at all frequencies is measured simultaneously by a single detector. An FTIR employ a poly-chromatic beam containing many frequencies. In order to measure all the infra-red frequency simultaneously, an optical device called interferometer (Michelson interferometer) is added, which is equipped with a fixed and a rotating mirror are shown in figure 2.7. The 'spectral encoding' takes place here. The beam then passes through the sample. The beam reflected from the sample surface or transmitted through the sample goes to detector. The interferogram's signal measured by the detector is sent to computer. The computer processes the raw data (light absorption for each mirror position) into the desired result (light absorption for each wavelength). The digitalization of data and fast Fourier Transformation takes place before the final FTIR spectrum of sample is displayed. The FTIR has many advantages over conventional IR spectroscopy. All the signals measured simultaneously, therefore it is fast.

It has high sensitivity and good signal to noise ratio. The FTIR spectrum is quite reproducible and accurate. These advantages make the FTIR very useful analytical tool.

The intensity of an electromagnetic wave (I) is directly proportional to the square of the amplitude if wave i.e. I α A^2. When interference of two electromagnetic waves propagated in same direction takes place, the resultant amplitude and intensity would be -

$$A = A_1^2 + A_2^2 + 2A_1A_2\,cos\delta$$

$$I = I_1^2 + I_2^2 + 2\sqrt{I_1I_2}cos\delta$$

Where, δ is the phase difference between the two waves.[56]

The FTIR is an excellent analytical tool for the binding study of proteins adhered to the surface of biomilled NPs was performed by FTIR.

In this thesis, the FTIR spectra were obtained using a Perkin Elmer Spectrum One instrument. The samples for FTIR studies were mixed with KBr powder and allowed to dry under Infra-red lamp. The powered samples were then pressed using hydraulic press to form pellet. The spectrometer operated in the diffuse reflectance mode, at a resolution of 2 cm^{-1}. To obtain a good signal to noise ratio, 256 scans were taken in the range 1200–3000 cm^{-1}.
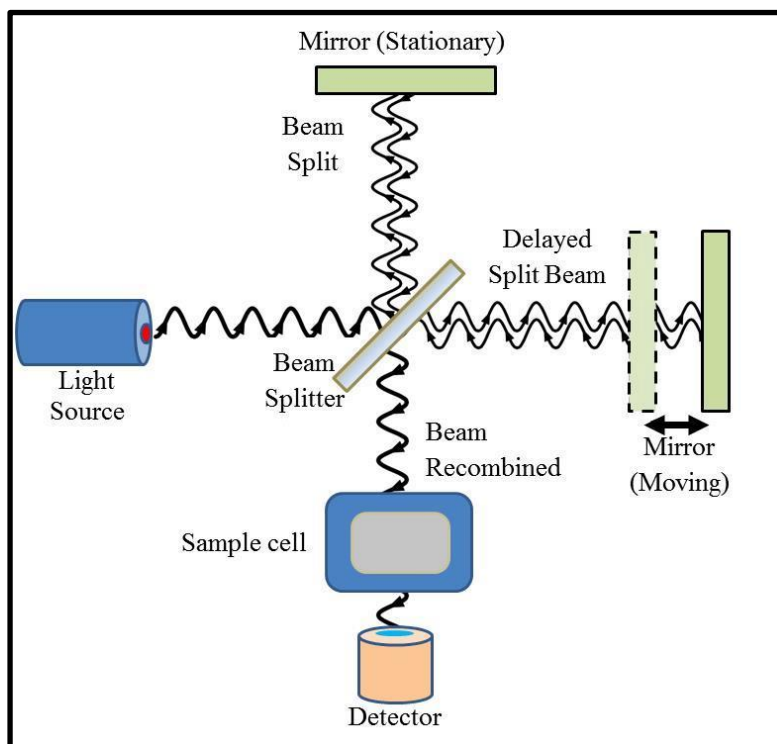
Figure 2.7: Schematic of a Michelson interferometer showing mirror arrangement and beam path.

2.5   Inductively Coupled Plasma – Optical Emission Spectroscopy (ICP-OES)

It is also known as inductively coupled plasma atomic emission spectroscopy (ICP–AES). The ICP-OES is a kind of emission spectroscopy, has been widely used for the quantitate determination of elements present in a solution. However, it can also be done for fine particulate solids or even for the gases.

The argon aerosol is mixed with the analyte and passes up through a tube. Radiofrequency radiation, with a frequency of 25–60 MHz and a power of 0.5–2.0 kW, is supplied through a copper coil around the tube. A high-voltage spark is applied to initiate

the plasma flame, which is then maintained through the inductive heating of the gas by the radiofrequency radiation. The electric current produced in the coil used to form plasma, hence its name. It produces excited atoms and ions that emit electromagnetic radiation at a characteristic wavelength of a particular element. This spectrum of radiation is analyzed for the quantitative determination of elemental composition.[47]

In this thesis, the ICP-OES were carried out using, Spectro Arcos (ARCOS-FHS-12) from SPECTRO Analytical Instruments GmbH. The sample solutions were filtered with 0.2 μm pore size nylon membrane filter before measuring the metal content.

2.6   X-ray Diffraction (XRD)

The X-ray is discovered by Wilhelm Rontgen in 1895. When an electron is bombarded to a metal target, it penetrates through the outer shells and transfers its energy to inner shell electrons. If the transferred energy is more than the critical energy required to escape the electron from attractive force of nucleus. The inner shell electron is ejected out; leaving an empty space (termed as hole or electron-hole) in the inner shell. To fill this space of missing electron (hole), an electron from outer shell jumps to inner shell (ground state). This transition led to the emission of an electromagnetic radiation (X-ray) or an Auger electron. The wavelength of these radiations are in order of 10^{-10} m (0.01 to 10 nm), which is comparable to the distance between the planes of crystal lattices. The commonly used metals targets for generation of X-rays are Cu Kα and Mo Kα which generates an X-rays of wavelengths 1.5418 Å and λ = 0.71073 Å, respectively.

The X-ray diffraction technique was started with Laue's discovery in 1912.When these X-rays strike to atoms of a crystal; it undergoes both elastic and inelastic scattering. The elastically scattered beams are interested as it gives information about the arrangement

of atoms in the crystal lattice. Initially X-Ray diffraction used only for the determination of crystal structure.

The crystalline materials are characterized by the long-range periodic arrangements of atoms. It has a basic repeating unit with maximum symmetry that uniquely defines the crystal structure is known as unit cell. These unit cells repeat in all dimensions to fill to form a macroscopic grains or crystals of the material.

2.6.1 Bragg's Equation for the Diffraction of X-ray
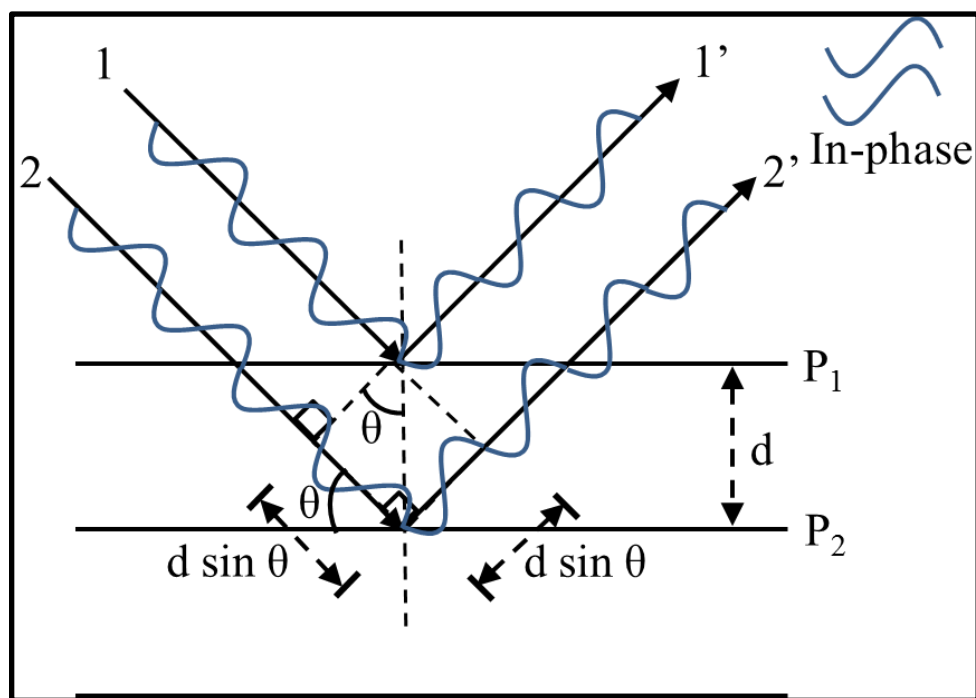
Figure 2.8: *The schematic depiction of Bragg's law, showing X-ray diffraction by a crystal. Where, n is an integer, d is inter–planar spacing, 2 d sin θ is path difference between the two beams, λ is the wavelength of X-ray.*

When X-ray beams incident on a pair of parallel planes P_1 and P_2, separated by an inter–planar spacing d. The two parallel incident rays 1 and 2 make an angle (θ) with these planes.

If the difference in path length between 1 to 1' (d sin θ) and 2 to 2' (d sin θ) is an integral number of wavelengths, the emergent beams are then in-phase and have maximum intensity (figure 2.8). This relationship is represented mathematically in Bragg's law.[57,58]

$$2\ d\ sin\ \theta = n\lambda$$

The crystals have been classified into six crystal families. This classification has been expanded slightly into seven crystal systems (table 2.2). The crystal systems are sets of reference axes, which have a direction as well as a magnitude, and hence are vectors.[58]
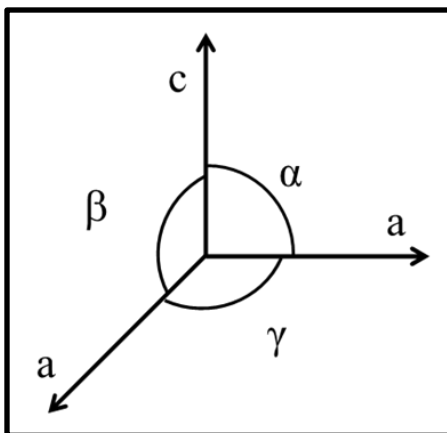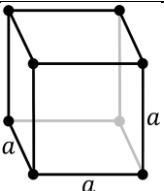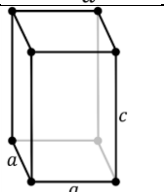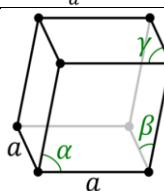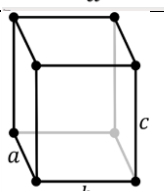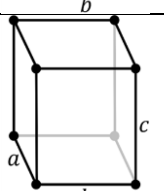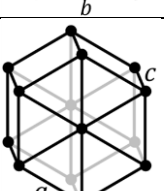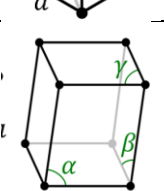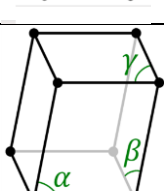
Figure 2.9: *The reference axis and angles, used for the characterization of crystal system.*

Table 2.2: The classification of crystal systems

S. N.	Crystal Family	Crystal system	Axis System (Axial relationships)	Unit cell Structure
1	Isometric	Cubic	$a=b=c$, $\alpha=\beta=\gamma=90^o$	
2	Tetragonal	Tetragonal	$a=b\neq c$, $\alpha=\beta=\gamma=90^o$	
3	Orthorhombic	Orthorhombic	$a\neq b\neq c$, $\alpha=\beta=\gamma=90^o$	
4	Hexagonal	Hexagonal	$a=b\neq c$, $\alpha=\beta=90^o$ $\gamma=120^o$	
		Trigonal or Rhombohedral	$a=b\neq c$, $\alpha=\beta=\gamma$ or $a'=b'\neq c'$, $\alpha=\beta=90^o$, $\gamma = 120^o$	
5	Rhombohedral	Rhombohedral	$a=b=c$, $\alpha=\beta=\gamma\neq90^o$	
6	Monoclinic	Monoclinic	$a\neq b\neq c$, $\alpha=\gamma=90^o$ $\beta\neq90^o$	
7	Anorthic	Triclinic	$a\neq b\neq c$, $\alpha\neq\beta\neq\gamma\neq90^o$	

2.6.2 The Determination of Crystal Structure using XRD

Crystal structure   Diffraction pattern

Unit cell $\longleftrightarrow$ Line positions

Atom positions $\longleftrightarrow$ Line intensities

The powder method of X-Ray diffraction was devised independently in 1916 by Debye and Scherrer in Germany. In 1935 Le Galley first constructed X-ray powder diffractometer. Largely metallurgists and mineralogists use powder diffraction primarily to study structural imperfections. The crystal structure of a substance determines the diffraction pattern of that substance or, more specifically, that the shape and size of the unit cell determines the angular positions of the diffraction lines, and the arrangement of the atoms within the unit cell determines the relative intensities of the lines.[59]

This method has been proved to be very useful to get the structural information of a material. Later this development in X-ray diffraction methods, now a days it is used for measurement of particle size, determination of the orientation of one crystal or the ensemble of orientations in a polycrystalline aggregate, chemical analysis and stress measurement, to the study of phase equilibrium etc.

2.6.3 The Determination of a Crystallite Size by Scherrer's Equation

$$L = \frac{k\lambda}{\beta\,cos\theta}$$

Where; L is the mean size of the ordered (crystalline) domains, which may be smaller or equal to the grain size, λ is the wavelength of the X-ray radiation in nanometers (CuKα = 0.15406 nm), k is a constant called shape factor, taken as 0.9 (it value depends on

shape parameters), θ is the diffraction angle and β is the line width (after subtracting the instrumental line broadening) at half maximum height, broadly termed as Full width half maxima (FWHM) intensity. Note: The angle can be either in degree or in radian, since both are same for the cosine values.

This is a widely accepted method for the estimation the mean crystalline size of nanoparticles.[60] This equation has later been modified implementing least square technique to minimize the errors.[61]

For XRD study, the samples were drop-casted on a glass substrate and dried under infra-red lamp. The PXRD patterns were recorded by using a PHILIPS X'PERT PRO instrument working at tension of 40 kV and 30 mA current, It is equipped with X'celerator, a fast solid state detector with Iron-filtered Cu-Kα radiation (λ = 1.5406 Å), was used to line-scan the samples at 2θ range of $10^{o} - 80^{o}$.

2.7 X-ray Photoemission Spectroscopy (XPS) Measurements

The X-ray photoelectron spectroscopy (XPS) is also known as electron spectroscopy for chemical analysis (ESCA). It has been developed by Professor Kai Siegbahn. For this great discovery, he awarded half share of the Nobel Prize in Physics in 1981.[62] The Photoelectron spectroscopy utilizes photo-ionization and energy-dispersive analysis of the emitted photoelectrons to study the composition and electronic state of the surface region of a sample.[47,63]

In this thesis, the XPS data were recorded using Thermo Scientific ESCALAB X-ray photoelectron spectrometer with Al Kα source (hν = 1486.6 eV). The sample measurements were done at ultra-high vacuum (UHV) pressure of $\sim 10^{-9}$ Torr. Both incidence and take off angles are set to 55° with respect to normal of the sample surface.

The spectra were analyzed with EA-125 Hemispherical energy analyzer of Omicron NanoTechnology GmbH in pulse-count mode. The energy pass of 50 eV used for broad range survey scan and energy pass of 25 eV used for narrow range core-level transitions. The narrow range core-level spectra of C1s, O 1s and Fe 2p were plotted, separately. The minimum numbers of peaks were fitted to functions Lorentzian-Gaussian functions after a Shirley background correction using the XPSPEAK41 software.

2.8   Polyacrylamide Gel Electrophoresis (PAGE)

Ferdinand Frederic Reuss in 1807 first time observed the movement of dispersed clay particles under the influence of constant electric field.[64] The electrophoresis method was developed with the earliest work of Arne Tiselius in the 1930s, for the electrophoretic analysis of colloidal mixtures.[65] It led to the development of electrophoresis for the separation of macromolecules based on their electrophoretic mobility. The electrophoretic mobility is the rate of migration of the substance measured in (cm/s) under the influence of a potential gradient of 1 (V/cm), and is expressed in (cm/V/s). The poly acrylamide gel electrophoresis (PAGE) is widely used method for the separation of for proteins. It has two main types (A) sodium dodecyl sulfate (SDS)–PAGE and (B) native–PAGE. The SDS [CH_3 (CH_2) CH_2OSO_3- Na^+] is an anionic detergent; on average one SDS molecule binds for every two amino acid residues. Samples are firstly boiled for 5 min. in sample buffer containing β-mercaptoethanol and SDS which denatures the protein's tertiary structure, and imparts a negative charge on the proteins. The sample buffer also contains a tracking dye, usually bromophenol blue which allows the monitoring of gel running, and sucrose or glycerol, which gives density to protein to settle at bottom in the loading well. Running the protein under electric field, in stacking gel, concentrate protein into a sharp band, which

are formed due to negatively charged glycinate ion have lower electrophoretic mobility than protein SDS-complex which in turn have lower mobility than chloride ion of loading buffer. The three species [Cl⁻] > [protein − SDS] > [glycine] arrange themselves in this order during electrophoresis in stacking gel, leading to the formation of a tight band of protein. This protein band when further electrophoresed in running gel, separates into different protein bands of specific molecular weight (M_r). The M_r of protein bands can be estimated by comparing it with standard protein marker, which runs simultaneously in adjacent well in the same gel. Therefore, in SDS-PAGE the proteins get separated based on the size *i.e.* molecular weight.

2.9   Dynamic Light Scattering (DLS)

It is also known as photon correlation spectroscopy or quasi-elastic light scattering. It is used to estimate the size distribution of small particles, typically in sub-micrometer, present in a suspension. It is a powerful technique for size estimation of nanoparticles and molecules.[66] In general smaller the particles, larger it's Brownian movement and vice versa. The Brownian movement occurs due to bombardment of solvent molecules to the particle.

When an electromagnetic wave (light) interacts with a matter, the electric field of the light induces an oscillating polarization of electrons in the molecules. Therefore, the molecules provide a secondary source of light and subsequently scatter light.

The Rayleigh approximation tells us that

$$I \; \alpha \; d^6 \quad \text{and} \quad I \; \alpha \; \frac{1}{\lambda^4}$$

Where, I is intensity of scattered light, d is particle diameter, λ is the wavelength of laser light used. In general the wavelength is fixed, for He-Ne laser it is 633 nm.

The rate of change of intensity of scattered light is related to the diffusion coefficient of the particles, which in turn is related to particle size by the Stokes-Einstein equation, as shown below.[67]

$$d\ (H) = \frac{kt}{3\pi\eta D}$$

Where, the d (H) is the hydrodynamic diameter, D is the translational diffusion coefficient, k is the Boltzmann's constant, T is the absolute temperature (in Kelvin) and η is the viscosity of the solvent.

The smaller particles cause fluctuation in the intensity more rapidly than the large ones (figure 2.10). Therefore, a digital autocorrelator (a signal comparator) is used to measure the degree of similarity between the signal at time (t), and same signal after a while at (t + δt). The (δt) is in the time scale of the molecular fluctuations. The intensities at successive time intervals were used to derive the rate at which the intensity is varying. The size particles can be obtained from the correlation function, by using various algorithms.

(1) Cumulants analysis: It is used to fit a single exponential to the correlation function to obtain the mean size (z-average diameter) and then estimate of the width of the distribution (polydispersity index).

(2) Intensity size distribution: It is used to fit a multiple exponential to the correlation function to obtain the distribution of particle sizes.
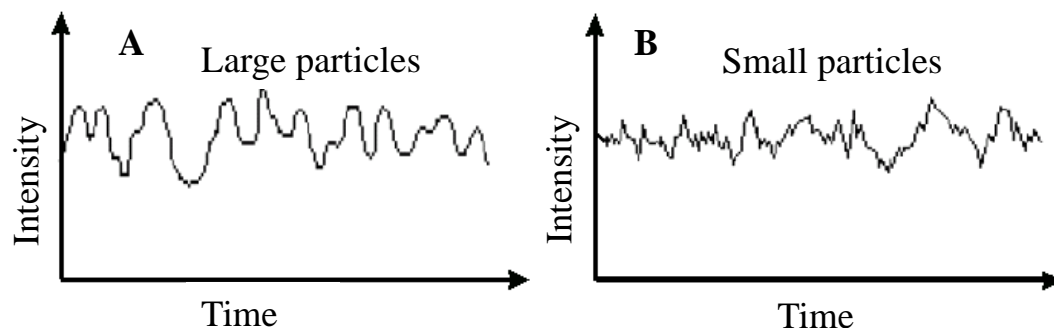
Figure 2.10: The schematic graph showing typical intensity fluctuations for large and small particles

In this thesis, a PALS Zeta Potential Analyzer Ver 3.54 (Brookhaven Instrument Corps.) equipped with He-Ne Laser (λ = 633 nm), was used to determine the electrophoretic motilities of particles, which is converted to zeta potential (z) using the Smoluchowski model.

2.10 Thermogravimetric Analysis (TGA)

The TGA is used to measure the physical property of a substance as a function of temperature. The sample to be analyzed is kept in a platinum crucible which is attached to an automatic recording weighing balance. The temperature of the crucible is increases at constant rate at constant rate. Furnace temperature is continuously monitored by a thermocouple. The weight loss versus temperature graph is plotted and is used to quantify the change in weight of substance, associated with transitions.

The TGA experiments were carried out in the temperature range of 25–750 $^{\circ}$C on a SDT Q600 TGDTA analyzer. The non-oxidising, neutral condition is maintained by constant flow of nitrogen gas at the heating rate of 10 $^{\circ}$C per min.

2.11 References

1   A. Foster and W. Hofer, *Scanning probe microscopy: Atomic Scale Engineering by Forces and Currents*, Springe-Verlag Berlin Heidelberg New York, 2006.

2   G. Binnig, C. F. Quate and C. Gerber, *Phys. Rev. Lett.*, 1986, **56**, 930–934.

3   D. Sarid, *Scanning Force Microscopy With Application to Electric, Magnetic and Atomic Forces*, Oxford University Press, Inc., New York, Revised Ed., 1994.

4   M. Kandpal, C. Sharan, V. Palaparthy, N. Tiwari, P. Poddar and V. R. Rao, *RSC Adv.*, 2015, **5**, 85741–85747.

5   M. Kandpal, C. Sharan, P. Poddar, K. Prashanthi, P. R. Apte and V. R. Rao, *Appl. Phys. Lett.*, 2012, **101**, 104102.

6   B. T. Marshall, K. K. Sarangapani, J. Wu, M. B. Lawrence, R. P. McEver and C. Zhu, *Biophys. J.*, 2006, **90**, 681–692.

7   J. Grobelny, N. Pradeep, D.-I. Kim and Z. C. Ying, *Appl. Phys. Lett.*, 2006, **88**, 091906.

8   W. Sun, P. Neuzil, T. S. Kustandi, S. Oh and V. D. Samper, *Biophys. J.*, 2005, **89**, L14–L17.

9   Q. Ouyang, K. Ishida and K. Okada, *Appl. Surf. Sci.*, 2001, **169**, 644–648.

10   T. Eastman and D. Zhu, *Langmuir*, 1996, **12**, 2859–2862.

11   S. Gourianova, N. Willenbacher and M. Kutschera, *Langmuir*, 2005, **21**, 5429–5438.

12   B. Dordi, J. P. Pickering, H. Schönherr and G. Julius Vancso, *Eur. Polym. J.*, 2004, **40**, 939–947.

13   B. Dordi, J. P. Pickering, H. Schönherr and G. J. Vancso, *Surf. Sci.*, 2004, **570**, 57–66.

14   O. H. Pakarinen, A. S. Foster, M. Paajanen, T. Kalinainen, J. Katainen, I. Makkonen, J. Lahtinen and R. M. Nieminen, *Model. Simul. Mater. Sci. Eng.*, 2005, **13**, 1175–1186.

15   N. E. Kurland, Z. Drira and V. K. Yadavalli, *Micron*, 2012, **43**, 116–128.

16   C. M. Franz, A. Taubenberger, Z. Sun, A. Trache, K. Meissner, G. a. Meininger, T. Ando, T. Uchihashi, N. Kodera, M. Shibata, D. Yamamoto, H. Yamashita, L. Redondo, Morata, D. Kiracofe, J. Melcher, A. Raman, A. Ikai, R. Afrin, T. Watanabe-Nakayama, S. I. Machida, J. J. Heinisch, Y. F. Dufrêne, T. Fukuma, M. J. Higgins, C. M. Franz and A. Taubenberger, *At. Force Microsc. Liq. Biol. Appl.*, 2012, 331–354.

17   E. Dague, D. Alsteens, J. Latge, C. Verbelen, D. Raze, A. R. Baulard and Y. F. Dufre, *Nano Lett.*, 2007, **7**, 3026–3030.

18   O. Klymenko, J. Wiltowska-Zuber, M. Lekka and W. M. Kwiatek, *Acta Phys. Pol. A*, 2009, **115**, 548–551.

19   C. Rotsch, F. Braet, E. Wisse and M. Radmacher, *Cell Biol. Int.*, 1997, **21**, 685–696.

20   J. Wong, A. Chilkoti and V. T. Moy, *Biomol. Eng.*, 1999, **16**, 45–55.

21   Y. Yang, H. Wang and D. A. Erie, *Methods*, 2003, **29**, 175–187.

22   I. Sorel, O. Piétrement, L. Hamon, S. Baconnais, E. Le Cam and D. Pastré, *Biochemistry*, 2006, **45**, 14675–14682.

23   A. Berquand, M.-P. Mingeot-Leclercq and Y. F. Dufrêne, *Biochim. Biophys. Acta - Biomembr.*, 2004, **1664**, 198–205.

24   S. E. Cross, Y.-S. Jin, J. Rao and J. K. Gimzewski, *Nat. Nanotechnol.*, 2007, **2**, 780–783.

25   M. Lekka, D. Gil, K. Pogoda, J. Dulińska-Litewka, R. Jach, J. Gostek, O. Klymenko, S. Prauzner-Bechcicki, Z. Stachura, J. Wiltowska-Zuber, K. Okoń and P. Laidler, *Arch. Biochem. Biophys.*, 2012, **518**, 151–156.

26   K. Tomankova, H. Kolarova, M. Vujtek and H. Zapletalova, *Mod. Res. Educ. Top. Microsc.*, 2007, 23–28.

27   S. E. Cross, Y. Jin, J. Tondre, R. Wong, J. Rao and J. K. Gimzewski, *Nanotechnology*, 2008, **19**, 384003.

28   C. Le Grimellec, E. Lesniewska, M. C. Giocondi, E. Finot, V. Vié and J. P. Goudonnet, *Biophys. J.*, 1998, **75**, 695–703.

29   N. H. Thomson, *J. Microsc.*, 2005, **217**, 193–199.

30   L. Zitzler, S. Herminghaus and F. Mugele, *Phys. Rev. B*, 2002, **66**, 155436.

31   C. Möller, M. Allen, V. Elings, A. Engel and D. J. Müller, *Biophys. J.*, 1999, **77**, 1150–1158.

32   R. Garcia and R. Preze, *Surf. Sci. Rep.*, 2002, **47**, 197–301.

33   C. Yang, I. Hwang, Y. F. Chen, C. S. Chang and D. P. Tsai, *Nanotechnology*, 2007, **18**, 084009.

34   K. L. Babcock and C. B. Prater, *Veeco Instruments Inc. (Santa Barbar. CA Digit. Instruments)*, 2004, 1–4.

35   G. Haugstad, *Atomic Force Microscopy*, John Wiley & Sons, Inc., Hoboken, NJ, USA, 2012.

36   B. R. Eby, *Veeco Instruments Inc. (Santa Barbar. CA Digit. Instruments)*, 2002, 1–2.

37   B. F. M. Serry, K. Kjoller, J. T. Thornton and D. Cook, *Veeco Instruments Inc. (Santa Barbar. CA Digit. Instruments)*, 2004, 5–12.

38   S. Hosaka, in *Roadmap of scanning probe microscopy*, ed. S. Morita, Springer Berlin Heidelberg New York, 2007, vol. I, pp. 53 – 61.

39   S. Kalinin, A. Rar and S. Jesse, *IEEE Trans. Ultrason. Ferroelectr. Freq. Control*, 2006, **53**, 2226–2252.

40   S. V Kalinin and D. A. Bonnell, *Phys. Rev. B*, 2002, **65**, 125408.

41   S. Jesse, A. P. Baddorf and S. V Kalinin, *Nanotechnology*, 2006, **17**, 1615–1628.

42   Y. Takemura and J.-I. Shirakashi, *J. Magn. Magn. Mater.*, 2006, **304**, 19–22.

43   E. Dubois and P. A. Fontaine, in *27th European Solid-State Device Research*

Conference, 1997, vol. 43, pp. 1085–1089.

44   P. J. Thomas, G. U. Kulkarni and C. N. R. Rao, *J. Mater. Chem.*, 2004, **14**, 625–628.

45   J. M. Kinsella and A. Ivanisevic, in *Applied Scanning Probe Methods IV*, eds. B. Bhushan and H. Fuchs, Springer-Verlag Berlin Heidelberg, 2006, pp. 1 – 33.

46   L. M. Prescott, *Microbiology*, The McGrow-Hill Companies, Fifth Ed., 2002.

47   J. M. Hollas, *Modern Spectroscopy*, John Wiley & Sons, Ltd, Fourth Ed., 1987.

48   B. Nolting, *Methods in Modern Biophysics*, Springer-Verlag Berlin Heidelberg, Second Ed., 2006.

49   G. Indebetouw, Y. Tada, J. Rosen and G. Brooke, *Appl. Opt.*, 2007, **46**, 993–1000.

50   R. F. Egerton, *Physical Principles of Electron Microscopy: An introduction to TEM, SEM, and AEM*, Springer Science + Business Media Inc., 2005.

51   J. J. Bozzola and L. D. Russell, *Electron Microscopy Principle and Techniques for Biologists*, Jones and Bartlett Publishers, 1999.

52   G. G. Hammes, *Spectroscopy for the biological sciences*, Wiley-interscienc; A John Wiley & Sons, Inc., 2005, vol. 34.

53   G. Gauglitz and T. Vo-Dinh, *Handbook of Spectroscopy*, Wiley-VCH Verlag GmbH & Co. KGaA, 2003.

54   W. W. Parson, *Modern Optical Spectroscopy with Examples from Biophysics and*

Biochemistry, Springer-verlag Berlin Heidelberg, Washington, 2007.

55   M. Hof, R. Hutterer and V. Fidler, in *Springer Series on Fluorescence Methods and Applications*, ed. O. S. Wolfbeis, Springe-Verlag Berlin Heidelberg New York, 2005, pp. 1–305.

56   J. Kauppinen and J. Partanen, *Fourier Transforms in Spectroscopy*, Wiley-VCH Verlag GmbH, 2001.

57   Y. Waseda, E. Matsubara and K. Shinoda, *X-Ray Diffraction Crystallography Introduction, Examples and Solved Problems*, Springer-verlag Dordrecht London New York, 2011.

58   R. J. D. Tilley, *Crystals and Crystal Structures*, John Wiley and Sons, Ltd., 2006.

59   B. D. Cullity, *Elements of X-Ray Diffraction*, Addison-Wesley Publishing Company, Inc., 1956.

60   P. R. Parmar, M. H. Mangrola, B. H. Parmar and V. G. Joshi, *Multi Discip. Edu Glob. Quest*, 2012, **1**, 146–154.

61   A. Monshi, M. R. Foroughi and M. R. Monshi, *Sci. Res.*, 2012, **2**, 154–160.

62   J. Pearce, *New York Times*, 2007.

63   E. M. E. Kristensen, F. Nederberg, H. Rensmo, T. Bowden, J. Hilborn and H. Siegbahn, Langmuir, 2006, 22, 9651–9657.

64   F. F. Reuss, *Mémoires la Société Impériale des Nat. Moscou*, 1809, **2**, 327–337.

65   A. Tiselius, *Trans. Faraday Soc.*, 1937, **33**, 524.

66   M. Kaszuba and M. T. Connah, *Part. Part. Syst. Charact.*, 2006, **23**, 193–196.

67   H. G. Merkus, *Particle size measurements: Fundamentals, Practice, Quality*, Springer Science + Business Media B.V., 2009.

Chapter III

The Synthesis of Metal Oxide Nanoparticles using Biomilling and Understanding the Role of Proteins

This chapter describes the top-down synthesis of metal oxide nanoparticles using biomilling. In this method we have synthesized quasi-spherical, protein-capped nanoparticles (NPs) below 10 nm by the break-down of chemically-synthesized anisotropic rod NPs using yeast; *Saccharomyces cerevisiae.* In the process of synthesis, the yeast cells secrete different types of proteins which participate in the breakdown of precursor particles into nanoparticles. It also led to the formation of 'protein corona' around the synthesized NPs. We have investigated the dynamic nature of protein corona and the expression profile of intracellular as well as extracellular proteins of the yeast (microorganism). In this chapter, we have made efforts to address some of the challenges associated with the biomilling process, (1) isolate the biomilled NPs from biomass, (2) separate the top-down biomilling and bottom-up biosynthesis processes (if the organism itself, has NP synthesis ability by extra/intracellular reduction of free zinc ions to form NPs), and (3) distinguish the yeast cell involvement in the biomilling process.

A part of the work presented in this chapter is published.[1]

3.1 Introduction

Metal oxides possess unique functionalities and play important roles in many areas of physics, chemistry, life sciences, materials sciences etc. As the nanotechnology flourishes, the interests in the synthesis and use of oxide nanostructures have also exponentially increased. The interest lies in the nanomaterials due to its unusual properties, for example quantum confinement effect, superparamagnetism etc. The overall chemical and physical characteristics of materials, such as hardness, thermal stability, low chemical reactivity etc. as well as their distinctive, optical, magnetic, electrical properties etc. have drawn the significant attention.

With the progression and applicability of metal oxide nanomaterials; the necessity for the development of reliable and ecofriendly method of synthesis, has also been hugely increased. Today, a number of reliable physical and chemical methods of synthesis are available nevertheless; there is a great concern over the use of harmful chemicals and high energy consuming processes. In addition, these methods sometime required special devices or equipment and the processes that required extreme conditions, such as high temperature, pressure etc. Altogether, all these requirements raised the apprehension for the environment.

To consider the future sustainability of these methods, there is always a great demand for the development of energy intensive, eco-friendly routes for the synthesis of nanomaterials. For the development of such eco-friendly ways, scientists sometimes look towards the nature to get knowledge and ideas. The nature always inspires with the sustainable, eco-friendly processes, which have already been utilized in various ways *e.g.*

in biomimetic engineering,[2,3] bio mineralization,[4] bioleaching,[5,6] bioremediation,[7] and biotransformation[8] etc.

There are two antagonistic ways, for the synthesis of nanomaterials (1) bottom-up; in which, the NPs are synthesized from their precursor molecules and, (2) top-down; in which, the bigger particles are broken-down to the nanoscale size by physical methods such as ball-milling, laser ablation[9] etc. Among the two,, the bottom-up methods are more popular among bionanotechnologists for the synthesis of nanomaterials of metals,[10,11] and metal oxides[12] etc. from their precursors; whereas, the microbiology based top-down methods such as "biomilling", which has been developed by our group.[13–15] is in its infancy, and drawing considerable attention.

There are many chemical/physical methods available in the literature for the synthesis of ZnO NPs such as sol–gel,[16] simple solution combustion method,[17] chemical vapor synthesis,[18] hydrothermal method,[19] microwave assisted synthesis of microcrystals,[20] microwave assisted hydrothermal synthesis, [21] and laser ablation.[9] However, the green top-down biological method to synthesize ZnO NPs is not reported so far. As the microorganims are endowed with various biomolecules, some of them can potentially break-down the larger particles, the biomilling technique efficiently utilizes these cells for the synthesis of protein-capped quasi-spherical ZnO NPs. The biomilling method is quiet a new method as compared to other existing methods of synthesis of nanomaterials. For the first time this method was demonstrated for the break-down of chemically synthesized BiOCl particles into very small nanoparticles of size less than 10 nanometers, and this method was named "bio-milling".[13] After this report this method has been used for many

materials such as $BaTiO_3$,[14] Gd_2O_3,[15] ZnO,[1] and $FeOOH$.[22] However, in order make it industrially feasible, we need to address several challenges and some of them include –

A.   Isolation of Biomilled NPs from the Biomass: In this method the large particles that have to be broken-down into nanoparticles are fed to the microbial culture. These microbes secrete a number of biomolecules such as proteins. These biomolecules interact with the precursor materials in order to break them down into nanoparticles. Conventionally, this process is carried out in the culture flask in a batch culture. Therefore, the microbes, their secreted biomolecules, precursor particles as well as the biomilled nanoparticles are still present in this medium. This made it highly heterogeneous system. Therefore, to get rid of unwanted things and to isolate nanoparticles from this mixture is remain challenging.

B.   Understanding the Biochemical Mechanism of Biomilling: During the biomilling process, the microbe secretes a number of biomolecules and all together in a mixture form, making this system highly complex one. Therefore, it is hard to understand the complete mechanism of this method. However, in order to optimize and improve the method, it is utmost important to understand the underlying mechanism.

Scale-up of the Process: To use this method industrial feasible, the system should be simple, yet can easily be scaled–up.

In this chapter we have made efforts to address some of these challenges, so that we can develop better understanding about the mechanism and to find out the causes responsible for the breakdown of bigger particles into smaller one, we have made some modifications in the biomilling method. These details and pictorial view of modified experimental system have been described in the experimental section of this chapter.

3.2   **The Model System to Study Biomilling of Metal Oxides**

In this study, we chose the yeast *S. cerevisiae* as a model organism and ZnO as materials, to study the biomilling process. The main objectives of choosing the *S. cerevisiae* as a model system are – (1) It is a fast growing yeast (requires less generation time) and it can be easily cultured in the ambient conditions (robust in nature). (2) The culture can be economically maintained and preserved for a long duration. (3) It is highly tolerant to many metal ions.[23] (4) It can also accumulates certain metal ions such as zinc, copper and manganese, through various physicochemical processes.[24] (5) It has a well developed transport mechanism for the intake of zinc. [25–27] (6) It has been utilized since ancient times for the production of bread and beer etc. and are safe for human consumption,[28] and are used as probiotics.

On the other hand choosing ZnO has added advantages, as it is well known for its unique properties such as piezoelectricity,[29] UV absorbance,[30] sensitivity to gases and chemical agents,[31] catalysis[32] etc. Its distinctive properties lead to an widespread applicability *e.g.* for solar-photovoltaic,[33–36] piezoelectric-transducers,[37] short-wavelength lasers,[38] phosphors,[39] light emitting diodes[40] etc. Recently, ZnO is proved to be an excellent material for the biological applications such as antimicrobial agents,[39,41] UV-protectants in sunscreen lotions, cancer treatment[42,43] etc. The fate of NPs in the living systems is determined by nanoparticle–corona complex which interact with biological system, rather than the bare nanoparticles.[44,45] Therefore, the biomilled nanoparticles would be also be a potential candidate for biomedical applications.

3.3   Experimental Section

3.3.1   Materials

All chemicals procured for this work were of analytical grade unless otherwise described. The constituents of MGYP media used for the growth of yeast culture were Dextrose monohydrate (AR grade), mycological peptone (certified), yeast extract powder (type I), malt extract powder were purchased from Himedia laboratories. The dialysis tubing made of cellulose membrane (average flat width 33 mm, D 9652) was purchased from Sigma-Aldrich. Sodium hydroxide pellets (GR grade) and absolute ethanol were purchased from Merck. Zinc acetate dehydrate [(Zn (CH$_3$–COO)$_2$·2H$_2$O), extra pure, AR grade] was purchased from Sisco Research Laboratory Pvt. Ltd. All glassware were washed with aqua-regia (HCl/HNO$_3$ = 3:1) carefully and were rinsed with double-distilled water before being used in the reaction. All the aseptic works were carried out in the laminar flow hood, pre-treated with UV-radiation.

3.3.2   Chemical Synthesis of ZnO NRs

The rod-shaped ZnO NPs were synthesized by previously described method.[46] In this method, zinc acetate and sodium hydroxide were dissolved in double-distilled water in the stoichiometric ratio and were stirred for ~ 45 min at room temperature (RT) followed by the hydrothermal reaction in a stainless steel vessel which was coated with Teflon liner. The reactions were carried out for ~ 24 h, at ~ 120 ^{o}C. The resultant materials obtained were washed several times with deionized water and then absolute ethanol, to remove the ionic impurities. Then the samples were dried in a vacuum oven for 6 h at 60 ^{o}C which results into a white powder of ZnO NRs. After characterization, this ZnO NRs powder was used as precursor for the biomilling experiments.

3.3.3 **Biomilling of ZnO NRs**

The budding yeast *S. cerevisiae* (NCIM no. 3064) was obtained from National Collection of Industrial Microorganisms (NCIM) situated at CSIR-National Chemical Laboratory, Pune, India. The biomilling of ZnO NRs were carried out by modified biomilling method as shown by the schematic shown in the figure 3.1, and are briefly described here. The yeast culture was grown in a 500 mL Erlenmeyer flask containing 150 mL of the MGYP medium (0.45 g malt extract, 0.45 g yeast extract, 0.75 g mycological peptone, and 1.5 g dextrose).The above flask was incubated at 28 ^{o}C under constant shaking at 150 rpm. After 48 h of growth, when cells are at late log phase, were harvested by centrifugation at 5000 rpm for 5 min at 4 ^{o}C. These cells were washed three times with autoclaved normal saline solution. The yeast cells were then transferred to a sterile Erlenmeyer flask containing normal saline (0.9 w/v sodium chloride) solution. In this flask, a dialysis bag (molecular weight cutoff ~14 kDa) containing precursor ZnO NRs (10 mg) dispersed in 15 mL double distilled water was added. Then this flask was incubated for 168 h in a rotary shaker at 28 ^{o}C, 150 rpm. However, for monitoring the biomilling process, the samples were taken out at interval of 24 h till 168 h. Then the dialysis bag from the culture flask were taken out and further dialyzed in distilled water for 24 h. The distilled water changed at the interval of 6–8 h. The whole procedure was performed aseptically, in a laminar air-flow cabinet whenever, it is required.
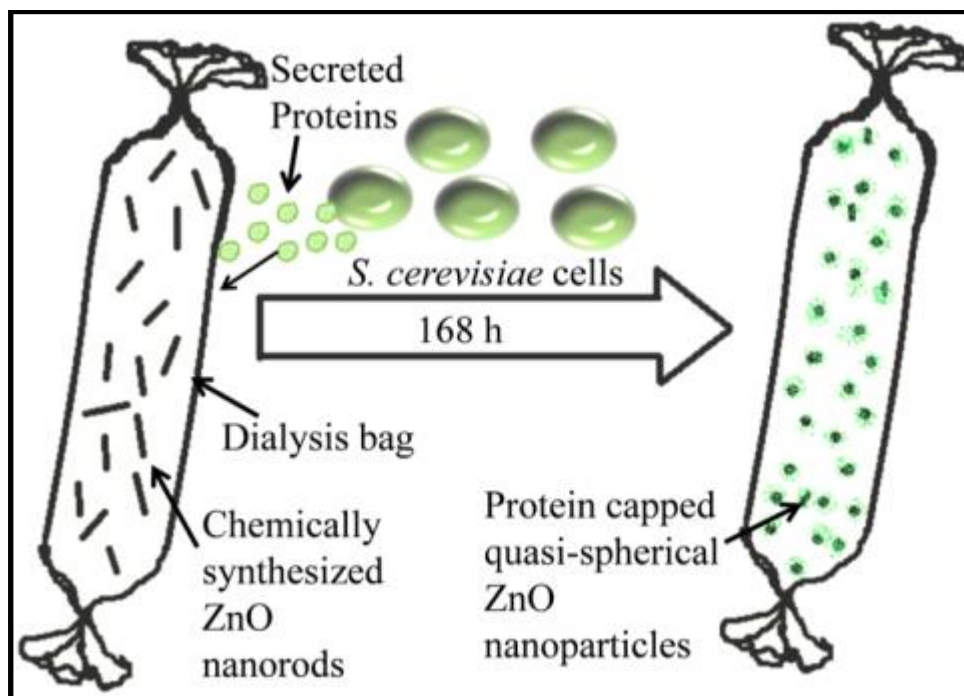
Figure 3.1: *The schematic showing modified biomilling process, in which the material (ZnO NRs) to be biomilled is kept in a dialysis bag.*[1]

3.4 Results and Discussion

3.4.1 The TEM Studies

The morphology of precursor ZnO NRs and the biomilled ZnONPs were characterized by TEM. The images were acquired from Tecnai F30 instrument of FEI Inc. This instrument was equipped with a field-emission electron gun, operated at 300 kV with S-TWIN objective lens having spherical aberration correction (C_S) value of 1.2 mm. The point resolution of the microscope was 0.24 nm. The sample was drop-casted on a carbon-coated copper grid having mess-size of 200 μm and air-dried in vacuum before being introduced into the TEM instrument.
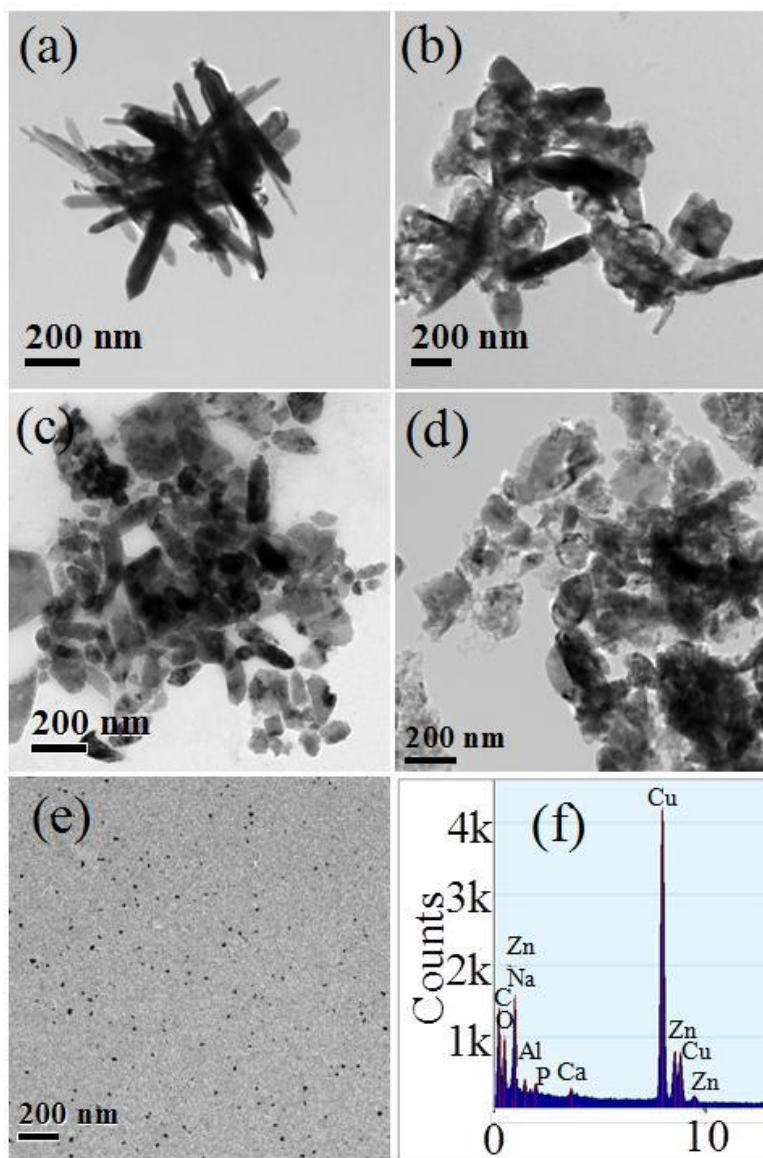
Figure 3.2: *TEM images showing the different stages of biomilling of the rod-shaped ZnO NPs. (a–e) TEM images of ZnO NPs at 0 h, 24 h, 72 h, 120 h and 168 h of biomilling, respectively. (f) EDS result demonstrates the presence of zinc in sample at 168 h.*[1]

From the TEM image in figure 3.2a, the presence of well-defined rods with an average diameter of ~45 nm and an average length of ~250 nm were observed. It was noticed from figure 3.2b that after 24 h of biomilling, the ZnO NRs were fully covered with a thick amorphous protein layer and the rods as a whole and specifically, at the edges, started to break-down and an overall reduction in length and diameter of rods was observed.

As the biomilling time was increased to 72 h, the average size of the ZnO NRs was decreased (Figure 3.2c). After 120 h of biomilling (Figure 3.2d), the spherical NPs were found to coexist with a significantly reduced population of smaller size of ZnO NRs. Further, the presence of uniformly distributed very small quasi-spherical NPs with size ~10 nm was found in the TEM image of 168 h of biomilled NPs (Figure 3.2e). The Zn, C, N and O elements were found in the corresponding Energy-dispersive X-ray spectrum (EDS) (Figure 3.2f).

3.4.2   The AFM Studies

For AFM imaging, the sample was drop-casted on the silicon-wafer and dried in vacuum. All the AFM measurements were done under ambient conditions using the tapping-mode AFM using Tap190Al AFM Budget Sensors® probes purchased from Innovative Solutions Bulgaria Ltd. The radius of curvature of tips used in this study was <10 nm and their height was 17 μm. The cantilever used had a resonant frequency of ca. 162 kHz and nominal spring constant of ca. 48 N m^{-1} with a 30 nm thick aluminum reflex coating on the backside of the cantilever of length 225 μm. For each sample, three locations with a surface area of 1 x 1 μm^2 each were imaged at a rate of 1 Hz and a resolution of 512 x 512

data points. AFM results were also confirmed the synthesis of very small spherical NPs with diameter ~10 nm as shown in figure 3.3a and its corresponding 3D image 3.3 b. The sizes of NPs were estimated by a drawing line profile drawn across the nanoparticles as shown in inset of figure 3.3a.
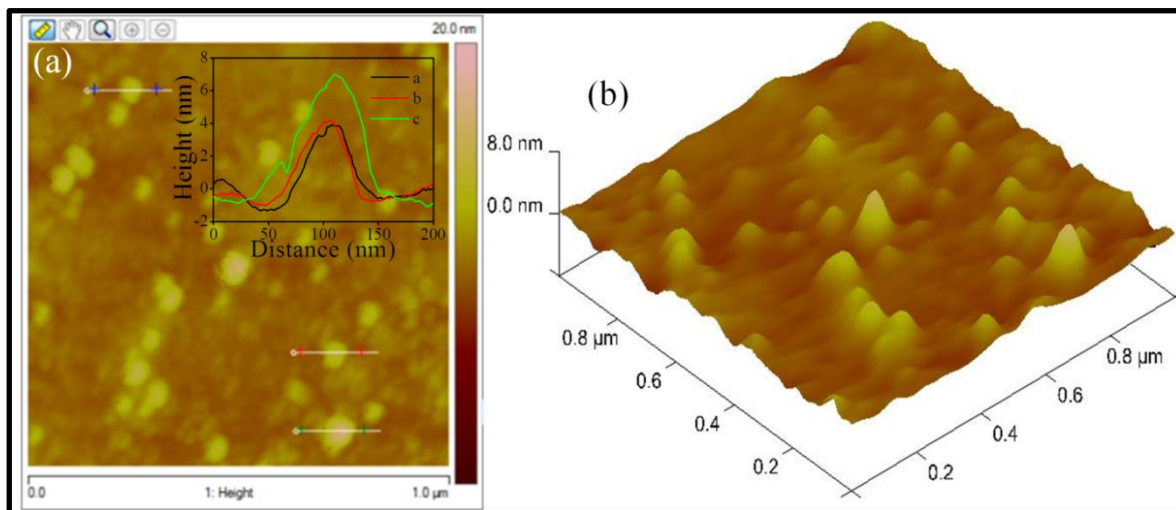
Figure 3.3: *The AFM image, (a) height image showing the presence of quasi-spherical ZnO NPs after 168 h of biomilling and (b) its 3D view.*[1]

3.4.3   The XRD Studies

To investigate the crystalline quality and crystalline phases of the precursor chemically synthesized ZnO NPs and the samples collected at different time intervals, the Powder X-ray diffraction (PXRD) pattern were carried out and presented in figure 3.4. The prominent peaks situated at 2θ values of 31.6^o, 34.2^o, 36.1^o, 47.3^o, 56.3^o, 62.7^o, 66.2^o, 67.5^o and 68.8^o correspond to the (100), (002), (101), (102), (110), (103), (200), (112) and (201) planes, respectively, and can readily be indexed to hexagonal wurtzite structure of ZnO (JCPDS card no. 36–1451).
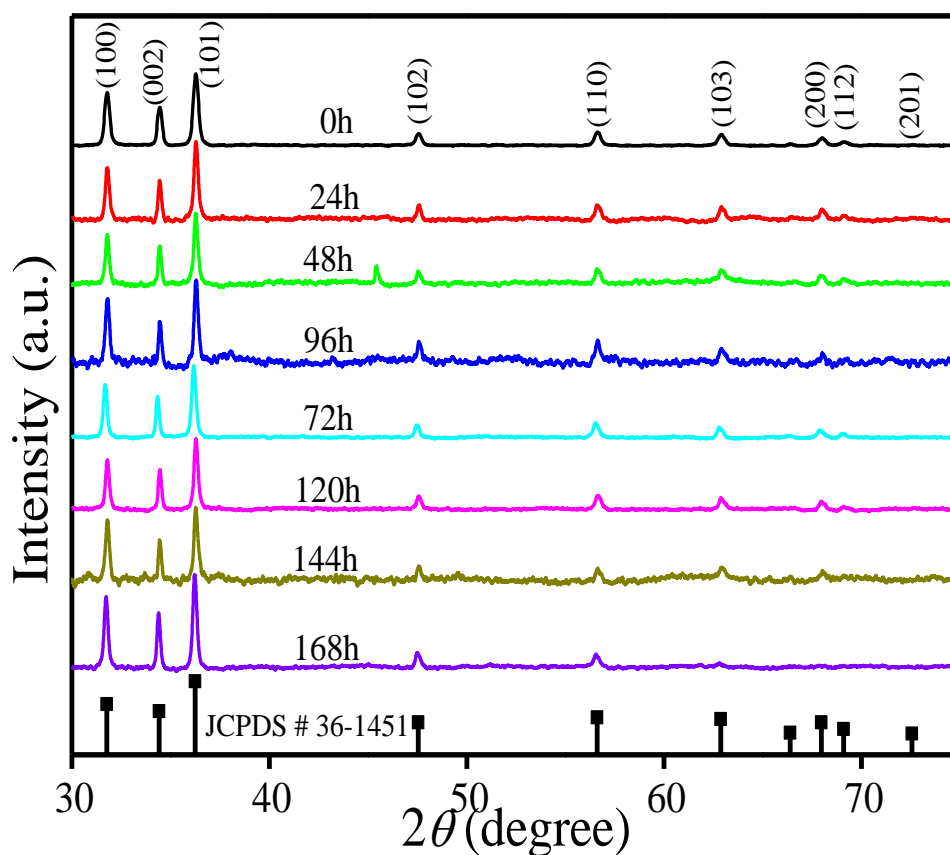
Figure 3.4: *The XRD patterns of ZnO NPs at different stages (0, 24, 48, 72, 96, 120, 144 and 168 h) of biomilling and was indexed to the JCPDS card no. 36–1451, depicted by black vertical lines.*[1]

The peak width is the measure of the crystallite size; broader the peak, smaller the crystallite size. In general, the crystallite size is proportional to the nanoparticle size. However, there was no significant change found in the relative peak intensities and peak widths, upon comparison of various XRD patterns. This was due to the fact that, after biomilling the crystallite size is remains the same, whereas, the particle size has decreased significantly. It suggest that breakdown of particles occur at grain boundaries. It is also possible that, not all the rod-shaped particles got biomilled into smaller quasi-spherical

particles and partially-biomilled/completely un-biomilled particles present in the sample may still contributes to the XRD signals. The effect of biomilling on the optical properties of ZnO NPs was studied by detailed UV-vis absorption and fluorescence emission spectroscopy measurements on the biomilled ZnO NPs taken out at a time interval of 24 h for a period of 168 h.

3.4.4   The Optical Properties of Biomilled ZnO NPs

UV-visible and photoluminescence spectroscopic studies were conducted to analyze the optical properties of the biomilled ZnO NPs.

The time-dependent changes in the UV-vis absorption spectra of the ZnO NPs after biomilling were shown in figure 3.5. It was noticed that most of the spectra show three characteristic features in the UV-vis range: (1) a broad absorption in the UV range centered at ~265 nm due to the π–π* transition in the aromatic amino acids containing coronal proteins,[47] (2) ~374 nm characteristic signature of ZnO NPs due to excitonic transition at room temperature,[48,49] and (3) ~400 nm (Soret band) due to the π–π* transition in porphyrin containing proteins.[50] The observed small shift in the ~265 nm peak with biomilling time was attributed to the dynamic nature of proteins binding to the ZnO NPs. Moreover, a small shift in the ~374 nm peak as a function of biomilling time was also observed which can be related to the change in the dielectric environment due to the change in the composition of coronal proteins.[51] The shift in ~374 nm peak with change in the size of particles cannot be attributed to the quantum size effect, because the mean diameter of particles after biomilling was~10 nm, which was higher than the reported excitonic Bohr diameter for ZnO (~6.5 nm).[52]

Further, the ratio of absorbance ~374 nm and ~265 nm (A374/265) was used to assess the relative concentration of ZnO NPs with respect to the concentration of proteins in the biomilled samples. It was observed that the ZnO NPs concentration with respect to protein concentration was increased almost linearly with time (Figure 3.5 inset).
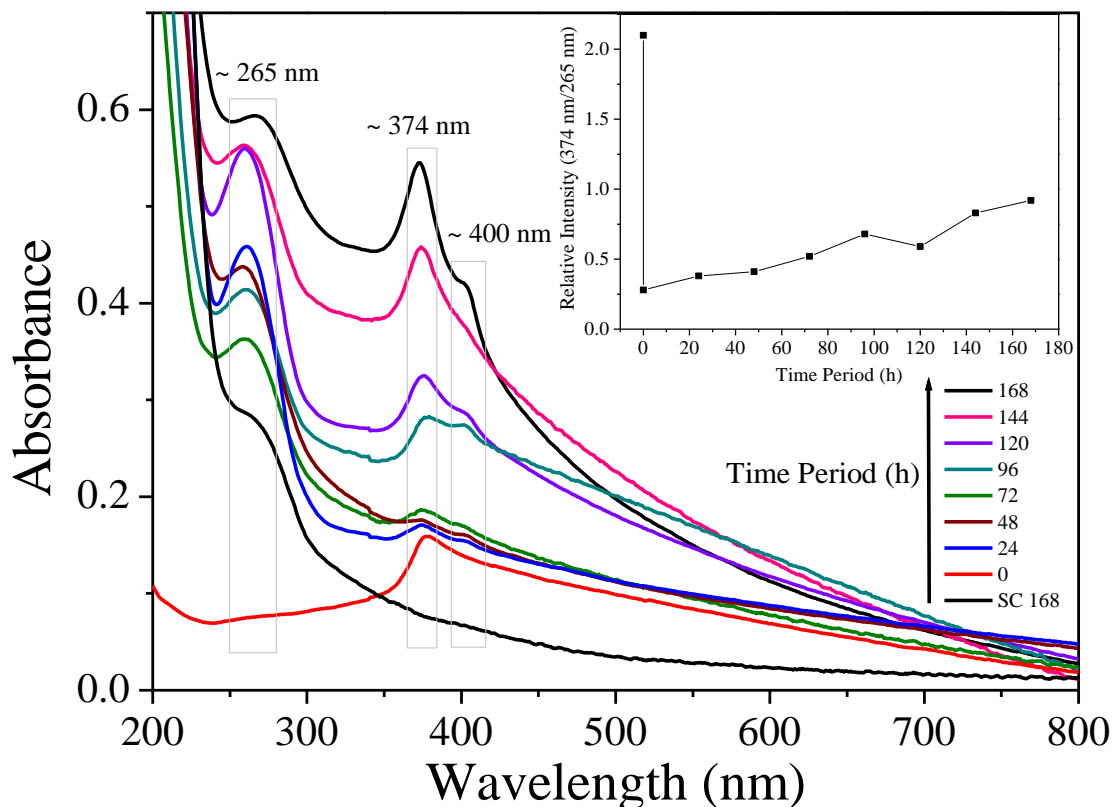
Figure 3.5: *A comparison of UV-visible spectra between the ZnO NPs at different stages of biomilling (0, 24, 48, 72, 96, 120, 144 and 168 h) and supernatant of S. cerevisiae culture after 168 h (without ZnO NPs, as negative control).*[1]

The PL results further supported the dynamic nature of coronal proteins (Figure 3.6). Generally, the PL spectrum of ZnO NPs show a narrow/strong peak in the UV region at ~ 370 nm, and broad/weak peak in the visible region at ~ 460 nm.[53] The PL peak in the UV range is assigned to near-band-edge transition (UV emission), which is due to the

photo-generated electron recombination with holes in the valence band. Whereas, the PL peak in the visible range is assigned to deep level emission and can be due to the recombination of an electron in singly occupied (deeply trapped) oxygen vacancy with a photo-generated hole in the valence band.[53] However, in our case, only one peak at ~ 380 nm was found which was consistent with many other reports in the literature.[33] However, there was no consistency in the change in the intensity of the PL peak of different biomilled samples. The reason can be the contribution of two major components in fluorescence: (a) fluorescence from ZnO NPs,[54] and (b) fluorescence from coronal proteins.[55] Both of these components were dynamic in nature i.e. decrease in the size of the ZnO NPs and change in the composition of protein corona as a function of biomilling time.
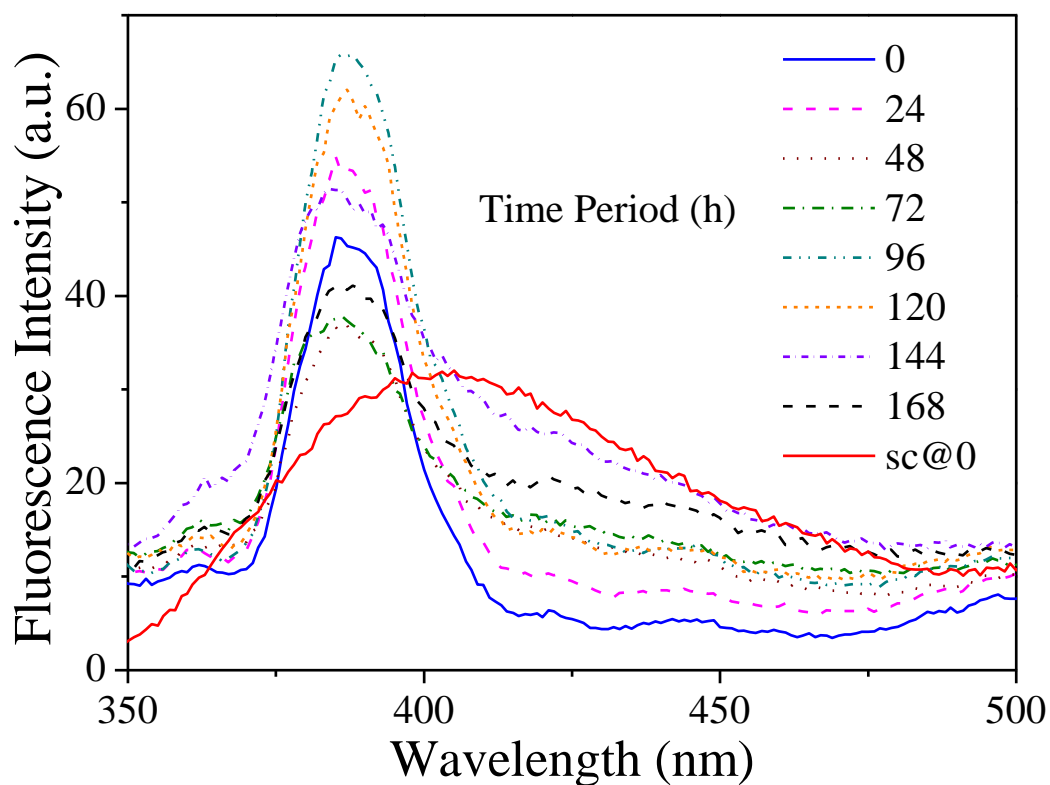
Figure 3.6: *A comparison between photoluminescence spectra of ZnO NPs after different stages of biomilling (0, 24, 48, 72, 96, 120, 144 and 168 h) and supernatant of S. cerevisiae culture after 168 h (without ZnO NPs, as control and represented by sc@0 h at an excitation wavelength of 325 nm.*[1]

3.4.5 The FTIR Studies

Binding study of proteins on the surface of biomilled ZnO NPs was performed by FTIR. The FTIR spectroscopic measurements were performed on all biomilled ZnO NPs samples to evaluate the binding of proteins with ZnO NPs as shown in figure 3.7.

Figure 3.7: *A comparison between FTIR spectra after ZnO NPs at different stages (24, 48,*
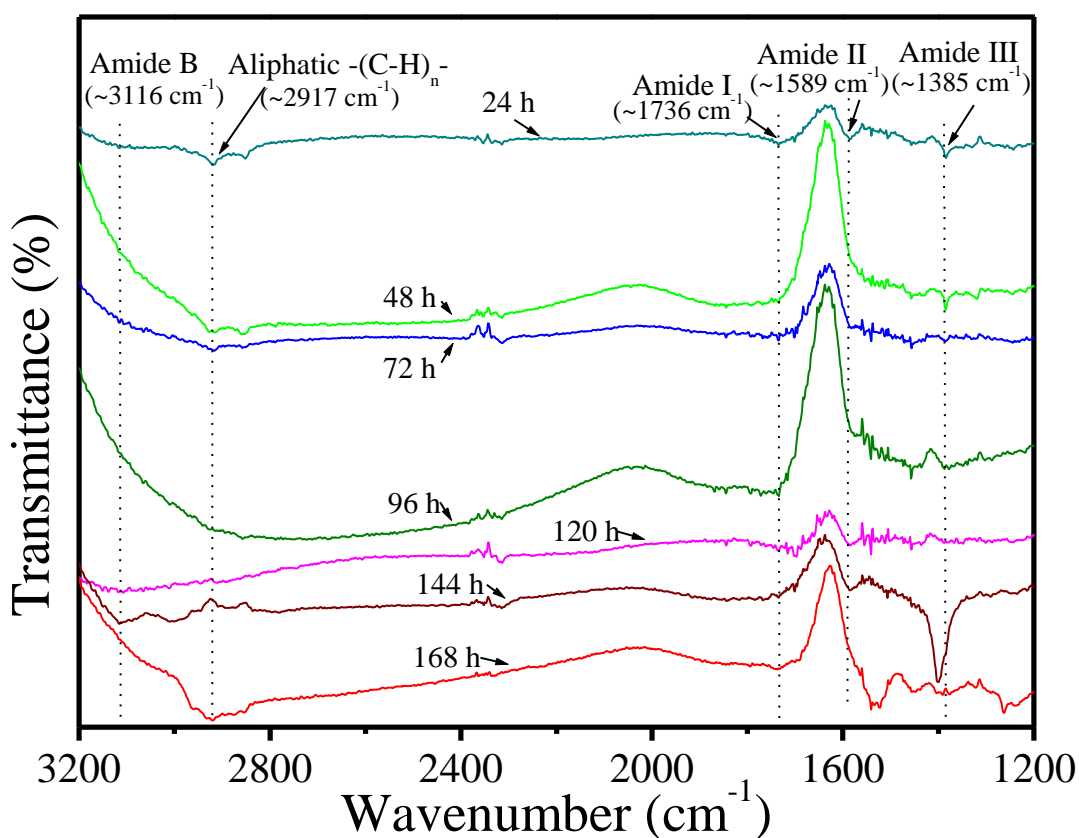
72, 96, 120, 144 and 168 h) of biomilling.[1]

The FTIR spectra of all the samples were shown the characteristic peak of proteins which was included the amide B, amide I, amide II, and amide III peaks, and was positioned around ~ 3116, 1736, 1589 and 1385 cm^{-1}, respectively.[56,57] However, the position and relative intensity of peaks were varied as a function of biomilling time, which

is related to the complex and dynamic nature of protein corona. These results further supported the dynamic nature of coronal proteins.

3.4.6 The Thermogravimetric Analysis

TGA analysis indicated the presence of protein corona on the biomilled ZnO nanoparticles. TGA analysis was performed on the chemically synthesized ZnO NRs and biomilled ZnO NPs to know the presence of proteins on the biomilled ZnO NPs. The percentage weight loss upon heating from RT to 750 ^{o}C was shown by Figure 3.8.
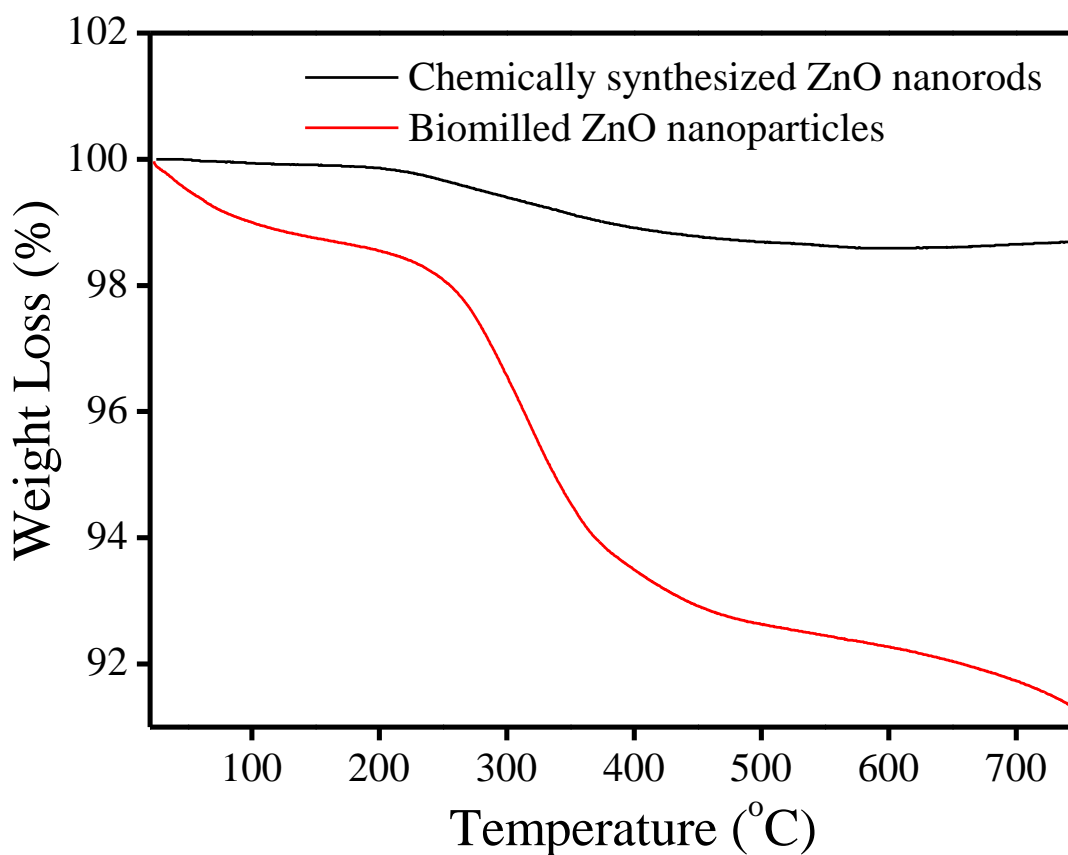
Figure 3.8: *A comparison between TGA curves for the chemically synthesized ZnO NRs (before biomilling, black) and biomilled ZnO NPs (after 168 h of biomilling, red).*[1]

It was noticed that the heating of biomilled ZnO NPs upto 400 ^{o}C leads to ~ 6.5% weight loss which was quite high in comparison to the weight loss (~ 0.5%) observed for

the chemically synthesized NRs and it was attributed to the loss of moisture and degradation of proteins.[58]

3.4.7   The Protein Expression Studies

In order to reveal the extracellular and intracellular protein expression profile as a function of biomilling time, sodium dodecyl sulphate-polyacrylamide gel electrophoresis (SDS–PAGE) (18%) was performed. The cells were harvested by centrifugation at 5000 rpm for 5 min at 4 ^{o}C, washed twice with normal saline. The intracellular protein was extracted from cells by using SDS and β-mercaptoethanol treatment. From the cell supernatant, the extracellular protein was extracted by precipitation with trichloroacetic acid (TCA). The protein samples were mixed in 1:1 ratio with 2X-loading buffer containing 4% SDS and 8% β-mercaptoethanol, were boiled for 5 min before loading to SDS-PAGE. We used standard molecular weight marker S8445 and M3913, obtained from Sigma Aldrich.

In order to gain deeper insight in to the mechanism of biomilling process, SDS-PAGE and ICP-OES analysis were performed to determine the intracellular and extracellular protein expression profile and aqueous zinc content in the cell and extracellular fluid, respectively, as a function of biomilling time. To study the expression profile of extracellular and intracellular proteins secreted by yeast, *S. cerevisiae* in the absence and presence of ZnO NPs as a function of biomilling time, SDS-PAGE analysis was performed. The expression profile of extracellular proteins in the absence and presence of ZnO NPs after every 48 h of time period such as 24 h, 72 h, 120 h and 168 h was shown in Figure 3.9.

It was observed that in presence of ZnO NPs, most of the proteins found to be under expressed. However, after 72 h of biomilling, two proteins with MW ~6.5 kDa and

~30 kDa were found to be over expressed. Furthermore, after 120 h of biomilling, only one protein with MW~39 kDa was found which was consistently present throughout the biomilling process and became more prominent at 168 h of biomilling.
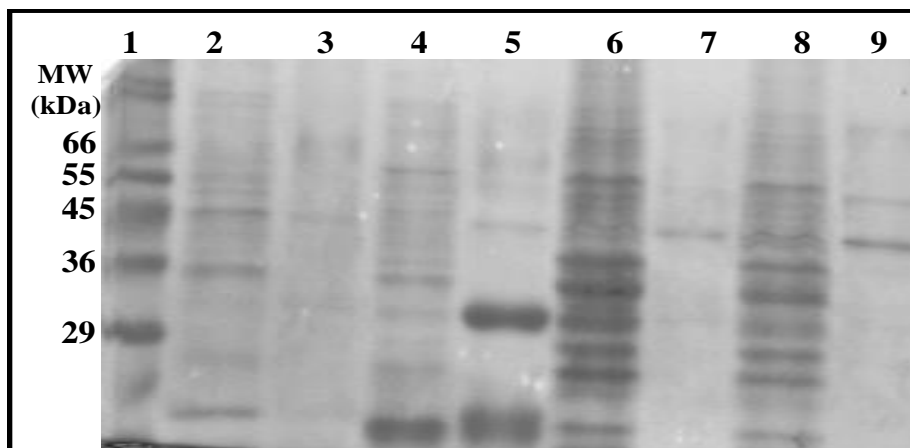
Figure 3.9: The SDS-PAGE data showing the extracellular protein expression profile. Column 1 shows marker S8445 protein bands ~ 66, 55, 45, 36 and 29 kDa from top to bottom. Columns 2, 4, 6, and 8 are for control samples and columns 3, 5, 7, and 9 are for test samples after 24, 72, 120 and 168 h, respectively.[1]

The expression profile of intracellular proteins in the absence and presence of ZnO NPs after every 48 h of time period was shown in the figure 3.10. It was observed that a protein with MW ~ 30 kDa showed increase in the expression with biomilling time and assumed to be related to the zinc transport in the yeast cells as zinc transporter.
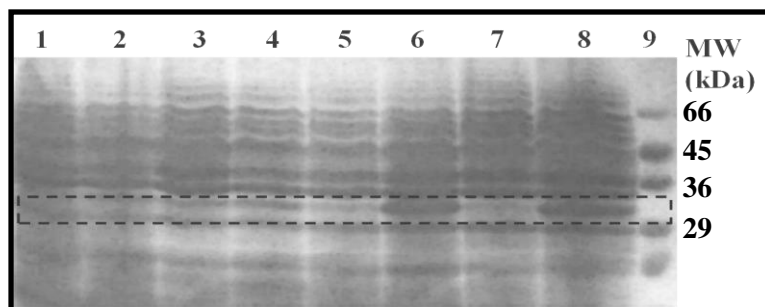
Figure 3.10: *SDS-PAGE data showing the intracellular protein expression profile. Columns 1, 3, 5, and 7 show control samples and columns 2, 4, 6, and 8 are for test samples after 24, 72, 120 and 168 h biomilling, respectively. Column 9 shows marker M3913 protein bands ~66, 45, 36 and 29 kDa from top to bottom.*[1]

3.4.8 Zinc Content Measurements

Inductively coupled plasma-optical emission spectroscopy (ICP-OES) was used to analyze the extracellular as well as intracellular zinc content as a function of biomilling time. For extracellular zinc content, the samples taken during biomilling were centrifuged at 10,000 rpm for 15 min at 4 ^{o}C. The as obtained supernatant was collected and filtered by nylon membrane filter paper with pore size of 0.2 μm before measuring the zinc content. The experiment was performed in duplicates. To analyze the intracellular zinc content, a modified method of Demirci[59,60] was used for sample preparation. Briefly, the *S. cerevisiae* cells were harvested by centrifugation at 5000 rpm for 5 min at 4 ^{o}C. The cells were washed twice with normal saline solution and allowed to dry. The cell dry mass of 100 mg were taken in a long neck flask and 5mL of conc. nitric acid was added and heated to 160 ^{o}C. Then, 2 mL of conc. sulphuric acid was added to it. To maintain the oxidizing environment, small amount of nitric acid was added till the solution gets colorless. After

cooling-down to RT, the deionized water was added to make the final volume 50 mL. The content was filtered with 0.2 μm pore size nylon membrane before measuring the zinc content by ICP-OES, model Spectro Arcos (ARCOS-FHS-12) from SPECTRO Analytical Instruments GmbH.

In order to analyze the change in concentration of extracellular and intracellular zinc content as a function of biomilling time, ICP-OES measurements were performed and presented in Figure 3.11. It was noticed from that at 0 h, zinc content in the extracellular fluid was found almost negligible whereas, it was ~1 mg L^{-1} for intracellular zinc content. After 24 h, the extracellular zinc content was increased to ~0.25 mg L^{-1} and remains almost constant up to 72 h. However, in the same time, the intracellular zinc content was continuously increased to ~18.4 mg L^{-1}. After 96 h, the extracellular zinc content was increased by 10 times to ~2.75 mg L^{-1} and can be related to the release of zinc from the cells which lead to decrease in the intracellular zinc content to ~14.5 mg L^{-1}. The intracellular zinc content was further decreased to its minimum level ~6.9 mg L^{-1}. However, the exact reason behind the decrease in the intracellular zinc content is not known. It was observed that after 120 h, the extracellular zinc content was further decreased to~1.25 mg $L^{-1}$and ~0.75 mg L^{-1} for 144 h of biomilling. Therefore, it is concluded that in the course of biomilling, yeast cells maintain the zinc content almost same in the extracellular fluid.
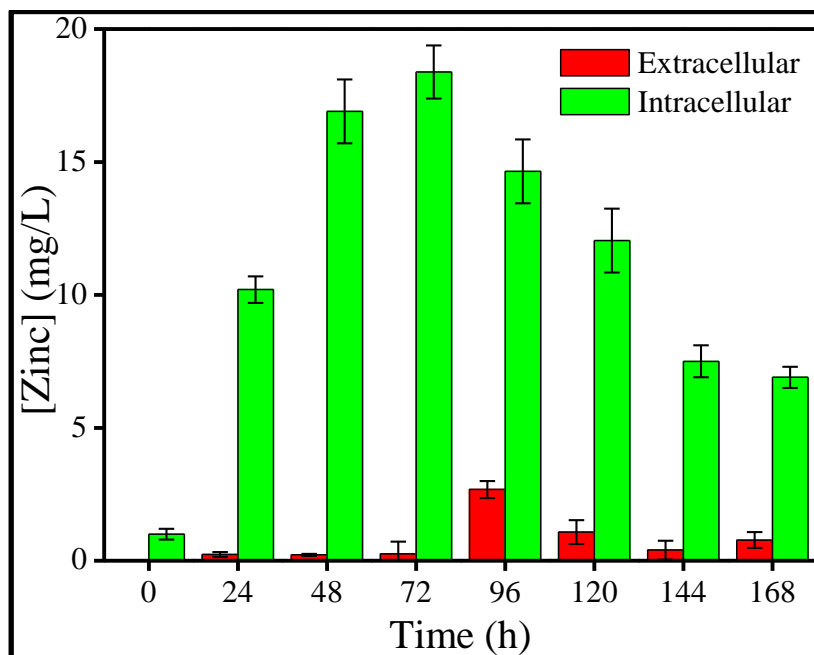
Figure 3.11: *The extracellular (red color) and intracellular (green color) zinc content at different stages (24, 48, 72, 96, 120, 144 and 168 h) of biomilling.*[1]

3.4.9   Zeta Potential Measurement

It is known that the yeast *S. cerevisiae* secretes a fair amount (few µg mL^{-1}) of proteins in the extracellular medium [61] which was also observed in our SDS-PAGE study. Some of these extracellular proteins may get attached to the positively charged ZnO NRs by electrostatic interaction and can form the protein corona. The change in the surface charge from ~ (+)12.3 mV for chemically synthesized NRs (at 0 h) to ~ (-)29.5 mV (after 24 h) for biomilled ZnO NPs was observed in our zeta potential study (Figure 3.12) which indicates the attachment of proteins to the surface of ZnO NPs. These proteins may act as chelating agents and leach-out the zinc ions.
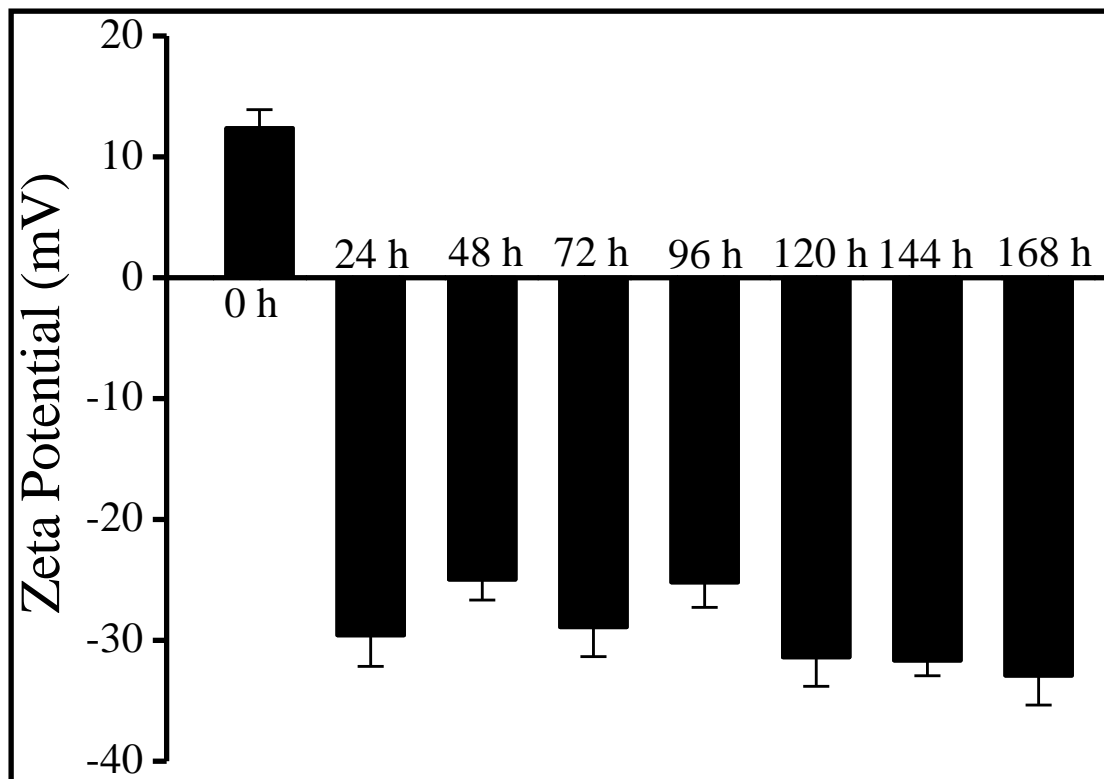
Figure 3.12: *Zeta potential study of various ZnO NP samples before and after different stages (24, 48, 72, 96, 120, 144 and 168 h) of biomilling.*[1]

3.4.10 **The Dispersibility of Nanoparticles in Aqueous Solvents**

The dispersibility of the biomilled ZnO NPs in the aqueous medium was compared with the chemically synthesized ZnO NRs and was shown in Figure 3.13. After 2 h, the absorbance at 374 nm was decreased by 10% for the biomilled ZnO NPs and 80% for chemically synthesized ZnO NRs. Further, the stability of both NPs suspension was compared at different time periods and biomilled ZnO NPs were found to be highly stable in aqueous suspension for a long time (Figure 3.13, inset).
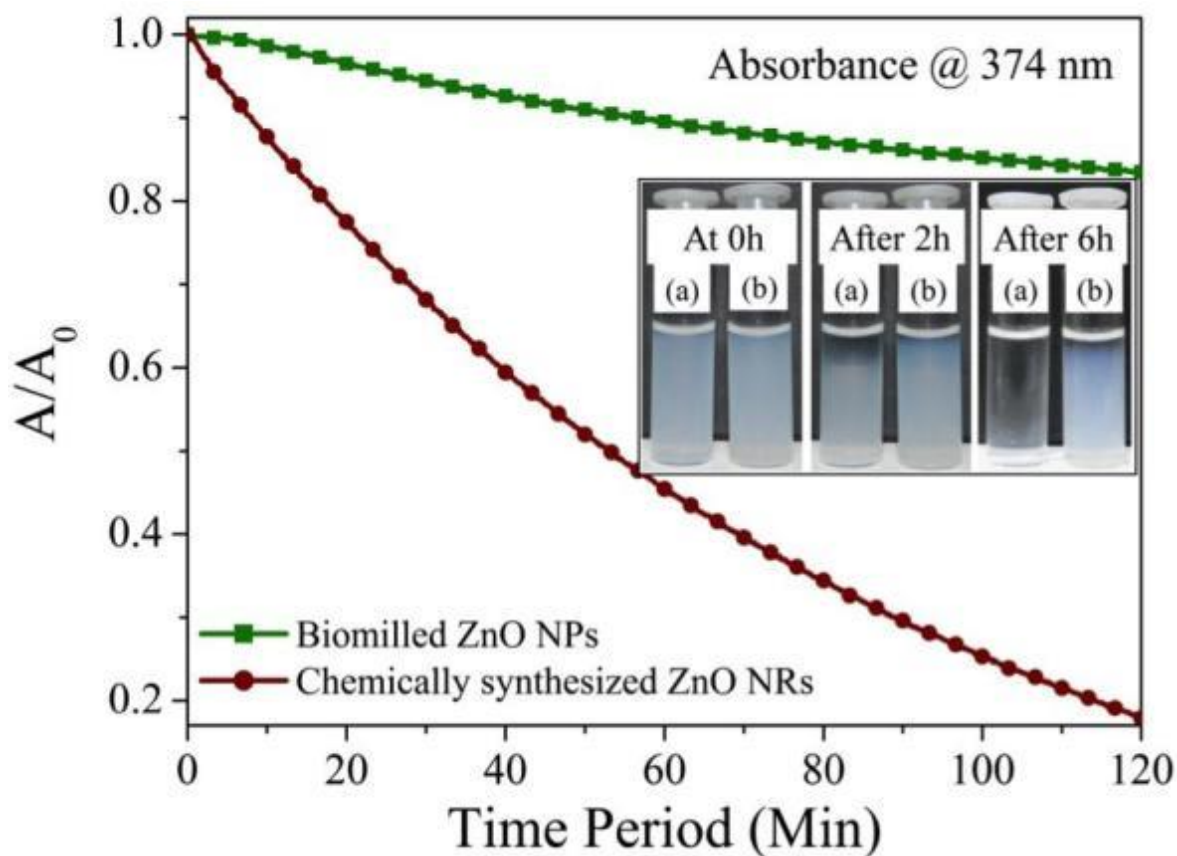
Figure 3.13: Dispersibility of the ZnO NPs in an aqueous medium as a function of time. Inset shows the stability of (a) the chemically synthesized ZnO NPs and (b) the biomilled ZnO NPs in aqueous suspension at different time periods of 0 h, 2 h and 6 h.[1]

3.5 Conclusion

In biomilling process, yeasts secrete a number of proteins. Some of these protein molecules interact with the particles in oreder to break it down to quasi-spherical nanoparticles. During this process the zinc ions leached-out ions can be taken up by yeast cells and stored in the vacuole, as it is the major site for zinc storage in the yeast cells.[62] The yeast *S. cerevisiae* is very well studied organism for zinc transport and trafficking.[25] This was also evident from our ICP-OES study that a higher amount of zinc content present inside the cells as compared to the extracellular zinc content. Therefore, we believe that the yeast

cells play an important role in the biomilling by secreting the proteins as well as maintaining the zinc content almost same in the extracellular fluid throughout the biomilling process

We have successfully developed a modified-biomilling process to transform the chemically synthesized ZnO NRs to protein capped quasi-spherical ZnO NPs at room temperature in a process spontaneously driven by *S. cerevisiae* as a stress response. Detailed time-dependent TEM and XRD studies have indicated the formation of quasi-spherical ZnO NPs with the size ~10 nm, and it has further confirmed by AFM study. UV-vis, PL and FTIR studies have shown the dynamic nature of protein corona as a function of biomilling time. Zeta potential study exhibited the abrupt change in the surface charge onto the NPs from ~+12.3 mV (for chemically synthesized NRs, at 0 h) to ~-29.5 mV (for biomilled ZnO NPs, after 24 h) which indicated the adherence of negatively charged protein molecules to the positively charged surface of ZnO NRs by electrostatic forces and formation of multiple layers of proteins. TGA analysis has also supported the presence of protein molecules with the biomilled ZnO NPs. The time dependent extracellular and intracellular protein expression profile by SDS-PAGE analysis has shown the over-expression of three different extracellular proteins with MW ~6.5 kDa, ~30 kDa and ~39 kDa; and one intracellular protein with MW ~ 30 kDa (assumed to be related to the zinc transport in the yeast cells), at different stages of biomilling. Moreover, the ICP-OES study has shown the accumulation of higher amount of zinc inside the cells in comparison to the extracellular fluid. Therefore, it is supposed that the yeast cells play an important role in biomilling by secreting the proteins as well as maintaining the zinc content almost same as in the extracellular fluid. Moreover, the biomilled ZnO NPs have shown higher

dispersibility and stability in aqueous medium than chemically synthesized ZnO NRs. However, there is further scope to explore the exact mechanism behind the biomilling process and the fate of biomilled nanoparticles upon interaction with biological systems. It is believed that this study will be of great potential applications in biology field because of its green biological approach and ability to synthesize water dispersible and stable protein-capped quasi-spherical ZnO NPs.

3.6   References

1   C. Sharan, P. Khandelwal and P. Poddar, *RSC Adv.*, 2015, **5**, 1883–1889.

2   R. R. Naik, S. J. Stringer, G. Agarwal, S. E. Jones and M. O. Stone, *Nat. Mater.*, 2002, **1**, 169–72.

3   C. Tamerler and M. Sarikaya, *Acta Biomater.*, 2007, **3**, 289–299.

4   K. Simkiss and K. Wilbur, *Biomineralization*, Academic Press New York, 1989.

5   C. Solisio, A. Lodi and F. Veglio, *Waste Manag.*, 2002, **22**, 667–675.

6   V. Bansal, A. Sanyal, D. Rautaray, A. Ahmad, M. Sastry, B. V. Bansal, A. Sanyal, V. Bansal and A. Sanyal, *Adv. Mater.*, 2005, **17**, 889–892.

7   A. Sanyal, D. Rautaray, V. Bansal, A. Ahmad and M. Sastry, *Langmuir*, 2005, **21**, 7220–7224.

8   V. Bansal, A. Ahmad and M. Sastry, *J. Am. Chem. Soc.*, 2006, **128**, 14059–14066.

9   P. V. Kazakevich, A. V. Simakin, V. V. Voronov and G. A. Shafeev, *Appl. Surf. Sci.*, 2006, **252**, 4373–4380.

10   P. Khandelwal, D. K. Singh, S. Sadhu and P. Poddar, *Chempluschem*, 2014, **79**, 134–142.

11   D. K. Singh, R. Jagannathan, P. Khandelwal, P. M. Abraham and P. Poddar,

Nanoscale, 2013, **5**, 1882–1893.

12 Z. R. Tian, J. a Voigt, J. Liu, B. McKenzie, M. J. McDermott, M. a Rodriguez, H. Konishi and H. Xu, *Nat. Mater.*, 2003, **2**, 821–826.

13 B. Mazumder, I. Uddin, S. Khan, V. Ravi, K. Selvraj, P. Poddar and A. Ahmad, *J. Mater. Chem.*, 2007, **17**, 3910–3914.

14 I. Uddin, A. Jaiswal and P. Poddar, *Int. J. Innov. Biol. Reaserch*, 2013, **2**, 1–5.

15 I. Uddin, P. Poddar, U. Kumar and N. Phogat, *J. Green Sci. Technol.*, 2013, **1**, 48–53.

16 S. Rani, P. Suri, P. K. Shishodia and R. M. Mehra, *Sol. Energy Mater. Sol. Cells*, 2008, **92**, 1639–1645.

17 Y. Ni, X. Cao, G. Wu, G. Hu, Z. Yang and X. Wei, *Nanotechnology*, 2007, **18**, 155603.

18 S. Polarz, A. Roy, M. Merz, S. Halm, D. Schroder, L. Schneider, G. Bacher, F. Kruis and M. Driess, *Small*, 2005, **1**, 540–592.

19 Y. Ni, X. Wei, J. Hong and Y. Ye, *Mater. Sci. Eng. B*, 2005, **121**, 42–47.

20 Y. Ni, S. Yang, J. Hong and P. Zhen, *Scr. Mater.*, 2008, **59**, 127–130.

21 S. M. Mahpeykar, J. Koohsorkhi and H. Ghafoori-fard, *Nanotechnology*, 2012, **23**, 165602.

22 C. Sharan, P. Khandelwal and P. Poddar, *RSC Adv.*, 2015, **5**, 91785–91794.

23 M. Batic, D. Lenarcic, J. Stupar, P. Raspor, M. Batic, D. Lenarcic, J. Stupar and P. SRaspor, *J. Rapid Methods Autom. Microbiol.*, 1996, **4**, 265–278.

24 V. Stehlik-tomas, V. G. Zeti, D. Stanzer and S. Grba, *food Technol. Biotechnol.*, 2004, **42**, 115–120.

25   D. J. Eide, *Biochem. Biophys. Acta*, 2006, **1763**, 711–722.

26   C. W. Macdiarmid, L. A. Gaither and D. Eide, *EMBO J.*, 2000, **19**, 2845–2855.

27   C. W. MacDiarmid, M. A. Milanick and D. J. Eide, *J. Biol. Chem.*, 2002, **277**, 39187–39194.

28   Biotechnology Program under the Toxic Substances Control Act (TSCA), http://www.epa.gov/biotech_rule/pubs/fra/fra002.htm

29   M. Kandpal, C. Sharan, P. Poddar, K. Prashanthi, P. R. Apte and V. Ramgopal Rao, *Appl. Phys. Lett.*, 2012, **101**, 104102.

30   Samuel M Soosen, L. Bose and G. Kc, *Acad. Rev.*, 2009, **16**, 57–65.

31   Y. Ma, *J. Wide Bandgap Mater.*, 2002, **10**, 113–120.

32   W.-J. Huang, G.-C. Fang and C. Wang, *Coloidal Surfaces A*, 2005, **260**, 45–51.

33   A. Khan and M. E. Kordesch, *Phys. E*, 2005, **30**, 51–54.

34   S. H. Ko, D. Lee, H. W. Kang, K. H. Nam, J. Y. Yeo, S. J. Hong, C. P. Grigoropoulos and H. J. Sung, *Nano Lett.*, 2011, **11**, 666–671.

35   K. S. Leschkies, R. Divakar, J. Basu, E. Enache-pommer, J. E. Boercker, C. B. Carter, U. R. Kortshagen, D. J. Norris and E. S. Aydil, *Nano Lett.*, 2007, **7**, 1793–1798.

36   A. B. F. Martinson, J. W. Elam, J. T. Hupp, M. J. Pellin, N. U. V, S. Road and E. V, *Nano Lett.*, 2007, **7**, 2183–2187.

37   N. K. Zayer, R. Greef, K. Rogers, A. J. C. Grellier and C. N. Pannell, *Thin Solid Films*, 1999, **352**, 179–184.

38   M. H. Huang, *Science (80-.).*, 2001, **292**, 1897–1899.

39   K. Vanheusden, W. L. Warren, C. H. Seager, D. R. Tallant, J. a. Voigt and B. E.

Gnade, *J. Appl. Phys.*, 1996, **79**, 7983.

40   M. Willander, O. Nur, S. Zaman, A. Zainelabdin, N. Bano and I. Hussain, *J. Phys. D. Appl. Phys.*, 2011, **44**, 224017.

41   N. Salah, S. S. Habib, Z. H. Khan, A. Memic, A. Ajam, E. Alarfaj, N. Zahed and S. Al-Hamedi, *Int. J. Nanomedicine*, 2011, **6**, 863–869.

42   N.-H. Cho, T.-C. Cheong, J. H. Min, J. H. Wu, S. J. Lee, D. Kim, J.-S. Yang, S. Kim, Y. K. Kim and S.-Y. Seong, *Nat. Nanotechnol.*, 2011, **6**, 675–682.

43   C. Hanley, J. Layne, A. Punnoose, K. M. Reddy, I. Coombs, A. Coombs, K. Feris and D. Wingett, *Nanotechnology*, 2008, **19**, 295103.

44   S. Tenzer, D. Docter, J. Kuharev, A. Musyanovych, V. Fetz, R. Hecht, F. Schlenk, D. Fischer, K. Kiouptsi, C. Reinhardt, K. Landfester, H. Schild, M. Maskos, S. K. Knauer and R. H. Stauber, *Nat. Nanotechnol.*, 2013, **8**, 772–81.

45   A. Salvati, C. Åberg, K. A. Dawson, M. P. Monopoli, C. Åberg, A. Salvati, K. A. Dawson, C. Aberg, A. Salvati and K. A. Dawson, *Nat. Nanotechnol.*, 2012, **7**, 779–786.

46   A. Jain, R. Bhargava and P. Poddar, *Mater. Sci. Eng. C*, 2013, 1247–1253.

47   E. Casals, T. Pfaller, A. Duschl, G. J. Oostingh and V. Puntes, *ACS Nano*, 2010, **4**, 3623–3632.

48   Ü. Özgür, Y. I. Alivov, C. Liu, A. Teke, M. A. Reshchikov, Ü. Özgür, Y. I. Alivov, C. Liu, A. Teke, M. A. Reshchikov, S. Do and V. Avrutin, *Appl. Phys. Lett.*, 2005, **98**.

49   A. B. Djurišić, Y. H. Leung, A. B. Djurisić and Y. H. Leung, *Small*, 2006, **2**, 944–61.

50   R. J. P. Williams, *Chem. Rev.*, 1956, **56**, 299–328.

51   A. K. Bhunia, P. K. Samanta, S. Saha and T. Kamilya, *Appl. Phys. Lett.*, 2013, **143701**.

52   S. Dhara and P. K. Giri, *Appl. Nanosci.*, 2011, **1**, 165–171.

53   H.-M. Xiong, *J. Mater. Chem.*, 2010, **20**, 4251.

54   L. Irimpan, V. P. N. Nampoori, P. Radhakrishnan, A. Deepthy and B. Krishnan, *J. Appl. Phys.*, 2007, **102**, 063524.

55   J. T. Vivian and P. R. Callis, *Biophys. J.*, 2001, **80**, 2093–109.

56   E. Fonseca, S. Fábia and H. Sander, 2006, **9**, 185–191.

57   K. K. Chittur, *Biomaterials*, 1998, **19**, 357–69.

58   U. Kumar, A. Shete, A. S. Harle, O. Kasyutich, W. Schwarzacher, A. Pundle and P. Poddar, *Chem. Mater.*, 2008, **20**, 1484–1491.

59   A. Demirci and A. L. Pometto, *J. Agric. Food Chem.*, 1999, **47**, 2491–2495.

60   A. R. Shet, L. R. Patil, V. S. Hombalimath, A. Deepak and B. B. Udapudi, *Biotechnol. Bioinf. Bioeng*, 2011, **1**, 523–527.

61   W. J., J. Dorfman, B. Soller and A. Friedmann, *Antonie Van Leeuwenhoek*, 1981, **47**, 193–207.

62   C. Simm, B. Lahner, D. Salt, A. Lefurgey, P. Ingram, B. Yandell and D. J. Eide, *Am. Soc. Microbiol.*, 2010, **6**, 1166–1177.

Chapter IV

The Mechanistic Insight into the Biomilling of Metal Oxy-Hydroxide Nanoparticles

In this chapter, the mechanistic insight of biomilling for a gradual transformation of anisotropic α-FeOOH rod-shaped nanoparticles into quasi-spherical nanoparticles below 10 nm size has been explored. The detailed UV-vis spectroscopy, transmission electron microscopy, atomic force microscopy, X-Ray diffraction, FTIR and X-ray photoelectron spectroscopic studies suggested that aquo group present at the α-FeOOH surface may provide the site for interaction with carboxyl ions of protein molecules which results in the formation of a stable coordination bonds with the surface Fe^{3+} ions and leads to leaching of the cations. This process will exposes another layer of Fe^{3+} ions on the surface of lattice which leads to the repetition of the process of protein complexation with Fe^{3+} ion and dissociation of complex from lattice. This causes the fragmentation of bigger nanoparticles into protein functionalized smaller nanoparticles.

A part of the work presented in this chapter is published.[1]

4.1   Introduction

The oxides, hydroxides and oxy-hydroxides of iron, which are collectively referred as iron oxides, are abundant in nature and found globally. Human beings have been using iron since the 'Iron Age'. Iron readily oxidizes in the presence of water to form various Fe_2O_3 and $FeO(OH)$ polymorphs (α, β, γ, δ, ε-Fe_2O_3/$FeOOH$). The α and γ polymorphs of Fe_2O_3 are known as hematite and maghemite, respectively and have many applications such as catalyst in Haber process, Fischer-Tropsch synthesis, water-gas-shift reaction, dehydration of ethyl benzene to styrene, vapor phase oxidation of alcohol to aldehyde and ketones,[2] decomposition of hydrogen peroxides,[3] lithium ion batteries,[4] gas sensors[5] etc.

Different forms of iron oxides are also extensively used in paint industries because of their different colors such as hematite for red, maghemite for brown, and magnetite for black.[6,7] The maghemite (γ-Fe_2O_3) and magnetite (Fe_3O_4) being magnetic, they have been extensively researched and used in magnetic data storage devices,[8,9,10] magnetic resonance imaging (MRI),[11] hyperthermia,[12] targeting and visualizing tumor,[13] drug delivery[14,15] etc. The β-$FeOOH$ (akaganeite) nanoparticles coated with various carbohydrate shells are being used for the treatment of hyperphosphatemia in dialysis patients and as intravenous and oral supplements for iron deficiency.[16]

Iron plays an important role in life-cycle of living beings as it serves both as an electron donor and an acceptor in redox reactions (heme-proteins of respiratory chain), for transport of oxygen (hemoglobin), cofactor for hundreds of proteins and enzymes, therefore, the cells have a developed mechanism to extract iron from various sources. However, free ionic form of iron is toxic and can damage the cellular organelles and even can lead to the death and hence cells utilize various ways, including few enzymes, that

neutralize the ionic form of iron and transport into the cell to store, in nontoxic form, inside ferritin protein cage.[17,18] Some organisms evolved to bio-mineralize the iron and utilize for their well-being. A fascinating example is magneto-tactic bacterium, which forms magnetic iron in a specialized organelle called magnetosome, which are responsible for the synthesis of long chain of magnetic nanoparticles of magnetite (Fe_3O_4) and less commonly greigite (Fe_3S_4). These magnetosomes arrange in the intracellular chain and facilitate bacterium to swim in response to the external magnetic field, this behavior is known as 'magnetotaxis'.[19,20]

People have reported the use of microbes for synthesis of iron oxide nanoparticles both by extracellular as well as intracellular ways because of their high surface area-to-volume ratio and the presence of charged chemical groups on the cell surface which is responsible for the potent mineral-nucleating ability of these cells.[21] Another way is a biomimetic synthesis of iron oxide nanoparticles through ferritin; a universal protein, which concentrates Fe and store it to maintain the intracellular iron level.[22,23] the microbes, proteins and drug molecules have been used for the synthesis of nanomaterials, through various methods such as biosynthesis,[24,25,26,27] bioleaching,[28,29] biotransformation,[30] enzymatic synthesis[31,32] etc.

There are numerous chemical methods available for the synthesis of rod or needle-shaped α-FeO(OH) nanoparticles with diameter approximately 30–50 nm and length 200–300 nm,[33,34,35,36] but very few reports are available for the synthesis of nanoparticles with spherical geometry and size less than 10 nm.[37,38] These small nanoparticles would be of great importance, especially for the purpose where specifically high surface area is required, for example, in catalysis, heavy metal removal from water etc. In this chapter, we

present an eco-friendly way of size reduction from anisotropic goethite particles to, quasi-spherical nanoparticles with size less than 10 nm.

4.2   The Model System to Study Biomilling of Metal Oxy-hydroxides

The goethite (α-FeOOH) is one of the most abundant forms of metal oxy-hydroxide, found globally. It was named after Johann Wolfgang von Goethe, in 1815. It is thermodynamically most stable iron oxide at ambient temperature. It is dark brown to black color when present in massive crystal aggregate whereas, it is yellow in powder form. It is also primarily responsible for the color of various rocks, soils and mineral ore deposits.[39]

It is the most common hydroxide which exhibits orthorhombic symmetry. It has three-dimensional structure build up with $FeO_3(OH)_3$ octahedral which form large tunnels spreading out along [010] direction. The (110) is a dominant face of goethite comprising about 80–95 % of crystal surface and is most prominent than other faces.[40,41] Each octahedron is linked to eight neighboring octahedral with four edges and three vertices.[34] The hydrated form of goethite {$FeO(OH).nH_2O$} is known as yellow iron oxide which has widely used in pigments and humidity sensing.[33] It has also used as the precursor for the synthesis of α-Fe_2O_3 (hematite)[33] because of its property to retain its original architecture upon transformation at elevated temperature into the oxide form.[42] The nano-sized iron oxide commonly applied for the removal of heavy metals Pb, Zn, Cu, Cd, Cr etc. from water/waste water include goethite α-FeO(OH), hematite (α-Fe_2O_3) amorphous hydrous Fe oxides, maghemite (γ-Fe_2O_3), magnetite (Fe_3O_4) and iron/iron oxide ($Fe@Fe_xO_y$).[43] The environment-friendly, nontoxicity, high stability in aqueous suspension and negligible risk of secondary contamination attract these materials for various applications.

4.3   Experimental Section

4.3.1   Materials

All chemicals were of analytical grade and used as-received without any further purification unless otherwise described. Dextrose monohydrate (AR grade), mycological peptone (certified), yeast extract powder (type I), malt extract powder were purchased from Himedia Laboratories. Dialysis tubing made of cellulose membrane (average flat width 33 mm, D 9652) was purchased from Sigma Aldrich. Ferric chloride hexahydrate ($FeCl_3 \cdot 6H_2O$), ferrous chloride tetrahydrate ($FeCl_2.4H_2O$), and hydrochloric acid (HCl) were purchased from Thomas Baker. Urea $[(CO(NH_2)_2]$ (GR grade), was purchased from Loba Chemie Pvt. Ltd. Acetone $[(CH_3)_2CO]$ (HPLC grade) purchased from Ranchem, RFCL Ltd. All glassware were washed with aqua-regia ($HCl/HNO_3 = 3:1$) carefully and were rinsed with double-distilled water before using for the reaction.

4.3.2   Chemical Synthesis of α-FeO(OH) Nanorods

We have synthesized the α-FeO(OH) nanorods by a low temperature, surfactant free route.[33] The $FeCl_3 \cdot 6H_2O$ and $FeCl_2.4H_2O$ were dissolved in 2 M HCl to make a final concentration of 1 M and 2 M, respectively. The solution temperature was increased to around 70 °C followed by the drop-wise addition of 2 M urea till the solution become slightly alkaline. The reaction mixture was allowed to precipitate. The obtained product was filtered and washed multiple times with deionized water and subsequently by acetone.[33]

4.3.3 Biomilling of α-FeO(OH) Nanorods

The *Saccharomyces cerevisiae* (NCIM No 3064) culture was obtained from National Collection of Industrial Microorganisms (NCIM) situated at CSIR-National Chemical Laboratory, Pune, India and grown in 500 mL Erlenmeyer flasks containing malt extract 3 g/L, D-glucose 10 g/L, yeast extract 3 g/L and mycological peptone 5 g/L in 200 mL double distilled water, incubated in shaker at 150 rpm and 28 ^{o}C temperature. At log phase of growth, the culture was harvested by centrifugation at 5000 rpm for 5 min at 4 ^{o}C, washed thrice with autoclaved double distilled water and transferred to sterilized Erlenmeyer flask contained a dialysis bag with 7.5 mg α-FeO(OH) nanorods suspended in 15 mL double distilled water. The samples were then incubated at 28 ^{o}C under shaking at 150 rpm. The aliquots were collected at every 24 h in sterilized condition and used for further characterization. The control sample (designated as 0 h) has not been interacted with the culture, but gone through the same treatment for 120 h.

4.4 Results and Discussion

4.4.1 The TEM Studies

The successive breakdown of chemically synthesized α-FeO(OH) nanorods in the biomilling process was imaged by transmission electron microscopy and atomic force microscopy techniques. For this purpose, the chemically synthesized α-FeO(OH) nanorods were added in yeast cell suspension (which did not supplement with culture media) and the samples were collected at successive time intervals. The TEM analysis of as-synthesized α-FeO(OH) nanoparticles exhibited the well-defined rod-shaped particles with the length from ~200 to 400 nm and diameter ~30 nm which is shown in figure 4.1 A. Initially, the change in the particle morphology was not significant but as the time progresses, these rod-

shaped particles were found to be covered with a thick amorphous protein layer. After 96 h, each particle was completely encapsulated by proteins as observed through a low contrast around nanorods in TEM image (figure 4.1D). At this stage, nanoparticles were fully covered with a thick amorphous protein matrix and the degradation of rods was observed. After 120 h, the as-synthesized nanorods were transformed to quasi-spherical nanoparticles with size below 10 nm as shown in figure 4.1E. The dark field imaging of the area corresponding to figure 4.1E was performed to clearly distinguish the encapsulated amorphous protein around biomilled nanoparticles were shown in figure 4.1 F, and the magnified view were shown in figure 4.1G, for better visibility the nanoparticle. The SAED pattern corresponding to figure 4.1E is shown in the figure 4.1H, which indicates the crystalline nature (bright spots) of biomilled nanoparticles, however, the diffused ring pattern can be attributed to the amorphous nature of protein corona around nanoparticles.[44] The SAED pattern was indexed according to (111) and (151) reflections of α-FeO(OH) on the basis of their d-spacing of 2.44 Å and 1.56 Å.
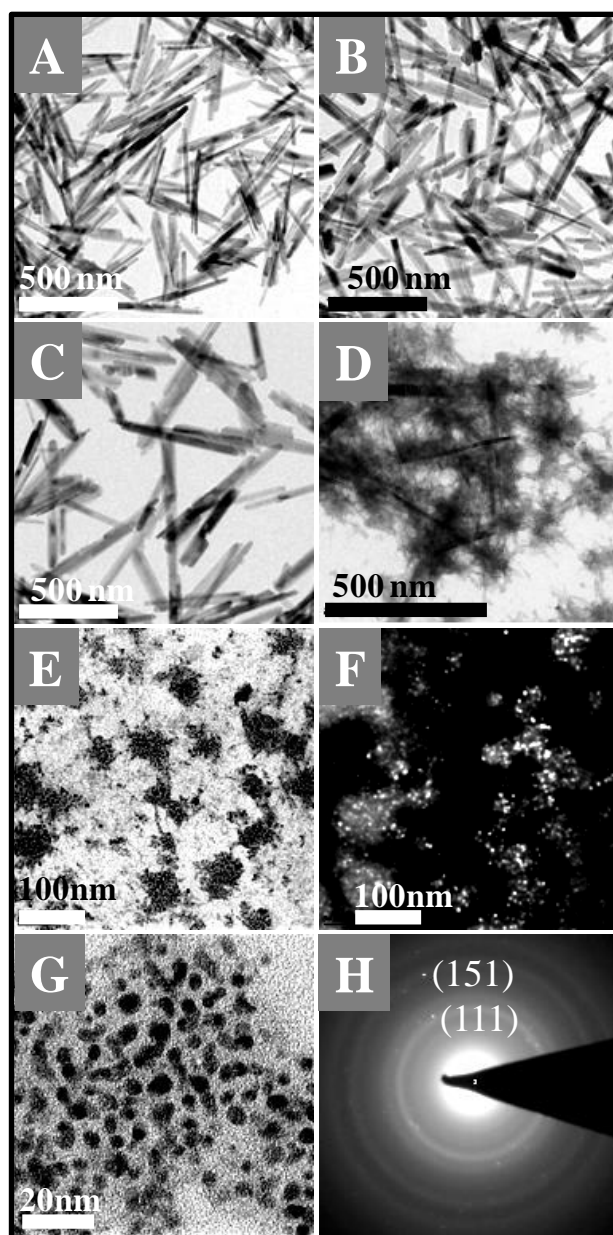
Figure 4.1: *The gradual transformation of rod shaped α-FeO(OH) nanoparticles to quasi-spherical ones. The bright field TEM images showing nanoparticles before (A) and after 48 h (B), 72 h (C), 96 h (D), and 120 h (E) biomilling. The TEM image in Figure(E) shows the fully transformed quasi-spherical nanoparticle aggregates after 120 h of biomilling (E), corresponding dark field image (F), magnified TEM image of 120 h biomilled sample showing particle size < 10 nm (G), and selected area electron diffraction (SAED) pattern (H).*[1]

4.4.2   The AFM Studies

The left panel of figure 4.2 shows the topography/height images and used for the analysis of shape and size of particles. The size of nanoparticles was estimated through height profile in figure 4.2 a, b, c which corresponds to the line drown across the nanoparticles in figure 4.2 A, B and C. The amplitude images of the same area shown in the right panel of figure 4.2, which indicates the amplitude variation in resonance frequency of AFM cantilever which is proportional to the first derivative of the topography.[45] The noteworthy breakdown events were observed after 96 h in figure 4.2C and D. At this stage, few smaller fragments of nanorods were observed together with intact nanorods with only minor change in the morphology.

After 96 h of biomilling, the diameter of nanorods were observed as high as ~ 80 nm, which may be due to the aggregates of two or more nanorods coated with a thick layer of proteins. After 120 h, the quasi-spherical nanoparticles were found to completely get embedded in the protein matrix and the average size was measured ~ 10 nm which can be easily seen from figures 4.2 E and F.
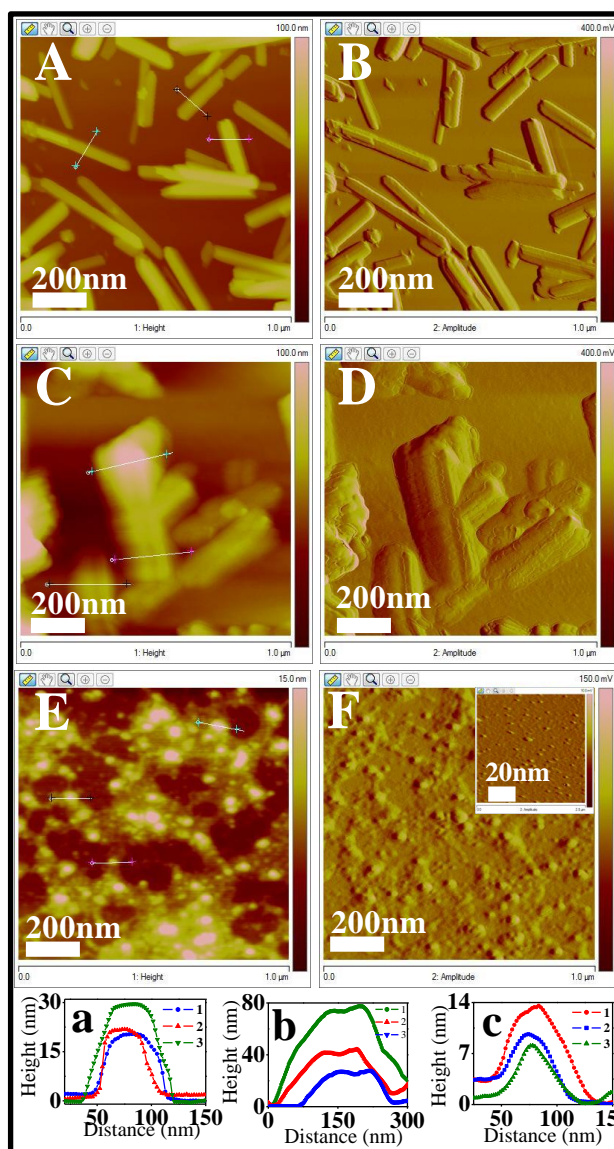
Figure 4.2: *The tapping mode AFM topographic (left panel, 2A, C, E) and corresponding amplitude images (right panel, B, D, F) showing the as-synthesized rod shaped nanoparticles at 0 h (A, B), aggregates of two or more nanorods coated with a thick layer of proteins after 96 h (C, D), and transformed quasi-spherical nanoparticle aggregates after 120 h (E, F) of biomilling, respectively. The approximate size of obtained nanoparticles was measured by height profile line scan analysis and plotted separately as figure a, b, c for their respective height images in figure 2A, C, and E.*[1]

The diameter of NRs before (20 – 60 nm) and after (<10nm) biomilling were as shown by a size distribution histogram in figure 4.3).
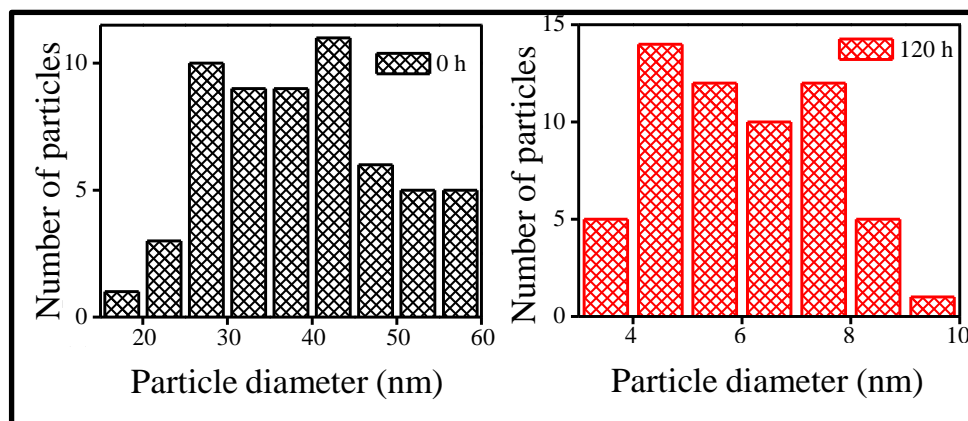
Figure 4.3: *The particle size (diameter) distribution of the α-FeO(OH) nanoparticles, before (0 h) and after (120 h) biomilling.*[1]

4.4.3   The Transformation of Nanorods into Quasi-spherical NPs

In order to get the better insight about the mechanism of biomilling, phase image and TEM image of the 96 h biomilled sample were compared and shown in figure 4.4. The phase shift in resonance frequency of AFM cantilever during tapping mode gives the information about the amount of dissipation of energy due to surface interactions, which is very sensitive to the composition, adhesion, friction, viscoelasticity as well as many other factors of the material.[45] In the phase images, the hard material (inorganic nanoparticles) supposed to show the different phase lag (dark color in image) compared to the soft materials (proteins, light color in image). Therefore, crevices on the surface of nanorods were clearly visualized in phase image in figure 4.4 A. The TEM image of a single biomilled nanoparticle and the enlarged view of certain specific areas on the rods (presented in white dotted circle) in TEM image 4.4 B, which confirm the finding from

AFM phase imaging results and suggest that the rods transform to spherical nanoparticles by formation of crevices in the rods.
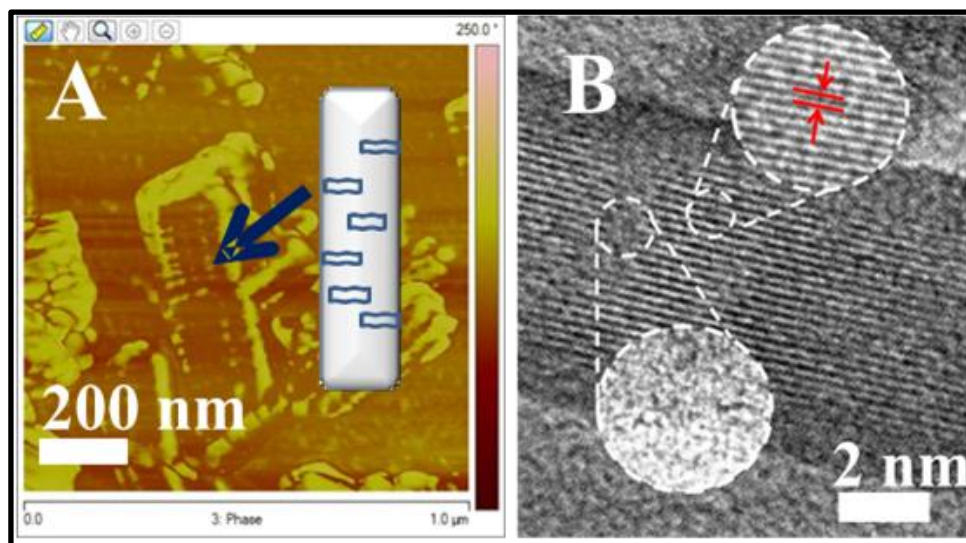
Figure 4.4: *The tapping mode AFM phase image (A) and HR-TEM image (B) of 96 h biomilled sample. The blue arrow in figure4.4A shows the region with soft organic material (light yellow color) such as protein molecules present in between the region with hard inorganic material (dark brown color) such as α-FeO(OH) nanorods. The figure 4.4 B supports the findings from AFM study and showing both the crystalline as well as amorphous regions in the rods (inset). The red mark shows the lattice fringes with d-spacing of 0.4 nm, which can be assigned to (110) crystal plane of α-FeO(OH) nanorods.*[1]

4.4.4 The Dispersibility of Biomilled Nanoparticles

The dispersibility of biomilled α-FeO(OH) nanoparticles in aqueous media, was compared with the chemically synthesized α-FeO(OH) nanorods and presented in figure 4.5. It can be easily seen from the UV absorbance at 373 nm as well as digital photographs (inset) that the biomilled α-FeO(OH) nanoparticles were more stable in aqueous suspension and did not settle down up to 2 h. These results support the presence of bulky ligands such as protein molecules on the nanoparticle surface which makes them dispersible in aqueous suspension.
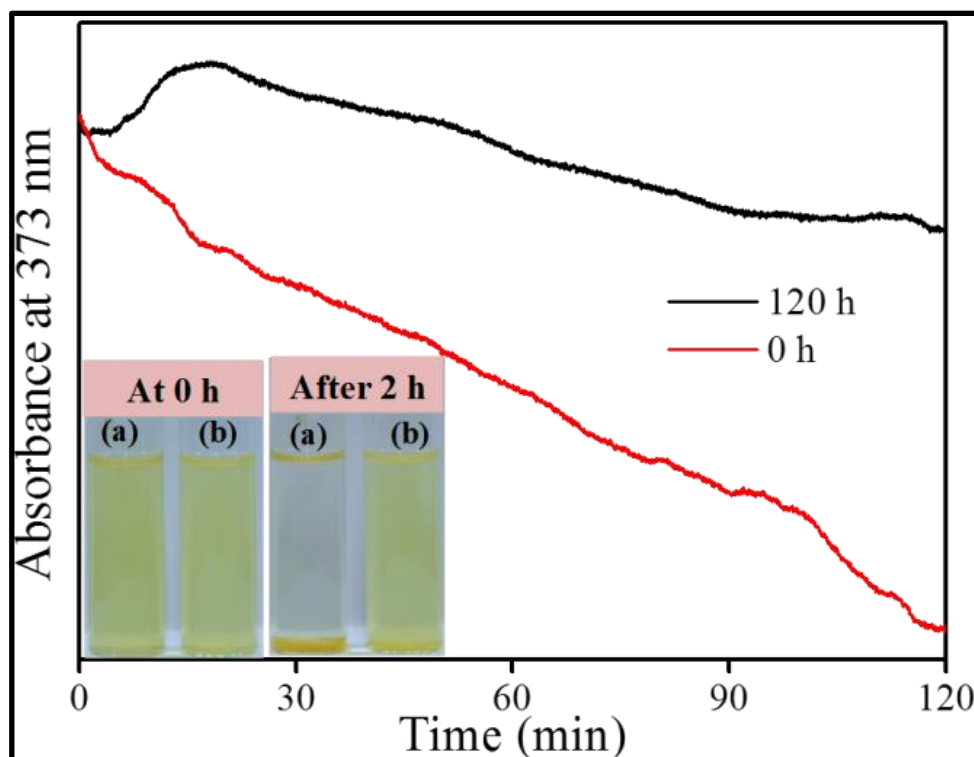
Figure 4.5: *The dispersibility of the α-FeO(OH) nanoparticles in aqueous suspension as a function of time. Inset shows the photographs of (a) 0 h sample, and (b) 120 h biomilled sample clearly indicates the instability of 0 h sample in aqueous suspension in comparison to 120 h sample.*[1]

4.4.5 The Role of Live Yeasts in Biomilling

To ensure that the biomilling process happens only in the presence of live yeast cells, the biomilling were carried out with live cells and dead cells. The biomilling were also carried without live or dead cells as control experiment.
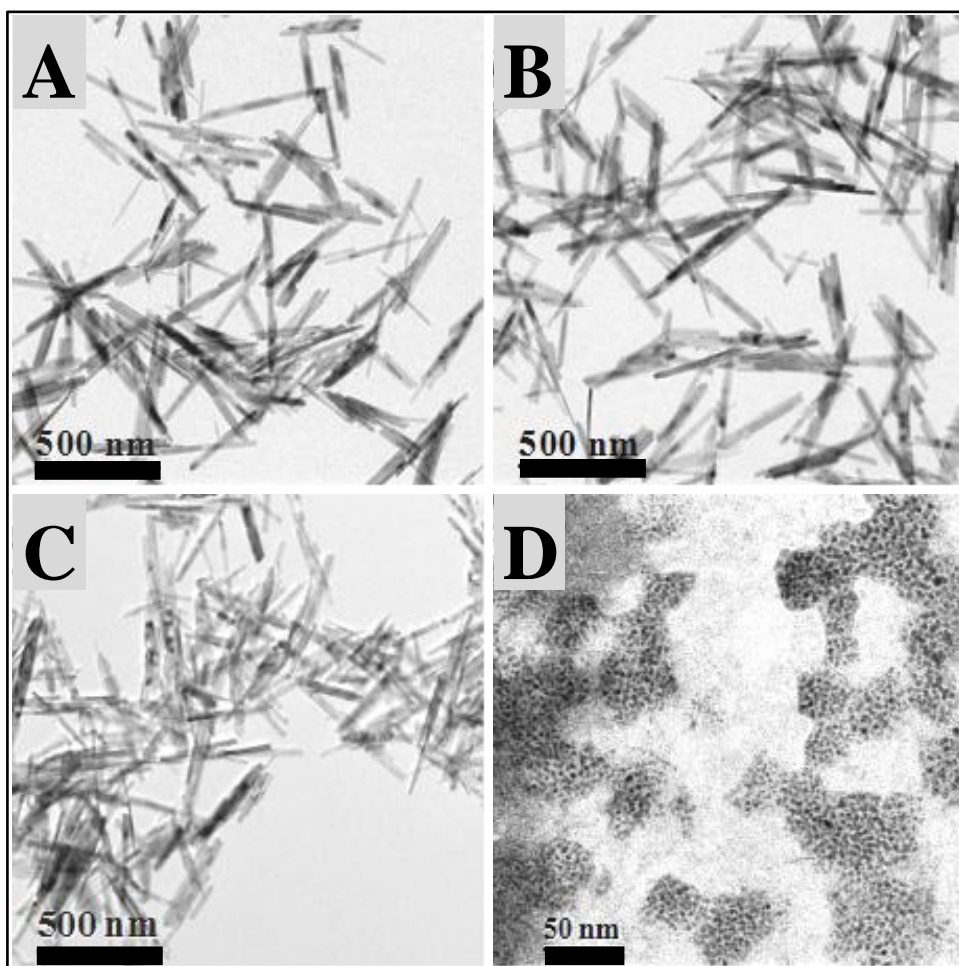
Figure 4.6: *The TEM images showing α-FeO(OH) nanorods , without biomilling at 0 h (A), at 120 h incubated without S. cerevisiae (B), with dead S. cerevisiae (C) and with live S. cerevisiae (D).*[1]

The TEM analysis of the α-FeO(OH) nanoparticles before (figure 4.6 A) and after exposure with PBS (in absence of yeast cells) (figure 4.6 B), dead yeast cells (figure 4.6

C), and live yeast cells (figure 4.6 D) for a period of 120 h indicates that the degradation of rods occurs only in the case of live yeast cells.

4.4.6   The XRD Studies

To study the effect of biomilling on the crystallinity of chemically synthesized α-FeO(OH) nanoparticles, PXRD measurements were performed on as-synthesized as well as biomilled samples, collected at different time intervals and shown in figure 4.7.
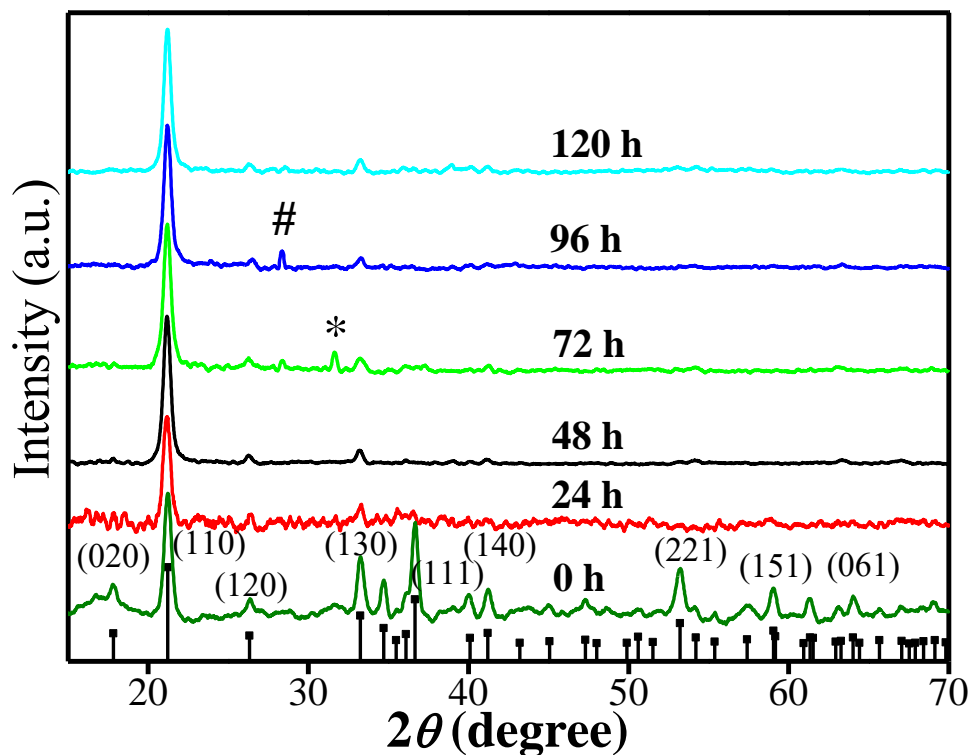
Figure 4.7: *Powder X-ray diffraction patterns of α-FeO(OH) nanoparticles at different time intervals (0 h, 24 h, 48 h, 72 h, 96 h, and 120 h) of biomilling. The patterns could be indexed to PCPDF 81-463. However, peak marked with * and # may be due to the traces of media.*[1]

The prominent peaks situated at 2θ values of 17.8°, 21.2°, 26.3°, 33.2°, 34.7°, 36.6°, 40.1°, 41.2°, and 53.2° correspond to the (020), (110), (120), (130), (021), (111), (210), (140) and (221) planes, respectively and could be indexed to α-FeO(OH) (JCPDS card no 81-463). The relative increase in the intensity of (110) crystal plane may be due to the possible size reduction of the crystallites during the course of biomilling.[46] However, peak marked with * and # may be due to the traces of media.

4.4.7 The Optical Properties of Biomilled NPs

UV-vis absorption spectroscopic measurements were performed at various time intervals of biomilling to acquire the information about the protein binding on the nanoparticle surface and presented in figure 4.8. The supernatant of control sample (having only protein molecules) shows a strong UV absorption at ~ 220 nm due to the presence of n-π* transition of peptide groups/carboxylic groups in the protein molecules.[47] The α-FeO(OH) nanoparticles (before and after biomilling) show the absorption at ~ 290 nm and ~ 380 nm wavelengths which may be due to the $^6A_1$ - $^4T_1(^4P_1)$ and $^6A_1$ - $^4E_1(^4D_1)$ ligand field transition of Fe^{3+}.[48] The strong UV absorbance ~ 220 nm due to peptide groups in the biomilled samples indicates the presence of protein molecules in the sample. The relative increase in absorption at ~ 290 nm in biomilled samples may also be due to the presence of romatic amino acids (Phe, Tyr, Trp) which again confirms the presence of protein molecules in the samples.[49]
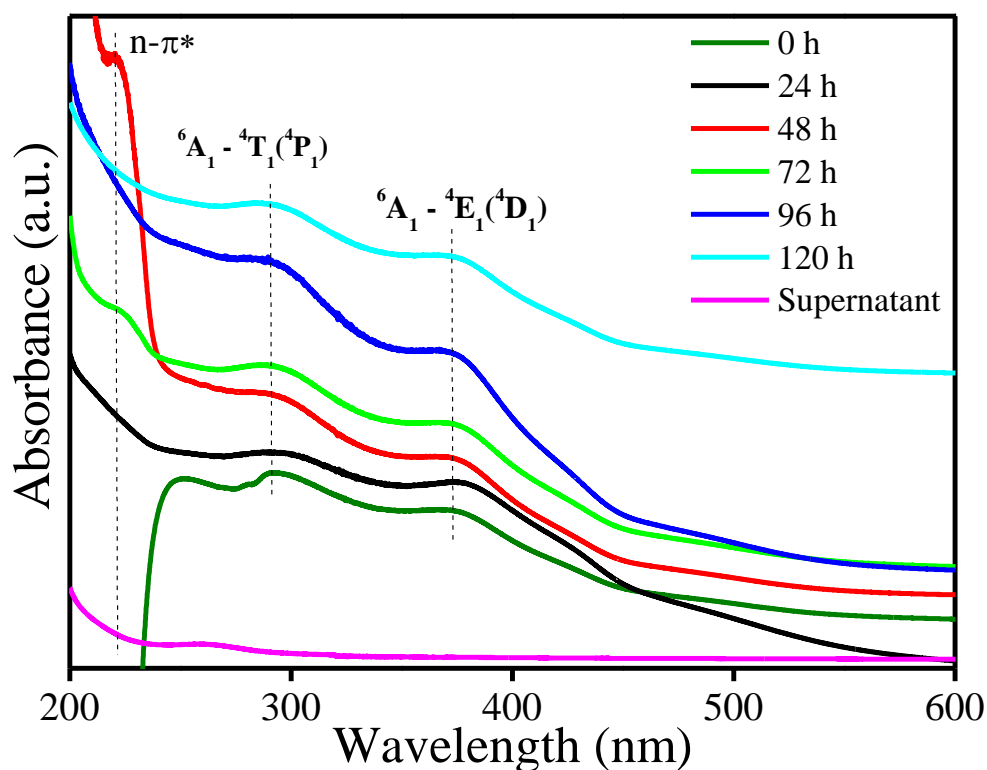
Figure 4.8: *The UV-visible spectra of α-FeO(OH) nanoparticles at different time intervals (0 h, 24 h, 48 h, 72 h, 96 h, and 120 h) of biomilling. The bottom pink color spectrum is for the supernatant of control sample (without α-FeO(OH)) showing the UV absorption below 230 nm (n-π* transition of peptide group) which is present in all the biomilled samples except 0 h sample indicates the presence of proteins. The absorption at ~ 290 nm and ~ 380 nm wavelengths in α-FeO(OH) containing samples may be due to the 6A₁ - 4T₁(4P₁) and 6A₁ - 4E₁(4D₁) ligand field transition of Fe³⁺. All the spectra were shifted vertically for the sake of clarity.*[1]

4.4.8 The FTIR Studies

In order to gain information about the functional groups of the proteins which are involved in the binding to α-FeO(OH) nanoparticles surface, the Fourier transformed infra-red

spectroscopy (FTIR) spectroscopic measurements were performed. At 0 h, α-FeO(OH) nanorods show the major peak at $\sim$ 1650 cm^{-1}. This peak was assigned to bending vibrations of hydroxyl group of goethite.[50,51] The peaks at 2337 cm^{-1} and 2360 cm^{-1} were observed in all the spectra, which could be due to the adsorbed CO_2 on the α-FeO(OH) surface.[52]
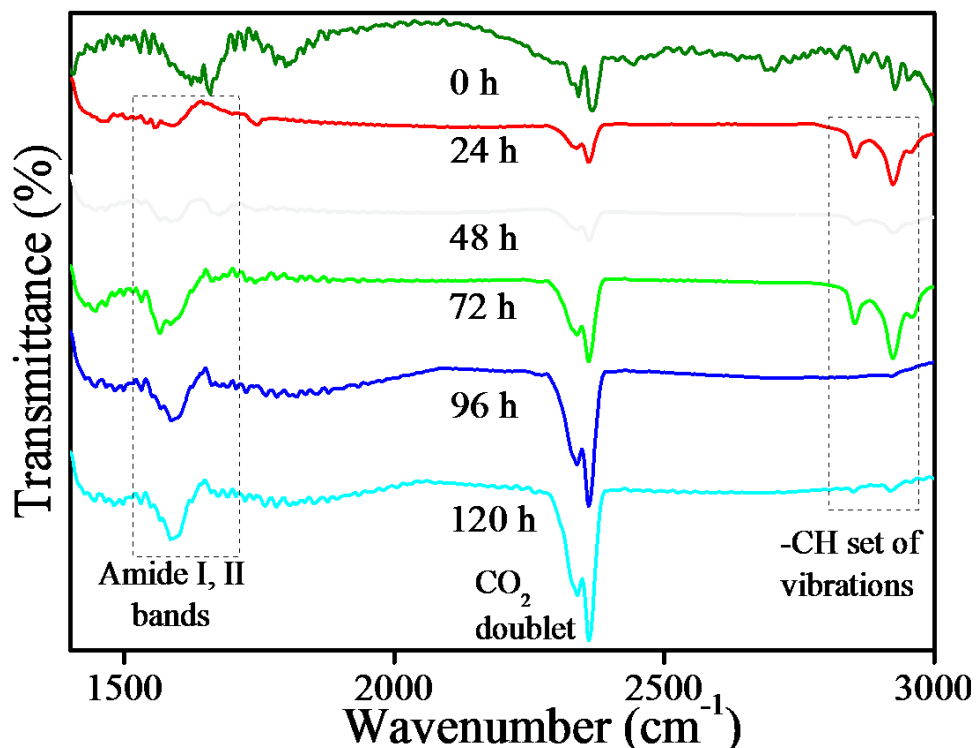
Figure 4.9: *The FTIR spectra of α-FeO(OH) nanoparticles at different time intervals (0 h, 24 h, 48 h, 72 h, 96 h, and 120 h) of biomilling, showing the appearance of amide bands in biomilled samples confirmed the presence of protein capping around nanoparticles.*[1]

FTIR spectra of all biomilled samples show the peak at $\sim$ 2852 cm^{-1} for symmetric stretching of CH_2 and its shoulder at $\sim$ 2870 cm^{-1} for symmetric stretching of CH_3, whereas, peak at $\sim$2923 cm^{-1} depicts the presence of asymmetric stretching of CH_2 and its

shoulder at 2958 cm^{-1} due to asymmetric stretching of CH$_3$.[53] Two other peaks at ~1630 cm^{-1} and ~1586 cm^{-1} correspond to amide I and II bands, respectively. The amide I band (1700-1600 cm^{-1}) is attributed to >C=O stretching vibration of peptide linkages in the backbone of the protein.[54] The amide II band (1620-1500 cm^{-1}) results from a combination of N-H bending and C-N stretching.[54] The presence of these bands confirms the protein capping around nanoparticles.

4.4.9　The XPS Studies

XPS is well suited for the characterization of proteins and other biomolecules adsorbed at the surface of nanoparticles.[55] It is also highly sensitive to detect the change in oxidation states of the elements. The XPS measurements were performed on 0 h and 120 h biomilled samples to validate the findings from FTIR study about the binding of the protein to α-FeO(OH) surface. For this purpose, the XPS spectra for binding energy of C 1s, O 1s and Fe 2p core level electrons for 0 h and 120 h sample were collected in high resolution, background-corrected by the Shirley algorithm, and chemically distinct peaks were resolved using a nonlinear least-squares fitting procedure.

The XPS survey scan has performed to get the information about the relative distribution of different elements before and after biomilling. For this purpose, the energy pass of 50 eV used for XPS survey scan at an energy resolution of 1 eV. The adventitious carbon (C 1s) peak was used for the charge correction reference and both the spectra were normalized against Fe 2p peak. The relative elemental contents were estimated by measuring the relative intensities of peaks. The 2.6 times increase in carbon and 1.7 times increase in oxygen content depicts the presence of organic molecules (proteins).[56] The

presence of sulfur (S 2*s*) and nitrogen (N 1*s*) depicts the presence of amino acids of protein.[57] Thus, these results support the presence of protein capping around nanoparticles. It can be noticed that in 120 h biomilled sample, the intensity of the C 1*s* and O 1*s* peaks was increased and the two new peaks (S 2*p* and N 1*s*) were appeared which confirms the presence of proteins capping around the biomilled nanoparticles.[57]
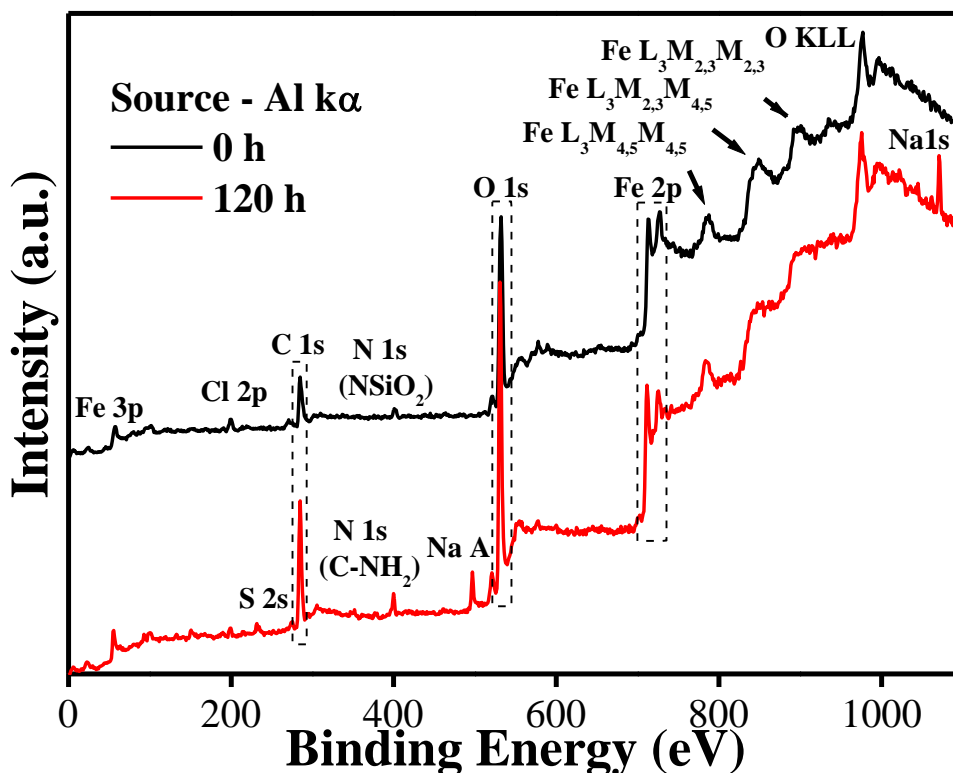
Figure 4.10: *The XPS survey spectra of 0 h and 120 h biomilled samples showing the relative distribution of various elements in the samples.*[1]

The C1*s* spectrum in figure 4.11 can be resolved in three components which are situated at 284.8 eV, 286.9 eV and 288.5 eV the binding energy for 0 h. The peak at 284.8 eV can be assigned to adventitious carbon (C-C, C-H), and served as charge reference standard to calibrate the whole spectrum for both 0 h and 120 h samples. The other two

peaks at 286.9 eV and 288.5 eV can be assigned to C-O and O-C=O groups, respectively.[57] For 120 h sample, the peaks were observed at 288.5 eV and 292.8 eV. The peak at 288.5 eV can be associated with carboxylic carbon.[58] Whereas, the peak at 292.8 eV can be assigned to the carboxyl carbon adjacent to the amino group (C^1) which is known to have highest binding energy in amino acids.[59]

Figure 4.11: *A comparison of XPS spectra for binding energy of C1s core level electrons for 0 h and 120 h biomilled samples showing the binding energy peaks for C-C/C-H, C-O-C, and O-C=O groups.*[1]

Figure 4.12: A comparison of XPS spectra for binding energy of O1s core level electrons for 0 h and 120 h biomilled samples showing that O 1s peak can be deconvoluted in three peaks at ~ 529.7, 531.2, and 533.4 eV binding energy which can be assigned to the lattice oxygen atom bound to Fe (Fe-O$_{lattice}$), hydroxide/hydrated or defective oxides component inherent to these oxide surfaces, and physisorbed water or organic oxygen, respectively.[1]

The O 1s core level spectrum in figure 4.12 for 0 h sample was deconvoluted in three peaks at 529.7, 531.2, 533.4 eV and can be assigned to the lattice oxygen atom bound

to Fe (Fe-O$_{lattice}$), hydroxide/hydrated or defective oxides component inherent to these oxide surfaces,[60] and physisorbed water, respectively.

These peaks were observed for 120 h sample at 529.6, 531.1, 532.8 eV. The major shift was observed in the third peak towards low binding energy 532.8 eV (which was situated at 533.4 eV in 0 h sample) and might be due to the replacement water molecules at 0 h, by protein molecules at 120 h.[61]

The Fe 2p spectra for 0 h sample was deconvoluted in four peaks situated at binding energy 713.2 eV (Fe 2$p_{3/2}$), 727 eV (Fe2$p_{1/2}$) and satellite features 719 eV (Fe2$p_{3/2}$ sattelite) and 734 eV (Fe2$p_{1/2}$ sattelite) as shown in figure 4.13. However, in 120 h biomilled sample, peaks were observed at 711 eV (Fe 2$p_{3/2}$) and 725 eV (Fe2$p_{1/2}$) and satellite features at 719 eV (Fe2$p_{3/2}$ sattelite) and 734 eV (Fe2$p_{1/2}$ sattelite).[62] The peaks at 711 eV and 725 eV can be assigned to the Fe atoms, bounded to lattice oxygen (Fe-O) and the lattice hydroxyls (Fe-OH$_{lattice}$), respectively.[63] The shifting of these peaks towards lower binding energy in comparison to 0 h sample, may be because of the replacement of adsorbed water molecules by the carboxylic group of protein molecules.[64] The satellite peaks are considered to be the characteristic feature of Fe^{2+} or Fe^{3+}.[65]
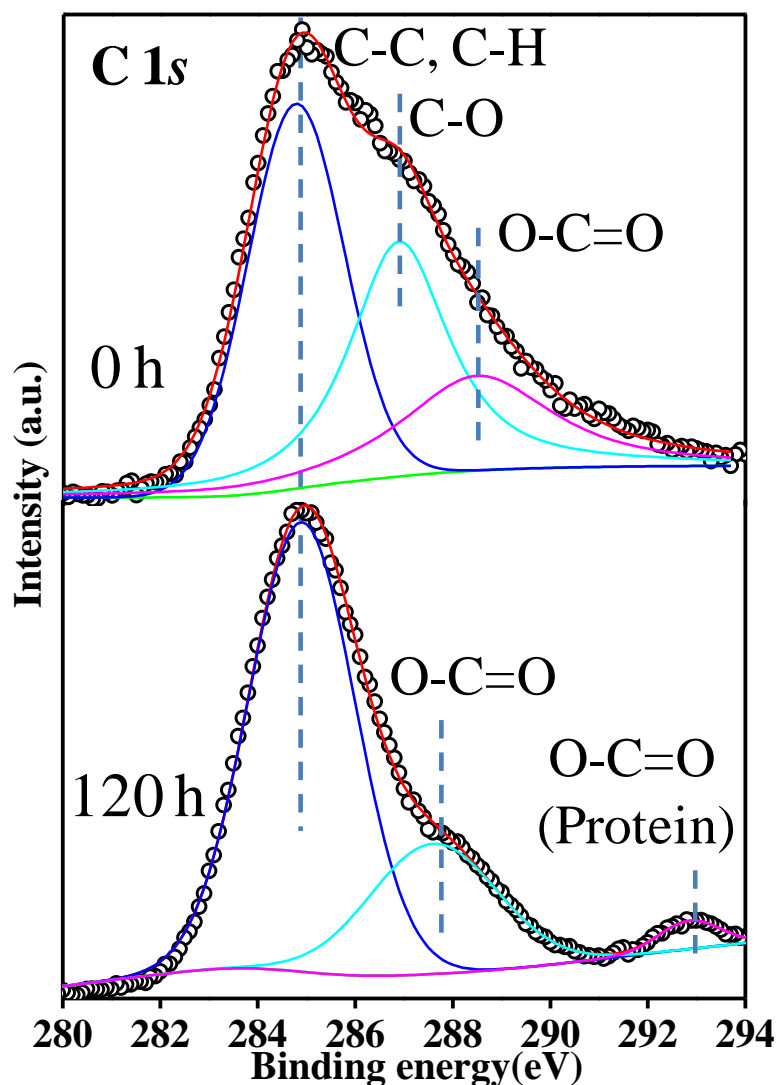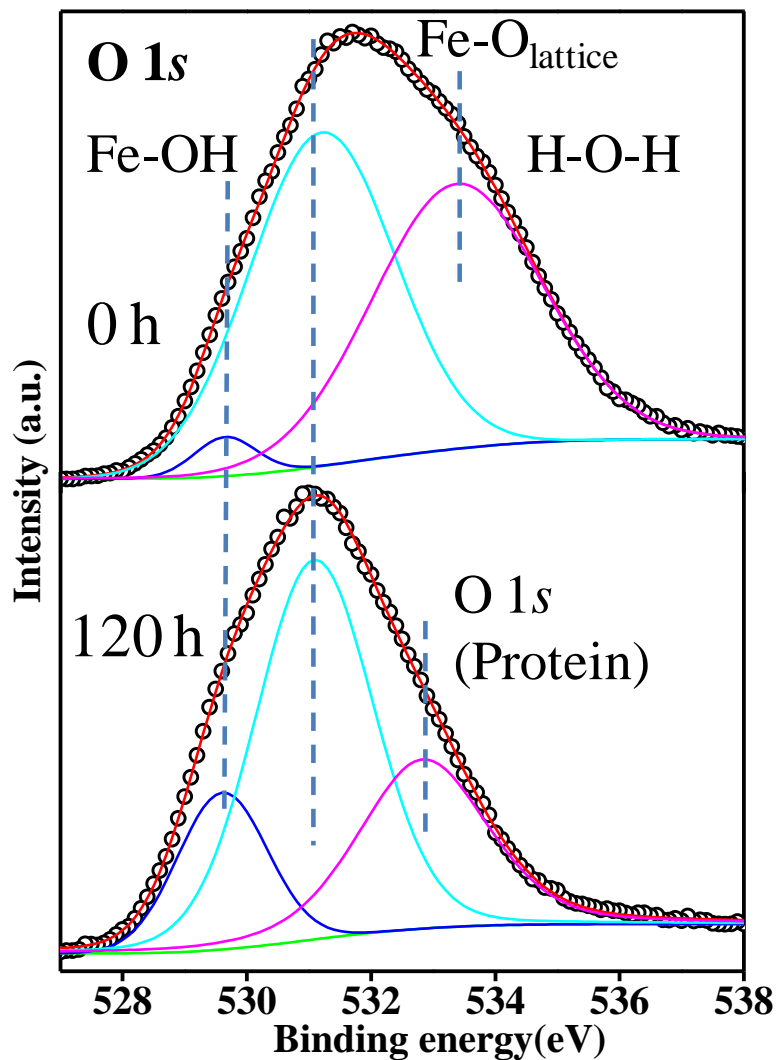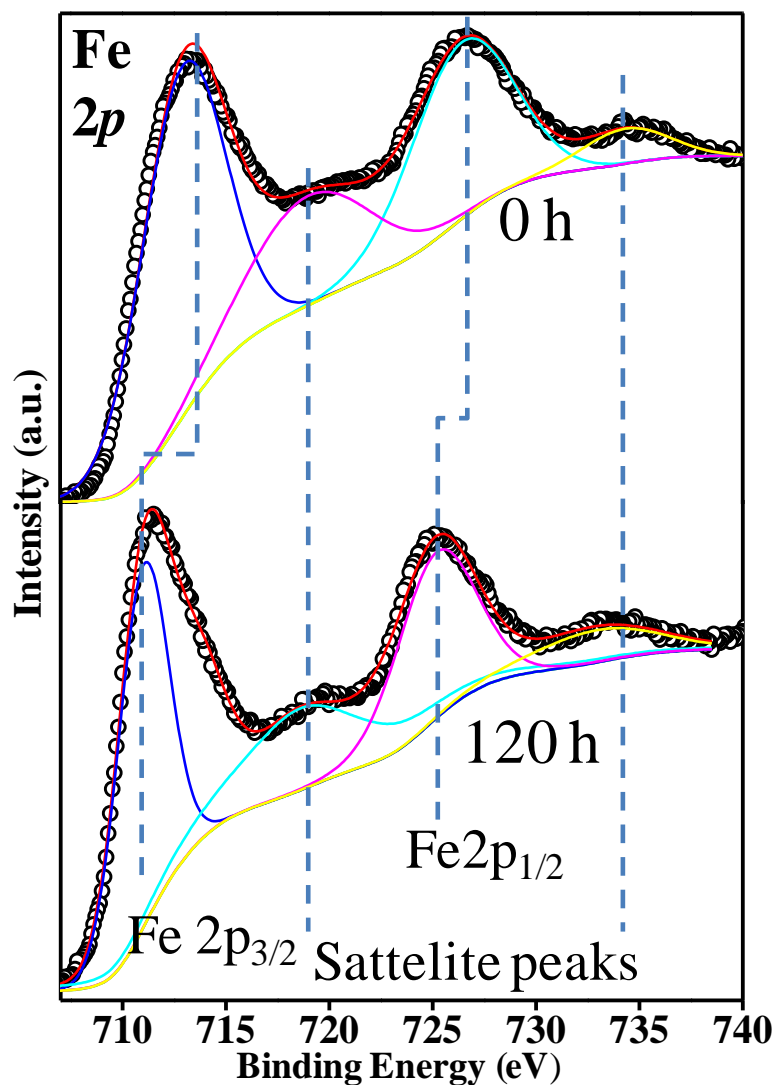
Figure 4.13: *A comparison of XPS spectra for binding energy of Fe2p core level electrons for 0 h and 120 h biomilled samples, showing the deconvolution of Fe2p peak in two major peaks at ~ 711 eV and ~ 725 eV binding energy for Fe bounded to lattice oxygen (Fe-O) and the lattice hydroxyls (Fe-OH$_{lattice}$), respectively.[1]*

4.4.10 The Proposed Mechanism of Biomilling

According to the literature, the (110) plane of goethite accounts for ~ 90% of the surface area and contains singly, doubly, and triply-coordinated oxygen, designated as $\equiv$FeOH$^{0.5}$,

$\equiv Fe_2OH$, and $\equiv Fe_3OH^{0.5}$, respectively. Singly- and triply-coordinated oxygen is responsible for the surface charge and, therefore, acid-base properties of the goethite.[41] Primarily, singly-coordinated oxygen is assumed to take part in ligand exchange reactions. Doubly-coordinated oxygen is generally to be inert in nature and do not supposed to take part in dissolution/biomilling of goethite.

The mechanism behind the degradation of anisotropic goethite particles into quasispherical NPs during biomilling is supposed to be started with the physisorption of water molecules to the surface of goethite nanorods. The theoretical double-hydrated double hydroxyl ((H_2O) - (H_2O) - OH - OH - Fe - O - O - Fe - R) termination model for the α-FeOOH surface best fit the interaction of goethite with water which propose the presence of two types of terminal hydroxyl (a) bidentate hydroxo and (b) monodentate aquo groups at the interface. The monodentate aquo group provides the effective Lewis base sites for interaction with cations of Lewis acid (via proton exchange), Lewis base exchange site and also the site for Columbic interaction with anions due to their excess positive charge.[66] This theory suggests that at the time of biomilling process, the aquo group may provide the site for interaction with carboxyl ions of protein molecules which results in the formation of a stable coordinate compound with Fe^{3+} ions[67] and is also supported by our XPS results. The Fe^{3+}-protein complexes get disassociated away from the lattice. This step exposes fresh Fe^{3+} ions on the surface of lattice and the process of protein complexation and dissociation from the lattice continues[68] which leads to the fragmentation of bigger particles into protein functionalized smaller nanoparticles as shown by a schematic in figure 4.14.
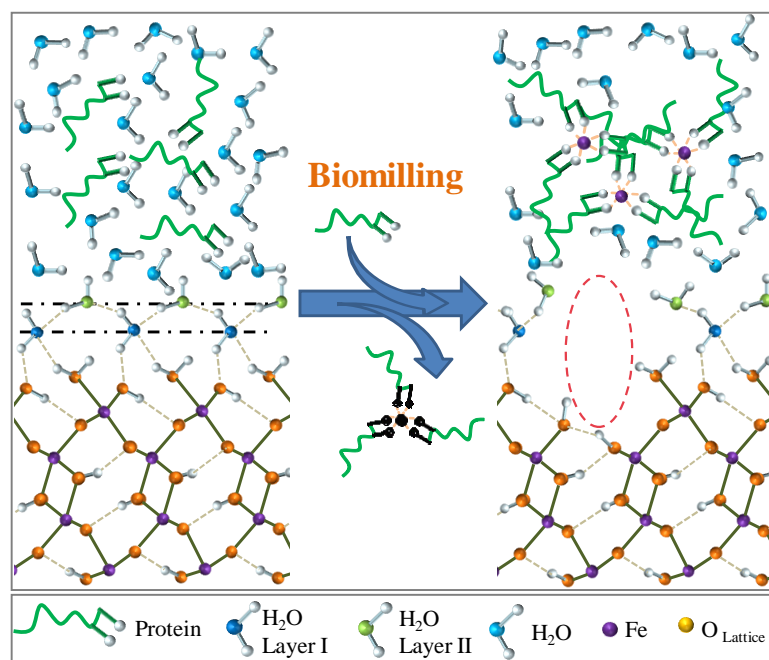
Figure 4.14: *Schematic of the mechanism behind biomilling of goethite.*[1]

4.5   Conclusion

Our study has shown that the degradation of rod-shaped α-FeO(OH) particles (length 200-400 nm and diameter ~ 30 nm) into small quasi-spherical particles with the size less than 10 nm is carried out by the proteins secreted by the *S. cerevisae* during the biomilling process. A detailed study using TEM, AFM, XRD, UV-vis spectroscopy, FTIR spectroscopy and XPS was performed to understand the mechanism behind biomilling. The HR-TEM and AFM phase imaging results have shown the formation of crevices on the nanorod surface at the time of biomilling. Further, UV-vis and FTIR results indicated the binding of protein molecules to the nanoparticles. XPS results show that the adsorbed water molecules on the goethite surface replaces by carboxyl group of protein molecules in the process of biomilling. According to the results from HR-TEM, AFM and XPS, it is

proposed that in the process of biomilling, the aquo group (present at the interface of α-FeO(OH) and water molecules) may provide the site for interaction with carboxyl ions of protein molecules which allows the formation of a stable coordinate compound with Fe^{3+} ions. Then, the chelated ion get dissociated from lattice and creates a new Fe^{3+} ion on the surface of lattice which results into the perforation of the nanorods and finally the formation of much smaller particles.

4.6   References

1   C. Sharan, P. Khandelwal and P. Poddar, *RSC Adv.*, 2015, **5**, 91785–91794.

2   U. T. Lam, R. Mammucari, K. Suzuki and N. R. Foster, *Ind. Eng. Chem. Res*, 2008, **47**, 599–614.

3   S. S. Lin and M. D. Gurol, *Environ. Sci. Technol.*, 1998, **32**, 1417–1423.

4   L. Zhang, H. Bin Wu and X. W. D. Lou, *Adv. Energy Mater.*, 2014, **4**, 1300958.

5   Q. Hao, S. Liu, X. Yin, Z. Du, M. Zhang, L. Li, Y. Wang, T. Wang and Q. Li, *Cryst. Eng. Comm.*, 2011, **13**, 806–812.

6   M. a. Legodi and D. de Waal, *Dye. Pigment.*, 2006, **74**, 161–168.

7   S. R. Prim, M. V. Folgueras, M. A. de Lima and D. Hotza, *J. Hazard. Mater.*, 2011, **192**, 1307–1313.

8   P. Poddar, T. Fried and G. Markovich, *Phys. Rev. B*, 2002, **65**, 3–6.

9   P. Poddar, M. B. Morales, N. A. Frey, S. a. Morrison, E. E. Carpenter and H. Srikanth, *J. Appl. Phys.*, 2008, **104**, 063901.

10   P. Poddar, T. Telem-Shafir, T. Fried and G. Markovich, *Phys. Rev. B*, 2002, **66**, 1–4.

11   C. Faure, M. Meyre, S. Trépout, O. Lambert and E. Lebraud, *J. Phys. Chem. B*, 2009, **113**, 8552–8559.

12   S. Laurent, S. Dutz, U. O. Häfeli and M. Mahmoudi, *Adv. Colloid Interface Sci.*, 2011, 166, 8–23.

13   K. Fan, C. Cao, Y. Pan, D. Lu, D. Yang, J. Feng, L. Song, M. Liang and X. Yan, *Nat. Nanotechnol.*, 2012, **7**, 459–464.

14   Wahajuddin and S. Arora, *Int. J. Nanomedicine*, 2012, 7, 3445–3471.

15   K. D. Wani, B. S. Kadu, P. Mansara, P. Gupta, A. V. Deore, R. C. Chikate, P. Poddar, S. D. Dhole and R. Kaul-Ghanekar, *PLoS One*, 2014, **9**, e107315.

16   J. Takagi, M. Ozaki, K. Shigemasa and T. Mizoguchi, *Mater. Trans.*, 2010, **51**, 1330–1339.

17   P. M. Harrison and P. Arosio, *Biochim. Biophys. Acta - Bioenerg.*, 1996, **1275**, 161–203.

18   C. Askwith and J. Kaplan, *Trends Biochem Sci.*, 1998, **4**, 135–138.

19   D. Faivre and D. Schüler, *Chem. Rev.*, 2008, **108**, 4875–4898.

20   J. Bunge, M. L. Sogin, J. Zhou, T. J. Gentry, Z. He, A. Boetius, T. Holler, K. Knittel, J. Felden, F. Wenzhöfer, M. Podar, M. Keller, P. Hugenholtz, T. M. Schmidt, A. E. Konopka, R. R. Colwell, S. S. Epstein, V. Miao, J. Davies, K. Lewis and K. Nealson, *Uncultivated Microorganisms*, springer-verlag Berlin Heidelberg, Third Ed., 2009, vol. 10.

21   S. Douglas and T. J. Beveridge, *FEMS Microbiol. Ecol.*, 1998, **26**, 79–88.

22   M. Uchida, S. Kang, C. Reichhardt, K. Harlen and T. Douglas, *Biochim. Biophys. Acta - Gen. Subj.*, 2010, **1800**, 834–845.

23   T. Wang, H. W. Choi and I. S. Yoo, *Molecular*, 2009, **505**, 386–395.

24   P. Mukherjee and S. Senapati, *ChemBioChem*, 2002, **5**, 461–463.

25   A. Ahmad, P. Mukherjee, D. Mandal, S. Senapati, M. I. Khan, R. Kumar and M. Sastry, *J. Am. Chem. Soc.*, 2002, **124**, 12108–12109.

26   M. Sastry, A. Ahmad, M. I. Khan and R. Kumar, *Curr. Sci.*, 2003, **85**, 162–170.

27   D. K. Singh, R. Jagannathan, P. Khandelwal, P. M. Abraham and P. Poddar, *Nanoscale*, 2013, **5**, 1882–1893.

28   V. Bansal, A. Sanyal, D. Rautaray, A. Ahmad, M. Sastry, B. V. Bansal, A. Sanyal, V. Bansal and A. Sanyal, *Adv. Mater.*, 2005, **17**, 889–892.

29   V. Bansal, A. Syed, S. K. Bhargava, A. Ahmad and M. Sastry, *Langmuir*, 2007, **23**, 4993–4998.

30   V. Bansal, A. Ahmad and M. Sastry, *J. Am. Chem. Soc.*, 2006, **128**, 14059–14066.

31   U. Kumar, A. K. Ranjan, C. Sharan, A. A. Hardikar, A. Pundle and P. Poddar, *Curr. Nanosci.*, 2012, **8**, 130–140.

32   R. Das, R. Jagannathan, C. Sharan, U. Kumar and P. Poddar, *J. Phys. Chem. C*, 2009, **113**, 21493–21500.

33   P. V. Adhyapak, U. P. Mulik, D. P. Amalnerkar and I. S. Mulla, *J. Am. Ceram. Soc.*, 2013, **96**, 731–735.

34   M. Mohapatra and S. Anand, *Int. J. Eng. Sci. Technol.*, 2010, **2**, 127–146.

35   J. Baltrusaitis, D. M. Cwiertny and V. H. Grassian, *Phys. Chem. Chem. Phys.*, 2007, **9**, 5542–5554.

36   V. H. Grassian, *J. Phys. Chem. C*, 2008, **112**, 18303–18313.

37   M. K. Ghosh, G. E. J. Poinern, T. B. Issa and P. Singh, *Korean J. Chem. Eng.*, 2012, **29**, 95–102.

38   E. Brok, C. Frandsen, D. E. Madsen, H. Jacobsen, J. O. Birk, K. Lefmann, J. Bendix, K. S. Pedersen, C. B. Boothroyd, A. A. Berhe, G. G. Simeoni and S. Mørup, *J. Phys. D. Appl. Phys.*, 2014, **47**, 365003.

39   R. M. Cornell and U. Schwertmann, *The Iron Oxids: Structure, Properties, Reactions Occurances and Uses*, Wiley-VCH Verlag GmbH & Co. KGaA, Second Ed., 2003.

40   T. Hiemstra and W. H. Van Riemsdijk, *J. Colloid Interface Sci.*, 1996, **508**, 488–508.

41   P. Venema, T. Hiemstra, P. G. Weidler and W. H. Van Riemsdijk, *J. Colloid Interface Sci.*, 1998, **295**, 282–295.

42   Y. Miao, Q. Zhang, H. Yang and H. Wang, 2006, **128**, 103–106.

43   M. Hua, S. Zhang, B. Pan, W. Zhang, L. Lv and Q. Zhang, *J. Hazard. Mater.*, 2012, **211-212**, 317–331.

44   D. B. Williams and C. B. Carter, *Transmission electron microscopy A Textbook for Materials Science*, Springer, Second Ed., 2009.

45   M. Stark, C. Möller, D. J. Müller and R. Guckenberger, *Biophys. J.*, 2001, **80**, 3009–3018.

46   B. Mazumder, I. Uddin, S. Khan, V. Ravi, K. Selvraj, P. Poddar and A. Ahmad, *J. Mater. Chem.*, 2007, **17**, 3910–3914.

47   L. B. Clark, *J. Am. Chem. Soc.*, 1995, **117**, 7974–7986.

48   D. M. Sherman and T. D. Waite, *Am. Mineral.*, 1985, **70**, 1262–1269.

49   R. K. Murray, D. K. Granner, P. A. Mayes and V. W. Rodwell, *Harper's Illustrated Biochemistry*, The McGrow-Hill Companies, 26 Ed., 2003.

50   R. G. Gast, E. R. Landa and G. W. Meyer, *Clays Clay Miner.*, 1974, **22**, 31–39.

51   H. D. Ruan, R. L. Frost and J. T. Kloprogge, *Spectrochim. Acta - Part A Mol. Biomol. Spectrosc.*, 2001, **57**, 2575–2586.

52   G. Lefèvre, T. Preočanin and J. Lützenkirchen, in *Infrared Spectroscopy – Materials Science, Engineering and Technology*, ed. T. Theophile, InTech, 2012, p. 510.

53   B. Stuart, *Infrared Spcetroscopy: Fundamentals and Applications*, John Wiley and Sons, Ltd., 2004.

54   S. Wang, T. Chen, Z. Zhang, X. Shen, Z. Lu, D.-W. Pang and K.-Y. Wong, *Langmuir*, 2005, **21**, 9260–9266.

55   S. L. McArthur, *Surf. Interface Anal.*, 2006, **38**, 1380–1385.

56   E. Johansson and L. Nyborg, *Surf. Interface Anal.*, 2003, **35**, 375–381.

57   E. Vanea and V. Simon, *Appl. Surf. Sci.*, 2011, **257**, 2346–2352.

58   J. F. Cardenas and G. Gröbner, *J. Electron Spectros. Relat. Phenomena*, 2005, **148**,

96–100.

59   D. Nolting, E. F. Aziz, N. Ottosson, M. Faubel, I. V. Hertel and B. Winter, *J. Am. Chem. Soc.*, 2007, **129**, 14068–14073.

60   M. C. Biesinger, B. P. Payne, L. W. M. Lau, A. Gerson and R. S. C. Smart, *Surf. Interface Anal.*, 2009, **41**, 324–332.

61   M. C. Biesinger, B. P. Payne, A. P. Grosvenor, L. W. M. Lau, A. R. Gerson and R. S. C. Smart, *Appl. Surf. Sci.*, 2011, **257**, 2717–2730.

62   M. Descostes, F. Mercier, N. Thromat, C. Beaucaire and M. Gautier-soyer, *Appl. Surf. Sci.*, 2000, **165**, 288–302.

63   Y. Jia, T. Luo, X.-Y. Yu, B. Sun, J.-H. Liu and X.-J. Huang, *RSC Adv.*, 2013, **3**, 15805–15811.

64   W. W. Parson, *Modern Optical Spectroscopy with Examples from Biophysics and Biochemistry*, Springer-verlag Berlin Heidelberg, Washington, 2007.

65   P. Graat and M. a. J. Somers, *Surf. Interface Anal.*, 1998, **26**, 773–782.

66   S. K. Ghose, G. a. Waychunas, T. P. Trainor and P. J. Eng, *Geochim. Cosmochim. Acta*, 2010, **74**, 1943–1953.

67   G. H. Jeffery, J. Bassett, J. Mendham and R. C. Denney, *Vogel's Textbook of quantitative chemical analysis*, Longman Scientific & Technical, 1989.

68   G. Svehla, *Vogel's Textbook of Macro and Semimicro Qualitative Inorganic Analysis*, Longman Group Limited London, Fifth Ed., 1979.

Chapter V

The Salient Features and Future Perspectives of the Work

_____

This chapter deals with the salient features and the future perspectives of the research work

presented in this thesis.

_____

5.1   Salient Features of the Work

In the modern era, the nanomaterials have revolutionized our lives and being virtually utilized in possible ways. The immense applicability has tremendously increased the demand of environmental-friendly production of nanomaterials. So far, people largely rely upon physical and chemical methods of synthesis of nanoparticles. However, the chemical ways are most of the times hazardous and pose a significant risk to the environment while physical methods demand specialized tools. Therefore, the synthesis of nanomaterials following the nature's way has always been of immense interest for the nanotechnologists. A number of bottom-up biological methods have been known. However, for the first time, our lab has used biological methods, for the top-down synthesis of nanomaterials. In top-down approach, microorganisms have been used for the controlled breakdown of large (micron-sized) particles into nanoparticles. This method can potentially be used for all kind of nanomaterials, however, this is especially useful for the synthesis of nanomaterials, which need to calcine at high temperature. In general the high temperature leads to grain growth and agglomeration of nanoparticles with improper crystallinity.[1] Therefore, for such materials, this method would be very useful.

First of all, the top-down method was demonstrated for the synthesis of BiOCl nanoparticles by break-down of chemically synthesized nanoplates and this method was termed as "biomilling". For this purpose, an alkalo-tolerant and thermophilic fungus, *Humicola sp.* (HAA-SHC-2), was isolated from self-heating compost. The biomilling was carried out for the synthesis of BiOCl nanoparticles from chemically synthesized nanoplates (edge lengths 150–200 nm).[1] Later, this method has been also used for the milling of Gd_2O_3,[2] $BaTiO_3$[3] etc. down to nanosize.

In the chapter III of this thesis, we discussed the synthesis the protein-capped, quasi-spherical ZnO NPs with size less than 10 nm from the chemically synthesized ZnO NRs (~250 nm in length). We have addressed some of the challenges associated with the biomilling process, which we have been facing. The modified biomilling procedure developed by us in this thesis work, has several inherent advantages over our earlier reported work. In this thesis we demonstrate that it is possible to (1) isolate the biomilled NPs with minimum efforts, (2) separate the top-down biomilling and bottom-up biosynthesis processes (if the organism itself, has NP synthesis ability by extra/intracellular reduction of free zinc ions to form NPs), and (3) differentiate the yeast cell involvement in the biomilling process. Detailed experimental investigation proves the formation of crystalline, small-sized protein-capped, quasi-spherical ZnO NPs after nearly 168 h of biomilling. The UV-vis, photoluminescence (PL) and FTIR spectroscopic studies as a function of biomilling-time, show the dynamic nature of protein corona on the ZnO NPs, which is further supported by the SDS-PAGE analysis of the extracellular fluid. The dynamic nature of proteins are due to the differential binding affinity of different proteins to the surface of nanoparticles, as well as the protein–protein interactions among the coronal proteins. We believe that the yeast cells provide an important role in the process of biomilling by accumulating a high amount of zinc content in the cells while the zinc content in extracellular medium almost same as shown by the ICP-OES analysis. The biomilled ZnO NPs show enhanced stability and improved dispersibility in aqueous medium than chemically synthesized ZnO NRs.[4]

In chapter IV, we have shown the degradation of rod-shaped α-FeO(OH) particles (length 200-400 nm and diameter ~ 30 nm) into small quasi-spherical particles with the

size less than 10 nm, carried out by the proteins secreted by the *S. cerevisae* during the biomilling process. A detailed study using TEM, AFM, XRD, UV-vis spectroscopy, FTIR spectroscopy and XPS was performed to understand the mechanism behind biomilling. The HR-TEM and AFM phase imaging results have shown the formation of crevices on the nanorod surfaces at the time of biomilling. Further, UV-vis and FTIR results indicated the binding of protein molecules to the nanoparticles. The XPS results show that the adsorbed water molecules on the goethite surface get replaced by the carboxyl groups of protein molecules in the process of biomilling. According to the results from HR-TEM, AFM and XPS, it is proposed that in the process of biomilling, the aquo group (present at the interface of α-FeOOH and water molecules) may provide the site for interaction with carboxyl ions of protein molecules which allows the formation of a stable coordinate compound with Fe^{3+} ions. Then, the chelated ions get dissociated from lattice and expose fresh lattice sites where this process can be repeated which results into the perforation of the nanorods and finally the formation of much smaller particles.[5]

In biomilling, we observed the synthesis of quasi-spherical nanoparticles with size below 10. During this process, the yeast cells secrete different types of proteins, which is responsible for the biomilling process and render negative surface charge on the nanoparticles. The obtained nanoparticles were quite stable in aqueous medium. However, despite of these similarities, the yeasts have shown faster response towards the metal oxide (ZnO), therefore the precursor particles are observed to be fully covered with proteins at 72 h as compared to that of 96 h in case of metal oxy-hydroxides. Whereas, the total time taken to biomill the metal oxide nanoparticles are higher (168h) as compared to metal oxy-hydroxides (120h).

5.2 Future Perspective of the Work

The biomilling method for the synthesis of nanoparticles is quite a new method as compared to other methods for synthesis of nanoparticles. Being in its infancy, it has been facing many challenges. In this thesis, we have modified the method which has many advantages such as – (a) isolate the biomilled NPs with minimum efforts, (b) separate the top-down biomilling and bottom-up biosynthesis processes (if the organism itself, has NP synthesis ability by extra/intracellular reduction of free zinc ions to form NPs), and (c) differentiate the yeast cell involvement in the biomilling process. During our study, we have observed that some proteins get overexpressed during biomilling. It would be very interesting to identify the proteins and understand their role in biomilling. It may also be a good idea to overexpress the yeast protein using recombinant DNA technology methods to get higher yield. However, biomilling using purified isolated protein of yeast or microbial cells, would be another aspects of study. There are some literatures which suggest that the proteins bind preferentially at some specific facets. So, it would open up the door to another direction of research where synthesis of tailored nanostructures can be possible.

5.3 References

1   B. Mazumder, I. Uddin, S. Khan, V. Ravi, K. Selvraj, P. Poddar and A. Ahmad, *J. Mater. Chem.*, 2007, **17**, 3910–3914.

2   I. Uddin, P. Poddar, U. Kumar and N. Phogat, *J. Green Sci. Technol.*, 2013, **1**, 48–53.

3   I. Uddin, A. Jaiswal and P. Poddar, *Int. J. Innov. Biol. Reaserch*, 2013, **2**, 1–5.

4   C. Sharan, P. Khandelwal and P. Poddar, *RSC Adv.*, 2015, **5**, 1883–1889.

5   C. Sharan, P. Khandelwal and P. Poddar, *RSC Adv.*, 2015, **5**, 91785–91794.

List of Publications

(1) Das, R.; Jagannathan, R.; **Sharan, C.**; Kumar, U.; Poddar, P. Mechanistic Study of Surface Functionalization of Enzyme Lysozyme Synthesized Ag and Au Nanoparticles Using Surface Enhanced Raman Spectroscopy. *J. Phys. Chem. C* **2009**, *113*, 21493–21500.

(2) Kumar, U.; Ranjan, A. K.; **Sharan, C.**; Hardikar, A. A.; Pundle, A.; Poddar, P. Green Approach Towards Size Controlled Synthesis of Biocompatible Antibacterial Metal Nanoparticles in Aqueous Phase Using Lysozyme. *Curr. Nanosci.* **2012**, *8*, 130–140.

(3) Kandpal, M.; **Sharan, C.**; Poddar, P.; Prashanthi, K.; Apte, P. R.; Ramgopal Rao, V. Photopatternable Nano-Composite (SU-8/ZnO) Thin Films for Piezo-Electric Applications. *Appl. Phys. Lett.* **2012**, *101*, 104102.

(4) **Sharan, C.**; Khandelwal, P.; Poddar, P. Biomilling of Rod-Shaped ZnO Nanoparticles: A Potential Role of *Saccharomyces cerevisiae* Extracellular Proteins. *RSC Adv.* **2015**, *5*, 1883–1889.

(5) Kandpal, M.; **Sharan, C.**; Palaparthy, V.; Tiwari, N.; Poddar, P.; Rao, V. R. Spin-Coatable, Photopatternable Magnetic Nanocomposite Thin Films for MEMS Device Applications. *RSC Adv.* **2015**, *5*, 85741–85747.

(6) **Sharan, C.**; Khandelwal, P.; Poddar, P. The Mechanistic Insight into the Biomilling of Goethite (α-FeO(OH)) Nanorods Using the Yeast *Saccharomyces cerevisiae*. *RSC Adv.* **2015**, *5*, 91785–91794.

List of Patents

(1)   **Patent Filed:** Gonnade, R. G.; Gawde, R. L.; Puranik, V. G.; Sharan, C. Novel heterocyclic probe, preparation method and application thereof. Application No 0207nf2016, 30/08/2016.